Muséum national d'Histoire naturelle

International Erasmus Mundus Master in
QUATERNARY AND PREHISTORY

Molar Size Determination in Hominins: Testing the Inhibitory Cascade Model

Chun Wing WONG

Tuteur/s : Florent DÉTROIT

Jérémie BARDIN

Pierre GOUSSET

Année académique 2024/2025

ACKNOWLEDGEMENTS

I would like to sincerely thank my supervisors, Florent Détroit, Jérémie Bardin, and Pierre Gousset, for their invaluable guidance and support throughout this project.

I am deeply grateful to Florent Détroit for his continuous advice, encouragement, and trust. From shaping the initial framework of this thesis to guiding the analyses and reviewing the written report, his insights have been indispensable. I greatly appreciate the time he devoted to our meetings and discussions, always making himself available without hesitation.

I thank Jérémie Bardin for his patience in explaining the principles of phylogenetic regression models, for his guidance in the interpretation of statistical results, and for mentoring me in the implementation of models in R. His expertise and mentorship equipped me with the fundamental skills to apply these methods and interpret their results, which have since become central to my work.

I am particularly indebted to Pierre Gousset for generously sharing his research materials, especially the dental metric database that constitutes a large part of my dataset and the 3D models of specimens unavailable in the museum collection, without which this project would have required considerably more time to complete. I am also grateful for the time he dedicated to teaching me the fundamentals of R and Avizo, and for always responding promptly and supportively whenever I needed help.

I would like to thank Guillaume Billet and Helder Gomes Rodrigues for their valuable comments and insightful discussions on the framework of this project.

Finally, I thank the Musée de l'Homme for granting me access to its collections, and I am especially grateful to Florent Détroit and Pierre Gousset for arranging this access and supporting me throughout the data collection process. I would like to acknowledge once again their kindness, which I did not have the opportunity to properly thank in my M1 internship report.

TABLE OF CONTENTS

LIST OF FIGURES

LIST OF TABLES

INTRODUCTION

A central quest in biology, since Charles Darwin, has been to understand the "laws of variation": an underlying rule that governs how new structures and forms arise for natural selection to act upon. While Darwin (1871) recognised that variation was the essential spark for evolution, the mechanisms that develop it remained a black box. With the advancement of developmental and molecular genetics that allow searches for the developmental blueprints that pattern morphological changes, the contents of the black box have now become visible (Brakefield, 2011). A key aim of evolutionary developmental biology (evo-devo) is therefore to find simple yet powerful rules that can predict evolutionary trajectories across the diversity of species. The inhibitory cascade (IC) model, which describes sequential molar development, marks a major step toward the aim by proposing a universal rule of elegant simplicity that may govern the evolution of mammalian dentition (Kavanagh et al., 2007). The critical question is, however, whether humans, and hominins in general, conform to this developmental rule, or if their distinctive dental patterns reflect departures from it.

The inhibitory cascade (IC) model

The inhibitory cascade model was introduced by Kavanagh et al. (2007) as a developmental mechanism that governs the relative size and number of molars in mammals, demonstrated through an experiment on *in vitro* cultured molars of mice (explants of mouse). The study suggests that as molars develop sequentially from anterior to posterior (first molar, then second molar, then third molar), their relative size is determined by a balance between activating and inhibiting molecular signals. The activator is thought to arise from the dental mesenchyme, while inhibitory signals originate from earlier developing molars, particularly from their enamel knots.

The enamel knot is an epithelial signaling centre. The primary enamel knot forms at the onset of tooth crown development, followed by secondary enamel knots appearing at the future positions of the major molar features (cusps), which contribute to shaping the morphology of the tooth crown. Since the first molar (M1) forms first, its enamel knots produce inhibitory signals that influence the initiation and growth of later molars (second molar - M2, and third molar - M3).

This mechanism creates a cascade of inhibition in which each newly forming molar is cumulatively affected by the development of the previous one. The process has been described as a “ratchet’:

when increasing inhibition cumulates and progressively reduces the size of posterior molars, a starting condition of equally sized molars (M1≈M2≈M3) can be shifted to a gradient M1>M2>M3 through the IC mechanism.

The IC model not only reveals the developmental mechanism of molar formation but also translates it into a statistical framework that can be empirically tested. Kavanagh et al. (2007) demonstrated that the relationship between M2/M1 and M3/M1 size ratios follows a reduced major axis (RMA) regression with a slope of 2.0 and an intercept of -1.0, meaning that an increase in the relative size of M2 predicts an even greater relative increase in M3. The clustering of species along the slope suggests that the regression captures evolutionary diversity and can be used to predict evolutionary change from developmental processes.

Kavanagh et al. (2007) also expressed the balance between activator (*a*) and inhibitor (*i*) signals in a simple mathematical formula: $1 + [(a - i)/i](x - 1)$, where x corresponds to the molar position. The finding that M2 accounts for roughly one-third of the total molar area reinforces the model's predictive potential. While the study involved 29 species of murine rodents, the authors proposed that the inhibitory cascade may be expected to apply across mammalian orders.

The IC model development in paleoanthropological context: testing on hominins

By linking developmental biology with precise quantitative prediction, the IC model offers a powerful framework to test macroevolutionary patterns across mammals (e.g., Billet and Bardin (2021) on placental mammals), including hominins. Evans et al. (2016) applied the model to both fossil hominins and modern humans. Rather than focusing on the standard molar triplet (M1-M2-M3), they extended the analysis to include deciduous premolars/ molars[1], based on the rationale that the principle of sequential inhibition should also be applicable outside the molar row. While it returned a positive result that the triplet "dp3-dp4-m1" (i.e., dm1-dm2-M1)[2] fit the linear IC pattern even more closely than the standard one, the approach has been criticized: the shift of

[1] The "deciduous premolars" in Evans et al. (2016) correspond to what are generally referred to as deciduous molars in hominin studies. In paleoanthropology, hominin deciduous molar 1 and 2 (dm1, dm2) are equivalent to Evans et al.'s "deciduous premolars 3 and 4" (dp3, dp4). Likewise, Evans et al.'s "m1, m2, m3" correspond to the permanent molars M1, M2, and M3 in hominin terminology

[2] As explained in Note1, the "dp3–dp4–m1" sequence in Evans et al. (2016) can be understood as dm1–dm2–M1 in standard hominin nomenclature

beginning and ending locations of study would imply a different system of cascades with different proportional dependencies from the original IC model (Roseman and Delezene, 2019). In addition, Hlusko et al. (2016:9262) argued that the study applied the IC model, originally proven on mice, "uncritically" to hominins, reducing the explanation of distinctive *Homo* dental morphology to the "simple rule" that decreased mesenchymal activation alone accounts for the proportional reduction of M3 (Hlusko et al., 2016; Evans et al., 2016).

More studies have applied the IC model to hominins since then. The results, however, have been varied. For instance, Boughner et al. (2021) tested modern humans and found that human dentition is far more variable than a signal linear pattern predicted by the IC mode, especially for the mandibular molars. Bermúdez de Castro et al. (2021) examined Middle Pleistocene hominins from Sima de los Huesos and reported that their molar proportions are largely in line with the IC model. Extending the scope further, D'Addona et al. (2024) applied the standard IC model (with triplet M1-M2-M3) on both fossil hominins and modern humans again. It was found that the model does not fit early hominins but aligns more closely with modern humans, particularly in maxillary molars. Whereas the outcome partly agrees with Evans et al. (2016), who also found that the standard IC triplet does not capture fossil hominin patterns well, it contradicts the findings of Boughner et al. (2021) on modern humans.

While the reasons leading to different results are uncertain, one possible reason is suspected to lie in the sampling strategy. Boughner et al. (2021) relied only on consecutive molars from modern human individuals, whereas Evans et al. (2016) assembled samples from consecutive teeth but also from isolated premolars and molars for all the species they analysed. Given that no single individual can simultaneously present both "dp3" (i.e., dm1 in hominins [1,2]) and M3, their data raises concerns about whether relative size during development was accurately represented. It is unclear whether D'Addona et al. (2024) used isolated molars for modern human, though a careful inspection of their supplementary materials indicate that fossil hominin data were likewise based on isolated molars.

The molar module component (MMC): a refinement?

Apart from the attempts at direct validation, some researchers have sought to move beyond the standard IC model by proposing refined frameworks. Hlusko et al. (2016) introduced two genetically patterned phenotypes: molar module component (MMC = M3 length/M1 length) and

premolar/molar module (PMM = M2 length/ P4 length). Unlike the IC model, which uses molar size defined as the computed area of the occlusal surface of the crown (mesiodistal (MD) diameter × buccolingual (BL) diameter), MMC and PMM rely solely on MD length, based on the rationale that BL width reflects systemic effects such as body size and sex, whereas MD length more directly reflects the underlying genetic patterning of relative tooth size. Hlusko et al. (2016: 9263) described that the MMC follows the IC model "but using only mesiodistal length". In this way, it preserves the IC model's ability to capture taxonomical variations while minimising pleiotropic influences brought by BL width. However, the MMC is not a direct analogue of the IC model: the IC focuses on the relationship between M2/M1 and M3/M1 ratios, whereas MMC isolates only the length ratio between M3 and M1.

The MMC was originally developed from quantitative genetic analyses of trait heritability in a pedigreed colony of baboons (Hlusko et al., 2016). As its introduction, the emphasis was on its potential to capture genetic variance across taxa, rather than on direct comparison with the IC model. Building on this foundation, Monson et al. (2022) evaluated the performance of the adjusted "IC model" (M3 size/ M1 size) and the MMC (M3MD/ M1MD) in reconstructing primate phylogeny and evolutionary history. While the results show broadly similar outcomes, Monson et al. (2022) argued that this reflects an overlap in the genetic factors influencing molar size variation between the two models, but with distinct emphases: the IC model frames variation in terms of developmental dynamics (posterior molar initiation modulated by the growth of M1), whereas the MMC captures genetic architecture underlying relative molar lengths, which appears particularly evolutionarily conserved in the mandible. Despite the modest differences between the two models found in the results, their comparative performance raises a broader question: whether size-based or length-based metrics provide a more precise proxy for capturing developmental patterns and/ or evolutionary variation.

Patterning cascade model on cusp formation

The concept of patterning cascade, i.e., the timing of sequential initiation influences the expression of dental traits, was not new when the IC model of molar size was introduced by Kavanagh et al. in 2007. Jernvall (2000) had already described a patterning cascade mechanism in seal teeth, where cusp height mirrors initiation sequence: the first cusp developed is the tallest, and subsequent cusps form later through continued epithelial folding, resulting in smaller cusps with greater variation

the later they appear. Enamel knots play a central role in this process. At the cusp level, the primary enamel knot provides positional information for tooth morphogenesis and induces a secondary enamel knot that regulates subsequent cusp growth. Salazar-Ciudad and Jernvall (2002) further emphasise that the size, shape, and position of the first-forming cusp influence those of later-forming cusps; a small change early in the development of the tooth germ can result in large differences in the fully formed tooth crown, including the number of cusps.

Studies of hominoids confirm the patterning cascade model. Skinner and Gunz (2010) examined cusp 6 at the enamel–dentine junction (EDJ) of chimpanzee molars and found the presence of cusp 6 consistent with the patterning cascade model: larger molars show higher cusp 6 frequency because increased tooth germ size reduces inhibition. Further to this perspective, Davies et al. (2021) analysed accessory cusps (i.e., cusp 6 and cusp 7) at the EDJ of hominins and concluded that they are not individually patterned nor genetically determined, but instead emerge following the patterning cascade model: dependent on the shape of the crown, size and the space of the primary cusps, and that of earlier forming accessory cusps.

Whereas accessory cusps arise from secondary enamel knots forming outside the inhibition zones of earlier cusps, the main cusps, especially the first cusp (i.e. the protoconid), follow a different trajectory. Governed by the molecular control of the primary enamel knot, the protoconid forms stably and consistently across molars. Bermúdez de Castro et al. (2022) measured protoconid size and crown size in modern humans and discovered that the absolute size remains stable across the row. As the molar size of modern humans decreases from M1 to M3, the relative size of the protoconid increases inversely. Since the test was only conducted on modern humans, it is uncertain whether this pattern holds for other hominin species with different molar size sequences across evolutionary history.

Research objectives

From the literature, it seems that the inhibitory cascade model is a developmental mechanism that determines the size of molars. Yet, as Hlusko et al. (2016) doubted, the balance between activator and inhibitor signals might not fully explain the complexity of dental morphology expressed by size. Evidence from cusp formation shows that cusp morphology is not determined by the cascade effect alone, but also by space availability. While these interactions shape cusps' expression, their influence on molar size is less certain.

In addition, comparative studies highlighted the differences in molar morphology between jaw types - for instance, Boughner et al. (2021) found mandibular molars with higher variability, and Monson et al. (2022) found mandibular MMC more conserved - raising the question of whether molar size and developmental dynamics differ between the mandible and maxilla. At a broader evolutionary scale, developmental outcomes also represent the translation of genotype into phenotype. While Hlusko et al. (2016) and Monson et al. (2022) argued that molar length, as a phenotype, may better reflect heritable genetic patterns, it remains unclear which metric is more effective in capturing patterns from the developmental process of molars in hominins.

Taken together, these issues converge on the central research question of this study: how is hominin molar size determined by the cascading developmental mechanisms? By analysing size as the development outcome, this study attempts to identify the factors that govern molar morphology across different organization levels, from cusp size to molar size, including in relation to the jaws.

To address this research question, this study follows five lines of analysis: **(1)** testing whether hominin molar morphologies follow the IC model, by applying the framework used in previous analyses to both consecutive molars (which capture relative size within the molar row) and isolated molars (as a comparison); **(2)** comparing molar size (i.e. area) and length (i.e. MD diameter) as alternative proxies to identify which of them more effectively reflects the underlying developmental pattern; **(3)** assessing how the availability of space in the jaw influences molar growth and size; **(4)** comparing molar development between the mandible and maxilla to evaluate the role of jaw type in determining molar size; **(5)** investigating cusps development under patterning cascade model, by quantifying its influence on the size (instead of just presence/ absence) of both main (protoconid) and accessory cusps (cusp 6 and cusp 7) across hominin species.

MATERIALS AND METHODS

Data collection

The analyses of the study were based on three types of data: 1) dental metrics, i.e., the mesiodistal (MD) and buccolingual (BL) diameters of the crown of molar, 2) the size of the cusps on the occlusal surface of molars, and 3) the width of the mandibular corpus. While dental metrics data and mandibular corpus data were collected from literature, cusp size data consists of both literary

data and my own measurements. Since this study focuses on the developmental mechanism of molars, i.e. a continuous developmental sequence where each molar influences the size of the next through activator and inhibitor signals, it is essential to study the full sequence of permanent molars (M1, M2, and M3) rather than just M1 and M2. While M3 generally erupts in adulthood (e.g. modern humans at their 18-20 years (Hillson, 2014); *Paranthropus robustus* between 11 and 14 years of age (Dean et al., 2020)), long after deciduous teeth are replaced, there is no temporal overlap between M3 and deciduous teeth. Not only the different trajectories would make it difficult to study both at the same time, the differences in sizes between deciduous teeth and the permanent teeth might not be comparable. For higher data consistency and availability, this study used exclusively permanent molars for analyses.

i. Dental metric data

The dataset was built on an extensive compilation of data from the literature (Appendix I). Metric data of mandibular and maxillary molars were recorded separately. When measurements on both left and right sides are available for the same specimen, to ensure standardised representation across individuals and to avoid disproportionate weighting from bilateral data, the mean value of both sides was used. This methodological choice is based on the rationale that proportions of the right and left sides of bilateral structures have the same genetic blueprint (Palmer & Strobeck, 1992). It is also justified by the fact that the sample sizes would have been very limited if data from both antimeric sides, or either the left or right side exclusively, were strictly required. To address the focus of this study on molar row development, data collection aimed to include three consecutive molars whenever preservation permitted; if one side preserved two molars and the other a non-overlapping third, data from both sides were combined to reconstruct a complete "composite" molar row. When measurement data for the same specimen were available from multiple sources but showed inconsistencies, preferences were given to the source that: 1) included more complete dental metrics (e.g., both MD and BL dimensions for a given molar); 2) applied correction for interproximal wear, as the original crown dimensions is prioritized over measurements affected by interproximal wear; and 3) in the few remaining cases not resolved by criteria (1) and (2), where the metric data from different sources were non-overlapping, data were combined across sources to form a single molar row, in line with the data collection strategy for maximizing the availability of complete sequences of three consecutive molars for analyses.

The analyses of this study were mainly conducted on the size of molars (i.e., computed occlusal area of the crown), which is defined as the mesiodistal length of the tooth multiplied by the mesial buccolingual width (area = MD x BL), where applicable. Counting molars whose size can be calculated (i.e. with both MD and BL diameters), the total sample sizes of this study are as follows: for mandibular molars, there was a total of 1,514 measured molars, including 831 consecutive molars, thus corresponding to n=277 complete individuals for M1 to M3; for maxillary molars, there were 1,615 measured molars in total, with 885 consecutive molars corresponding to n=295 complete individuals (M1-M3).

The hominin taxa, or Operational Taxonomic Units (OTUs), represented in this sample is inclusive of almost all species of fossil hominins, spans a wide chronological range (from Pliocene to Holocene), and a wide geographical range (Africa, Europe and Asia), aiming to reflect the diversity of hominin taxa throughout their evolutionary history as accurately as possible. Table 1 shows the counts of complete individuals (M1-M3) and of each molar distributed by OTUs.

Table 1. Sample counts by OTUs - (ranked by their first appearance datum (FAD))

- *molar sizes (Column "M1-M3" corresponds to the number of consecutive molar series; individual molar columns "M1", "M2" and "M3" refer to the number of isolated molars)*

	Mandible				**Maxilla**			
Operational Taxonomic Units (OTUs)	M1-M3	M1	M2	M3	M1-M3	M1	M2	M3
Sahelanthropus tchadensis		1		1			1	2
Orrorin tugenensis		1	1	1				2
Ardipithecus kadabba							1	1
Ardipithecus ramidus	2							
Australopithecus anamensis		1	2	2		3	3	4
Australopithecus afarensis	9	13	13	9	5	7	6	4
Australopithecus deyiremeda	1							
Australopithecus africanus	14	23	26	24	5	19	17	21
Paranthropus boisei sensu lato	6	10	6	19	3	6	5	1
Homo habilis sensu lato	6	12	7	13	8	10	3	4
Paranthropus robustus	8	28	20	26	9	36	26	27
Australopithecus sediba	2				1			1
Homo ergaster	4	11	6	3	2	6	4	2
Homo georgicus	3				2	1	1	
Homo erectus	4	8	14	7	3	10	4	1
Early Pleistocene China						1	2	1
Homo mauritanicus	5					1		
Homo antecessor	1	2	3	1		3	1	

Early *Homo floresiensis*		1						
Homo heidelbergensis	5	2	4	3	2	1	2	
Homo pekinensis	5	14	12	6	2	8	7	5
Early *Homo neanderthalensis*	19	15	14	14	12	12	13	16
Middle Pleistocene Levant			2	1			1	1
Homo rhodesiensis		1	1		1			
Middle Pleistocene Asia		3	4	2	2	6	4	3
Early *Homo sapiens*	9	13	9	9	7	25	16	7
Homo naledi	2	9	9	4	1	11	12	6
Homo neanderthalensis	18	27	28	21	18	24	34	20
Homo floresiensis	2					1	1	
Homo luzonensis					1			1
Homo sapiens	152	57	64	20	211	119	108	18
Total	277	252	245	186	295	310	272	148

The OTUs used here were initially defined in the frame of the PhD thesis of Pierre Gousset for the purpose of phylogenetic analyses. While most of them are widely used species, 6 worth mention: 3 of them are chronological OTUs widely used in the paleoanthropological literature (Early *Homo floresiensis*, Early *Homo neanderthalensis* and Early *Homo sapiens*). Keeping in mind that they were defined for phylogenetic analyses, they were defined as such to avoid long-branch attraction, as it has been shown that adding taxa may solve this issue (Wiens, 2005). 3 other OTUs are "paleo-demes" that have been argued to be identifiable based on anatomy but also well constrained in time and space. However, none of them received a clear taxonomical attribution, thus explaining why they are named after their chronological and geographical distribution (see Liu et al., 2022 for Middle Pleistocene Asia and Hershkovitz et al., 2021 for Middle Pleistocene Levant). While "Early Pleistocene China" are traditionally included in the *Homo erectus* hypodigm, they cannot be linked with high confidence to any of the "sub-groups" of *Homo erectus* used in this work (e.g. Xing et al., 2021; Pan et al., 2022).

ii. Cusps sizes

Areas of protoconid, cusp 6 and cusp 7 are used to study the possible relationships between the respective sizes of these cusps and of the total crown area. Data for protoconid were taken from the literature by Wood (1991) and Noerwidi (2020), and partly from my measurements, while that of cusp 6 and cusp 7 were partly collected from Wood (1991) and partly measured by myself The total sample collected for cusp size analysis corresponds to 148 molars for protoconid, 68 molars for cusp 6, and 38 molars for cusp 7 (Table 2). It includes hominin species which show different

patterns of relative molar sizes (for example, M1<M2<M3 or M1<M2>M3), to investigate whether the mechanisms of cusp development are consistent across species regardless of molar size pattern or whether they have evolved.

Regarding data selection to standardise sample representation, mean values were used only when both antimeric molars of a specimen exhibited symmetrical traits. However, cusp numbers and the presence of accessory cusps on antimeric teeth of a single individual are not always symmetrical, and data availability is often constrained by the degree of occlusal wear. Therefore, when selecting between left and right molars, two major criteria were taken into account:

1) Greater internal consistency within individuals. For instance, in the case of OH16, data were available for both the left (LLM3) and right (LRM3) lower third molars. While both exhibited six cusps in total, LRM3 possessed a cusp 7 (i.e. 5 main cusps + 1 cusp 7), whereas LLM3 had a cusp 6 (i.e. 5 main cusps + 1 cusp 6). The morphological differences make it inappropriate to average the two sides. We therefore considered the presence of, and/or data availability for, the other molars on both sides. For OH16, data for M1 and M2 were available only for the right side, so the LRM3 was selected to have a complete M1-M3 dataset corresponding to molars from the same side. The same criteria were applied to SK55b, whose M1s on both sides exhibited seven cusps. However, the data source did not include information on the presence or size of cusp 7 on the right, nor cusp 6 on the left. The right M1 was selected considering that there was also data available for the right M2. Whenever applicable, the same approach was applied to my measurements made on dental casts, with measurements taken from the side where morphological traits were present or more identifiable: for the Montmaurin Mandible, only the protoconid sizes of left M1-M3 were selected because the occlusal surface of right M1 and M2 are worn and the boundary between the major cusps are unclear.

2) Data completeness. When criterion 1) was not applicable for a particular specimen, the side for which a maximum of information is available was selected. For example, Taung 1 only had its first permanent molars: the right M1 exhibited seven cusps, but information on the presence and size of cusp 6 was missing. In contrast, the left M1 had six cusps, with measurements available for all of them. Given its completeness in terms of available data, the left M1 was selected. For our own measurements made on dental casts, priority was given to the side where the molars exhibited clearer occlusal surfaces, allowing for more detailed information to be obtained.

Table 2. Sample counts by OTUs - Cusp sizes and mandibular width

	Protoconid			Cusp 6			Cusp 7			Mandibular corpus width at M1
OTUs	M1	M2	M3	M1	M2	M3	M1	M2	M3	/
Orrorin tugenensis	1									
Australopithecus afarensis						1		1	1	9
Australopithecus africanus	6	5	7	1	4	5		2	5	5
Paranthropus boisei sensu lato	7	6	6	5	5	4		1		5
Homo habilis sensu lato	5	6	11		2	7	2	3	4	6
Paranthropus robustus	15	12	11	9	9	2	1		1	3
Homo ergaster	6	7	6		1	4	2	2	1	4
Homo georgicus					1	1	1	1	1	
Homo erectus	4	5	7		1	1	1	1		2
Homo mauritanicus					1	1			1	3
Homo heidelbergensis	1	1	1			1				4
Homo pekinensis				1			1			
Early *Homo neanderthalensis*	1	1	1			1				14
Early *Homo sapiens*	1	2	2				1			3
Homo neanderthalensis	1	1	2					1	3	18
Homo sapiens										4
Total	48	46	54	16	24	28	9	12	17	80

Our own cusp measurements were made on 1) good quality casts that were selected from the collections of the Muséum national d'Histoire naturelle (MNHN) stored at the Musée de l'Homme, and 2) 3D models of the individual molars (see Appendix II for the list of specimens).

a. Photographs of dental casts

Standardised high-resolution photographs of the occlusal surfaces of molars on the casts were taken using a reprographic stand. The molars on the mandibles (or mandibular fragments) were positioned so that the occlusal planes were perpendicular to the optical axis of the camera. The camera was mounted on the platform of the adjustable cross-arm attached to the vertical column to ensure a consistent distance and orthogonal angle relative to the occlusal surface.

In each occlusal photograph, a millimetre scale was included and parallelly placed at the same height as the occlusal surface for calibration. The photos were calibrated and measured by using

the ImageJ software program. Calibration was accomplished using the program's set scale function with the millimetre scale provided on each image.

b. Snapshots of 3D models

3D models of each individual molar were loaded into Avizo. The projection was set to Orthographic mode to avoid distortion of the depth and scale. The model was rotated manually to orient the occlusal surface facing directly up in the view. Best effort was made to achieve a symmetrical view of the molar crown in view without visible buccal or lingual tilt. Snapshots were loaded into ImageJ and calibrated by the program. However, rather than placing a physical scale next to the occlusal plane as in the photographs of dental casts, calibration was performed using the documented mesiodistal diameter from the literature. The mesiodistal diameter was defined following the protocol of Wood and Abbott (1983), as the maximum distance between the mesial and distal crown borders, measured parallel to the longitudinal axis of the crown. After the scale was set on the snapshot using this reference, a buccolingual measurement—defined as the maximum distance between the buccal and lingual crown borders at a right angle to the longitudinal axis, following Wood and Abbott (1983)—was taken for verification. If the resulting BL measurement closely matched the corresponding published value (within a tolerance of one decimal place), the calibration was considered suitable for further cusp measurements.

c. Cusp measurement

Measurement was taken by using the freehand line tool of the ImageJ program. Multiple attempts were made for each measurement, and the mean value of the two closest attempts was used to calculate the cusp size. The overall intra-observer measurement error between the two closest attempts is approximately 0.4%.

Following the protocol of Wood et al. (1983), the base areas of each individual cusp were demarcated by tracing the course of the primary fissures separating the principal cusps. When a fissure did not extend to the outer crown margin, its course was projected by following the direction of the fissure before it became attenuated (Bailey et al., 2004). Using the protocol of Wood and Engleman (1988), in case the tooth possessed additional cusps, the primary fissure was extended to the crown base margin and the appropriate proportions of the area of the additional cusps were added to the areas of the adjacent main cusps.

To assess the comparability of measurements obtained from 3D models to those of traditional dental casts, we compared results from the measurements of the lower right M3 (LRM3) of the Montmaurin Mandible, for which both cast photographs (Fig. 1a) and 3D model snapshots were obtained and measured on ImageJ following the same protocol. In addition to the snapshot of the occlusal surface taken from a direct superior view, additional images were captured with a slight oblique angle toward the right and left sides respectively. In this preliminary test, the size measurements obtained from the 3D model snapshot taken from a direct superior view (Fig. 1b) was approximately 8% smaller than the corresponding measurement from the photograph of the dental cast. When the orientation was adjusted to a slightly oblique leftward angle (Fig. 1c) the discrepancy widened to nearly 20% smaller than that of the cast. In contrast, the snapshot taken from a slightly oblique rightward angle (Fig. 1d) produced a different outcome: due to the position of cusp 6—located on the left side of the occlusal basin and sloping downward toward the center, the altered perspective visually flattened the cusp's profile, resulting in an overestimation in size. The measurement was approximately 5% larger than that of the dental cast photograph.

1(a) Dental cast- Superior view	1(b) 3D model- Superior view	1(c) 3D model- Superior view oblique leftward	1(d) 3D model- Superior view oblique rightward
	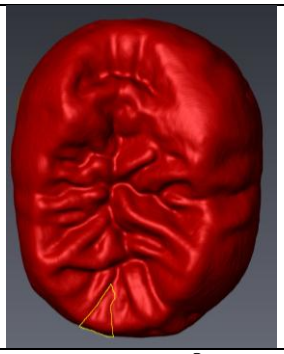	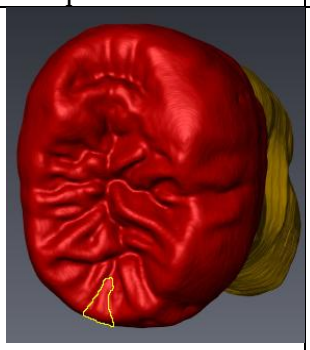	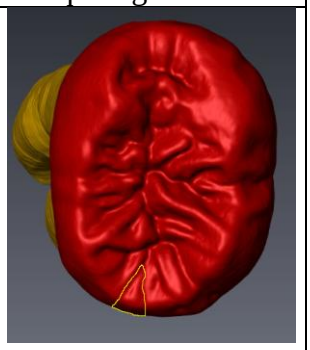
Size: 1.65 mm^2	Size: 1.52 mm^2 *versus* 1(a): -8%	Size: 1.34 mm^2 *versus* 1(a): -19%	Size: 1.74 mm^2 *versus* 1(a): +5%

Figure 1. Measurement comparison between the cast and the 3D model of the Montmaurin Mandible LRM3

While the intentionally adjusted orientations explain the discrepancy between Fig. 1c and Fig.1d from Fig. 1a, there are also obvious differences between the sizes measured in Fig. 1a and Fig. 1b. From the figures, the shapes of cusp 6 are different between Fig. 1a and Fig. 1b, while the former shows a clear curve on the right boundary, that on Fig. 1b shows a relatively straight boundary with just slight convexity. It might be partly due to the orientation differences despite our efforts

in capturing the most precise angle perpendicular to the camera/screen. However, from Fig. 1c and Fig. 1d, it is shown that even with a steepened or flattened slope of cusp surface, the right-side boundaries of cusp 6 on the 3D model are also straight, implying the orientations might not be the only factor to explain the variance. It is suspected that the visual effects caused by the various shades on the dental cast might affect the observer's judgement when defining the cusp boundary, or contrarily, the outline / convexity characteristic on the right side of cusp 6 on the monochromatic 3D models was not presented as pronouncedly as it does on the dental cast.

Despite observable discrepancies, the sole sample in this test makes it unable to draw a concrete conclusion about the causes of discrepancies, nor determine the better material reference (dental casts or 3D models) to perform cusps measurements However, given that the discrepancy between Fig. 1a and Fig. 1b remained within 10%, no further corrections were applied to the measurements obtained from 3D snapshots using ImageJ.

iii. Width of mandibular corpus

To investigate the possible relationship between space and size, i.e., whether "available space" in the dental arch determines the size of molars when they grow, we collected data on the width measurements of the mandibular corpus documented in the literature by Wood (1991), Richards et al. (2024) and Villmoare et al. (2015). The width of the mandible was used as the parameter to estimating space instead of one of the possible lengths, because 1) measurements such as total mandibular length or alveolar length include additional anatomical elements and/or particularities (e.g. ramus, incisors/ canines/ premolars or retromolar spaces), 2) even among mandibles with three consecutive molars preserved, very few of them are complete enough to allow reliable measurement of length, and 3) the total length of the molar row (M1–M3) itself would obviously be redundant given that we are comparing with molar sizes here.

The mandibular corpus width measured at the midpoint of M1 was collected to assess the relationship between M1 size and the space available for subsequent molar development. M1 was chosen as the focus because it is the first molar to form and emits inhibitory signals that limit the growth of later-developing molars (Kavanagh et al., 2007). This implies that within the molar row, M1 is the only molar that is not affected by inhibitory signals when it grows.

Following the same principle mentioned in (i), in case the mandibular width at M1 of both antimeric sides of one individual is available, the mean value of both sides was used for analysis. In total, measurements of mandibular width are available for n=80 individuals, covering 13 hominin OTUs belonging to 3 different genera (Table 2).

Statistical analyses

Reduced major axis (RMA) and Phylogenetic RMA (PRMA) regressions

Relationships between molar size, length and ratio —such as M2/M1 *versus* M3/M1, and M3MD *versus* M1MD—were analysed using reduced major axis (RMA) and phylogenetic reduced major axis (PRMA) regression with the R package *phytools* (Revell, 2024). RMA is appropriate when neither variable is dependent on the other because it treats both variables symmetrically (Clarke, 1980). This approach was adopted following the statistical framework used by Kavanagh et al. (2007) to investigate the relationship between M2/M1 and M3/M1 ratios (i.e., the inhibitory cascade model). To replicate their analysis with our hominin sample, the original RMA regression was followed, with extension of phylogenetic reduced major axis (PRMA), which integrates phylogenetic relationship to account for non-independence among species due to shared evolutionary history (Felsenstein, 1985).

PRMA results were computed using Pagel's lambda (λ), estimated by maximum likelihood of the observed data given different model coefficients (Pagel's λ not fixed), with a fixed Pagel's $\lambda = 1$ applied in supplementary cases. Pagel's λ is a scaling parameter that rescales the off-diagonal elements of the phylogenetic variance–covariance matrix, thereby quantifying the extent to which shared evolutionary history contributes to traits covariation among species under a Brownian motion model of evolution (Pearse et al., 2025). Typically, λ ranges between 0 (no phylogenetic correlation between species) and 1 (correlation between species corresponds to the Brownian expectation) (Pearse et al., 2025; Revell, 2012). The primary analyses presented in this report are based on λ values estimated by maximum likelihood, representing the best fit to the observed data given model parameters.

It should be noted that the optimised λ value in PRMA models is estimated using model residuals and is not an index of phylogenetic signal of the measured traits (Pearse et al., 2025; Revell, 2010): a λ value of 0 indicates no phylogenetic dependence in the residuals, even if the traits themselves

exhibit phylogenetic signal. A λ value approaching 1, on the contrary, suggests that the residuals covariation closely follows a Brownian motion model of trait evolution (Revell, 2010).

Since RMA (and PRMA) describes a symmetrical relationship between two observed variables (Clarke, 1980), there are no distinct independent and dependent variables in the regression. Under this context, R^2 no longer quantifies the proportion of variance in the dependent variable that is explained by the independent variable. Instead, R^2 is simply the square of the sample correlation coefficient (R) that reflects the strength of the linear relationship between *x* and *y* (Clarke, 1980). R^2 in RMA/PRMA calculated in *phytools* (Revell, 2024) is therefore linked to the statistical properties of the slope: a larger R^2 value means the data points cluster more tightly around the fitted line, representing a stronger and reliable slope estimate.

It is also noteworthy that the null hypothesis of 0.0 is not allowed in PRMA computation in *phytools* (Revell, 2024). It defaults to 1.0 with a null hypothesis that the phylogenetically corrected RMA slope equals 1, meaning that the scaling relationship between the two traits is consistent with isometry.

Ordinary least squares (OLS) and Phylogenetic generalised least squares (PGLS) regressions

For asymmetric variable pairs with an assumed predictive relationship, where one variable is considered dependent and the other independent, ordinary least squares (OLS) regression was used to quantify the influence of the independent variable on the dependent variable. A common application of this approach is the study of allometry, where regression slopes describe how a trait scales relative to overall body size (Huxley, 1932). In the analyses of this report, overall size refers to total molar size (i.e., the combined crown area of M1, M2 and M3).

To study allometric relationships, the size data, including the size of individual molars and the total molar size, were transformed by logarithm and scaled on log-log scatter plots with log(trait size) on the y-axis against log(overall size) on the x-axis, following the equation proposed by Huxley (1924b). The resulting slope line that fits through the points describes the allometric scaling of the structure (Kilmer and Rodríguez, 2017). Least squares regression is commonly used for describing allometric scaling (over the other linear regression models) because the slope is

sensitive to the changes in the steepness of the relationship without changing the scatter (Kilmer and Rodríguez, 2017).

Phylogenetic generalised least squares (PGLS) were also applied following the same rationale as for PRMA: to account for the non-independence of species due to their common history. PGLS models were fitted using maximum likelihood estimation, additionally run with a fixed phylogenetic signal ($\lambda = 1$) consistent with the PRMA analyses. Both OLS and PGLS regressions were computed using the R package *nlme* (Pinheiro et al., 2025).

Since the *nlme* package does not calculate the coefficient of determination (R^2) for OLS and PGLS models, the R^2 was additionally computed using the R package *rr2* (Ives, 2018), mainly with the *R2_pred* metric. *R2_pred*, where "pred" stands for prediction, is based on the variance in the difference between observed and predicted data, with prediction in PGLS computed by removing each data point from the dataset and estimating it from the predictor variables and the remaining data points (Ives, 2019). This approach "gives the most direct answer" to the question of how much variance in the data is explained by a model (Ives, 2019:2). In other words, it measures how well the model, including its specified covariance structures such as phylogenetic signal, predicts the observed data. A high R^2 calculated by *R2_pred* in PGLS, therefore, indicates that the model's predictions align closely with the observed values, signifying strong explanatory power of the entire model.

Phylogenetic signal: Blomberg's K

The function *phylosig* of the R package *phytools* (Revell, 2012) was used to calculate phylogenetic signal (i.e., the tendency of related species to resemble one another) by Blomberg's K statistics. The K-value is a variance ratio that scales the observed phylogenetic signal in data against the signal that would be expected if the trait evolved purely under a Brownian motion model along the phylogenetic tree (Blomberg et al., 2003). A $K > 1$ implies that close relatives are more similar than expected under Brownian motion evolution. While $K = 1$ indicates that the trait exhibits exactly the amount of phylogenetic signal expected under Brownian motion evolution along the specified tree, $K < 1$ means that the relatives resemble each other less than expected (Blomberg et al., 2003).

Visualisation

To visualise regression patterns within a phylogenetic framework, we used the *phylomorphospace* function from the *phytools* package (Revell, 2024) to project a phylogeny into the morphospace, based on the selected trait pairs from PGLS regression.

We used the *contMap* function from the *phytools* package (Revell, 2024) to visualise the distribution of continuous trait values by mapping them onto the branches of the phylogenetic tree with a colour gradient.

Phylogenetic tree

Tree typology is developed based on the phylogenetic tree used by D'Addona et al. (2024), which was previously obtained by Rocatti and Perez (2019) using molecular and craniodental data from fossil and extant hominins based on the initial work of Dembo et al. (2016). Node ages and first appearance datums (FADs) of species were referenced from Mongle et al. (2022) to calculate branch lengths. However, due to differences in tree topology—for example, the finer taxonomic resolution in our tree, such as the subdivision of *Homo sapiens* into Early *Homo sapiens* and recent *Homo sapiens*—some nodes in our phylogeny did not have corresponding node ages documented in Mongle et al. (2022). When a node age was unknown but bounded by two known ages, the temporal interval between them was divided by the number of branches between the two nodes; for example, the interval would be divided by three in a clade with three branches between the two known ages. The resulting prorated interval was then added to the more recent node age to estimate the timing of the preceding divergence, thereby inferring the older node age. The phylogenetic tree was written and manipulated by the R package *ape* (Paradis, 2024).

RESULT

A deconstruction of the IC model: relationships between molar size, length and ratio

The principal component analysis (PCA) result in Fig.2 summarises the relationship among all the variables measured at the molar level. Most variables— all the absolute measurement variables including size, MD, BL of each molar, total molar size and length, along with a pair of M2/M1 size and MD ratios—cluster strongly along Dimension 1 (Dim 1), which alone accounts for over 70% of the total variance. Dimension 2 (Dim 2), on the other hand, primarily captures variation in molar ratios, especially those involving M3, i.e. M3/M2 (M3.M2 and M3MD.M2MD in Fig.2), and M3/M1 (M3.M1 and M3MD.M1MD). While M2/M1 ratios fall within the main cluster

aligned with Dim 1, the distinct positions of M3/M2 and M3/M1 ratios suggest they may vary more independently from the rest. Notably, the M3/M2 ratios lie closest to Dim 2, whereas the M3/M1 ratios are positioned between Dim 1 and 2. This pattern likely reflects that part of the M3 developmental trajectory is independent of the other molars. Besides, in Fig. 2, the absolute measurements of M3 itself (size, MD, and BL) are oriented toward the positive end of Dim 1 but are slightly separated from the tightly clustered M1 and M2 variables, which are concentrated below the horizontal axis. The spatial distribution reinforces that M3 may vary, to some extent, independently of the more tightly correlated patterns seen in M1 and M2.

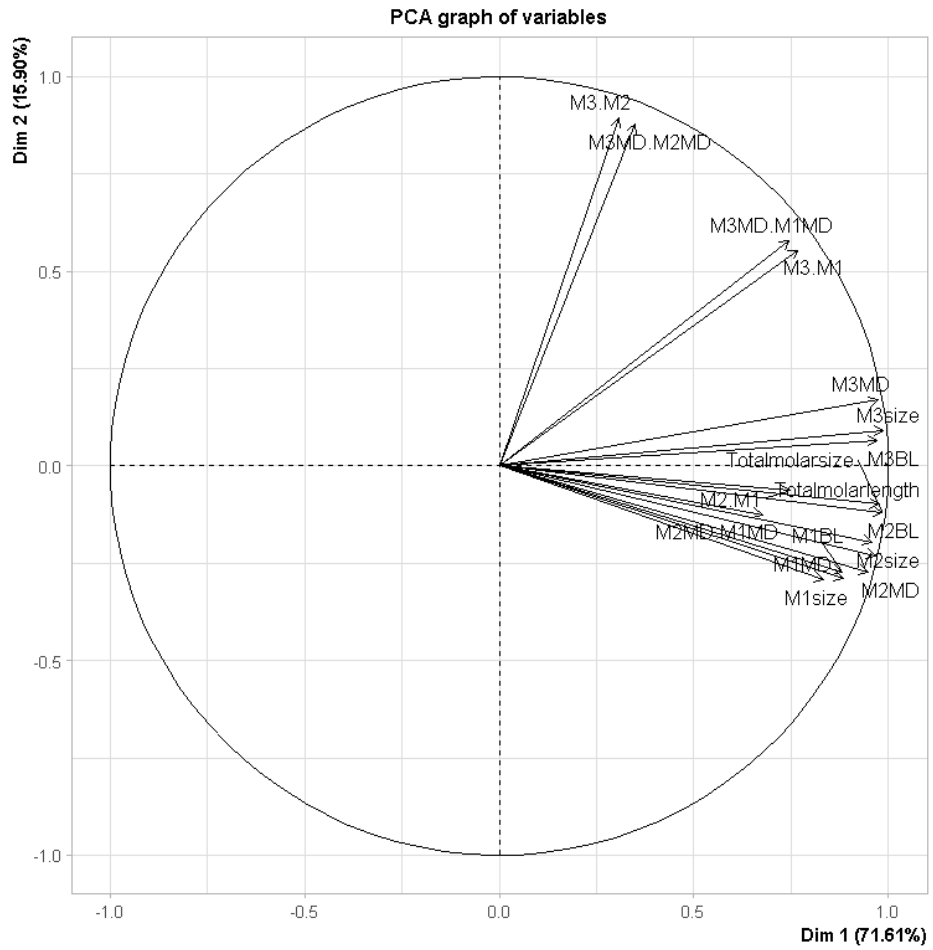

Figure 2. Principal component analysis of all molar metrics and proportion variables

including absolute size and length measures (e.g. "M1size"=absolute crown size of M1, "M1MD"= absolute mesiodistal length of M1), ratio between molars (e.g. "M2.M1"=ratio of M2 size/ M1 size; "M2MD/M1MD"=ratio of M2 length/ M1 length), and total molars series metrics ("Totalmolarsize"= M1 size+M2 size+M3 size; "Totalmolarlength"=M1 length+M2 length+M3 length).

This observation aligns with Kavanagh et al. (2007: 430)'s analogy of the inhibitory cascade model as a "ratchet": molars are initiated sequentially through the interaction between activators and inhibitors, with M3 forming last. Its development is influenced by inhibition from M2, which in turn is influenced by M1. As a result, the development of M3 relative to M2 or M1 may follow a less direct or less tightly coupled trajectory than the other molars. This helps explain the differing positions of M3/M1 and M3/M2 ratios in the PCA. The M3/M2 ratios reflect the relationship between the second and the third molars, i.e. the last two to be initiated, and are therefore less integrated with the other variables. In contrast, the M3/M1 ratios link the third molar to the first-initiated molar (M1), which likely contributes to their closer alignment with Dim 1. The M2/M1 ratios, involving the first two molars, cluster tightly with the majority of size and length variables and appear orthogonal to M3/M2 ratios in PCA. This pattern is further supported by pairwise scatterplots (Appendix III), where M2/M1 and M3/M2 show a weak correlation and lack clear clustering among individuals.

It is also noteworthy that, for each molar combination in Fig.2, the size and MD ratios consistently cluster together in the PCA, suggesting they may be shaped by a shared underlying mechanism. Although Monson et al. (2022) highlighted a fundamental distinction between the IC model and MMC, framing the IC as a rather hypothetical developmental mechanism and MMC as an inherited anatomical structure, they also acknowledged that both models capture overlapping genetic influences on molar variation. While IC is based on molar size ratios and MMC on MD length ratios, the PCA result showing that size and length tend to vary together aligns with their suggestion about the relationship between molar size and length.

Test 1: The application of the IC model on hominins

The verification of the IC model's application to our hominin sample is based on two main criteria: (1) the slope and intercept value under RMA/ PRMA regression match those defined by Kavanagh et al. (2007), i.e. slope= 2 and intercept=-1; (2) the size of M2 makes up roughly one-third of total molar area (Kavanagh et al., 2007).

(1) Reduced major axis (RMA)/ Phylogenetic RMA (PRMA) regressions
    a. Scenario 1: Lower consecutive (LC) molars

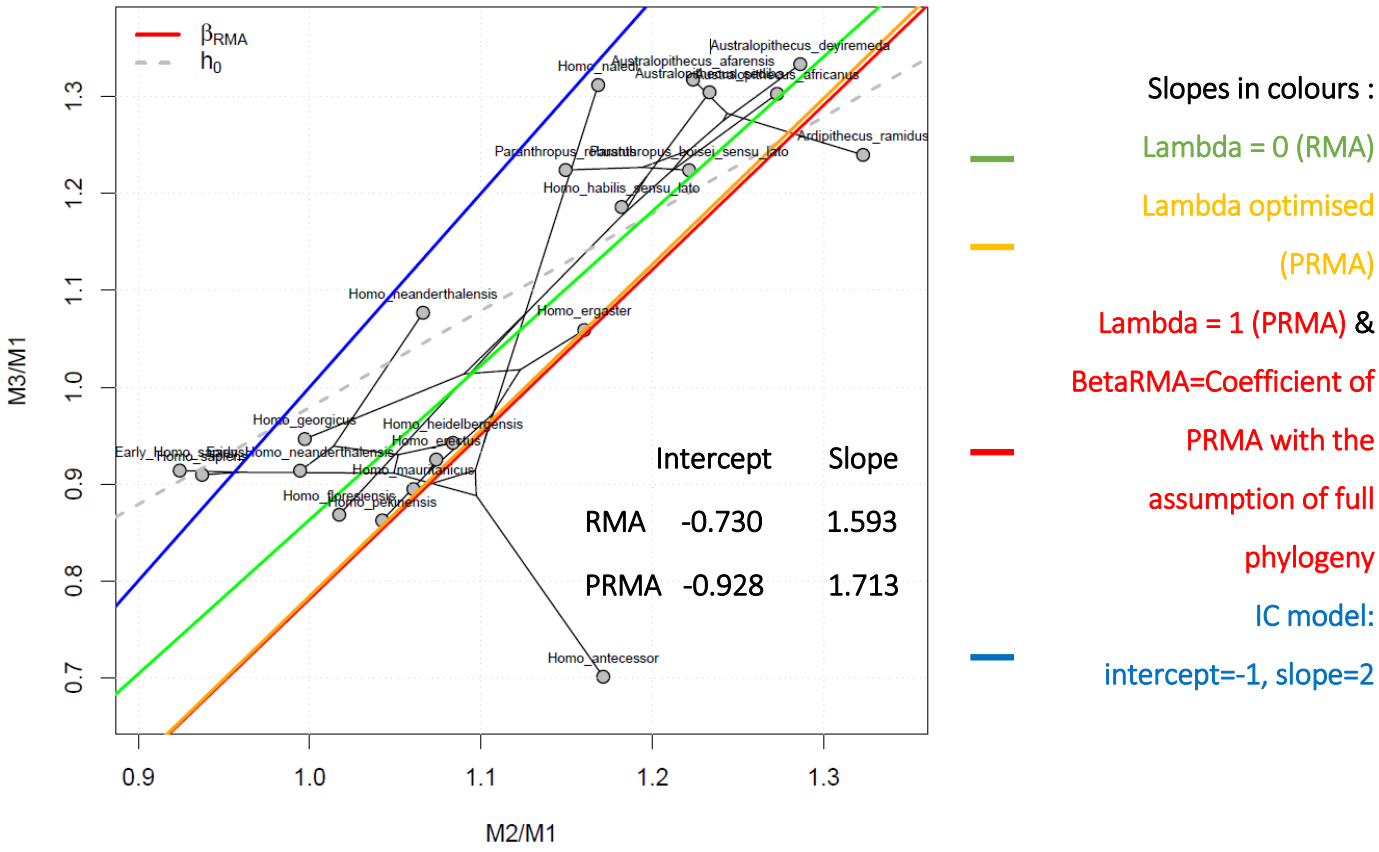

Figure 3. RMA/PRMA regression on consecutive mandibular molars (Scenario 1)

For consecutive lower molars, the RMA regression produced a slightly higher intercept (-0.730) and a lower slope (1.593) compared to the original IC model. When accounting for phylogenetic relationships, the PRMA regression yielded a lower intercept (-0.928) and a slightly higher slope (1.713). Billet and Bardin (2021) applied the IC model to placental mammalian species and reported that the intercept ranges from -1.239 to -0.433, and the slope values from 1.025 to 1.881. Some of them diverged markedly from the reference IC slope and appeared nearly perpendicular to it. In Fig. 3, the RMA slope (green line) and PRMA slope (orange line) remain broadly parallel to that of the IC model (blue line) despite the differences in regression values. This suggests that the molar size ratios follow a similar scaling pattern, though shifted along the y-axis. While the y-axis corresponds to the M3/M1 ratio, the higher intercept value of PRMA implies that, on average, hominins' mandibles have a slightly higher M3/M1 ratio for a given M2/M1 ratio, suggesting relatively larger M3 in relation to the M1 compared to that of murine rodents (the sample IC model based on).

The distribution of OTUs in the morphospace in Fig. 3 is primarily aligned along the RMA (green) and PRMA (orange) slopes. The upper portion of the slope is occupied mainly by earlier taxa, particularly *Australopithecus* and *Paranthropus*, which exhibit relatively large M2/M1 ratios and even larger M3/M1 ratios. OTUs of *Homo*, whose molar size is smaller, are concentrated in the mid-to-lower portion of the slope, corresponding to lower M2/M1 and M3/M1 ratios. One notable outlier is *H. antecessor*, which displays a high M2/M1 ratio but a comparatively low M3/M1 ratio.

b. Scenario 2: Lower isolated (LI) molars

We tested the same hypothesis using isolated lower molars, following the approaches of Evans et al. (2006) and D'Addona et al. (2024), as a comparison of the results obtained on consecutive molars.

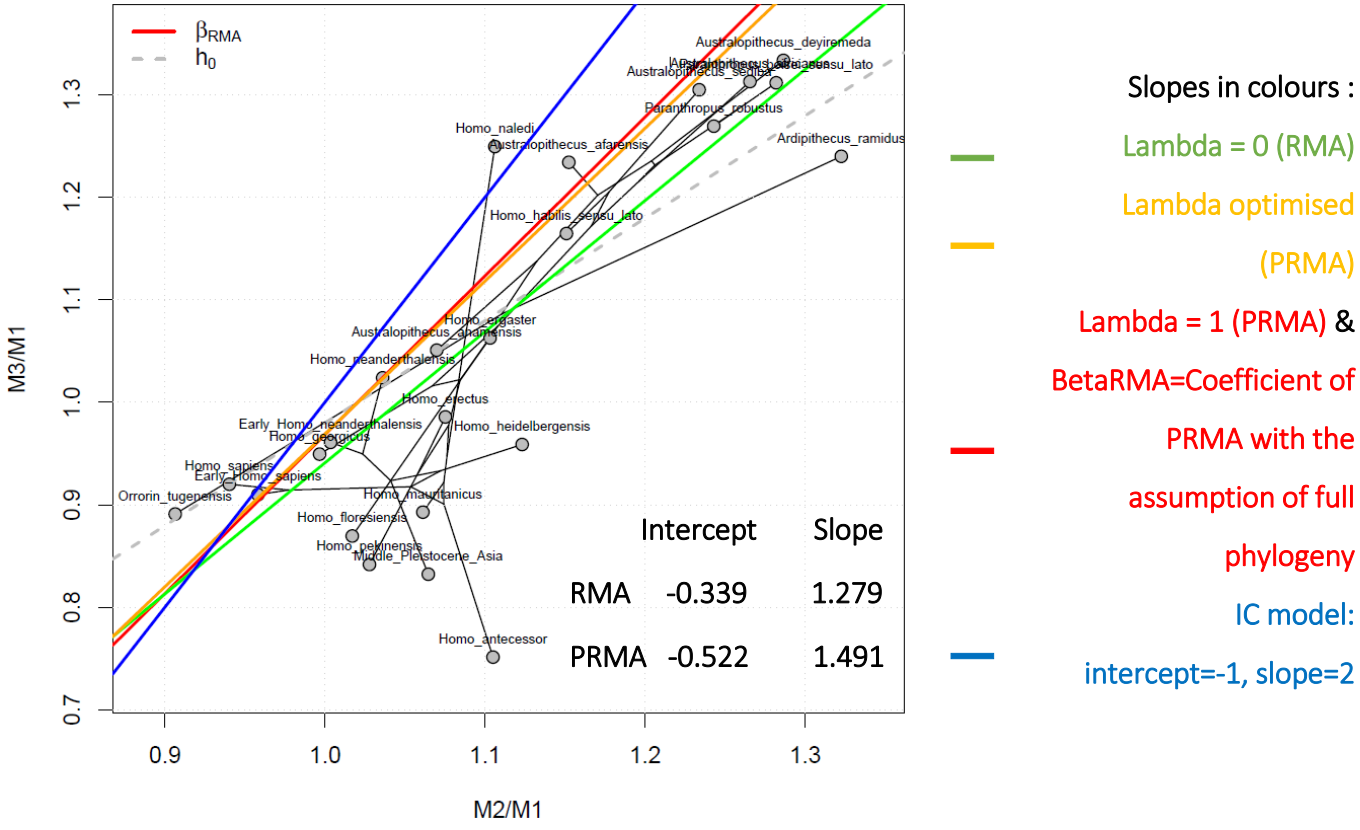

Figure 4. RMA/PRMA regression on isolated mandibular molars (Scenario 2)

The regression result for Scenario 2 (Fig. 4) yielded a higher intercept and lower slope than those observed in Fig. 3 and in the IC model, indicating an even higher baseline M3/M1 ratio and a smaller increment in M3/M1 as M2/M1 increases. As shown in Fig. 4, the RMA and PRMA slopes

are different from each other and less parallel than those in Fig. 3, indicating that the slope pattern observed in Scenario 1 is less evident here. For OTUs distribution, earlier hominins still approximate the upper portion of the slope, but several OTUs extend into the lower region of the plot and deviate from the expected slope trajectory. These two scenarios demonstrate that variation in sampling strategy can lead to noticeable differences in the results: the strength and structure of the relationship between M2/M1 and M3/M1 ratios, as reflected in slope orientation and OTUs positioning, are sensitive to how specimens are selected.

c. Scenario 3 and 4: Upper consecutive (UC) and upper isolated (UI) molars

A similar empirical validation was conducted using maxillary molars in Scenario 3 (UC; see the graphs in Appendix IV). The RMA results yielded a lower intercept (−1.112) and a slightly lower slope (1.940) compared to the IC model. The PRMA produced nearly identical results, with a marginally higher intercept (−1.098) and a slightly lower slope (1.933), suggesting a lower M3/M1 ratio than predicted by the IC model for a given M2/M1 ratio in the maxilla. In the graph (Appendix IV), the PRMA slope lies closest to the IC model, and with both RMA and PRMA slope values approaching 2, the results suggest the presence of a relationship very similar to the IC model within hominins, with or without accounting for phylogenetic dependency. In Scenario 4 (UI: upper isolated molars), PRMA returned a much lower intercept and a higher slope than the IC model. As in Scenario 2 (LI: lower isolated molars), regression results based on isolated molars show notable deviations from those based on consecutive molars (Scenarios 1 and 3), highlighting the sensitivity of slope and intercept estimates to sampling approach.

Table 3. Validation results of Scenario 1-4 by RMA/PRMA regressions

Scenario	Description	Regression	Lambda	Intercept	Slope	R^2	P-value
1	Lower consecutive	RMA	NA	-0.730	1.593	0.606	0.005
		PRMA	0.761	-0.928	1.713	0.239	0.015
2	Lower isolated	RMA	NA	-0.339	1.279	0.736	0.037
		PRMA	0.950	-0.522	1.491	0.359	0.029
3	Upper consecutive	RMA	NA	-1.112	1.940	0.822	0.000
		PRMA	0.595	-1.098	1.933	0.578	0.001
4	Upper isolated	RMA	NA	-1.105	1.927	0.511	0.001
		PRMA	0.940	-1.460	2.160	0.370	0.001

Table 3 summarises the regression results for Scenarios 1–4. The PRMA models in Scenarios 2 and 4, which are based on isolated molars, yielded higher lambda (λ) estimates than those based on consecutive molars (Scenarios 1 and 3). As discussed earlier, Pagel's λ in phylogenetic regression quantifies the extent to which phylogenetic relationships structure the model's residuals (Pearse et al., 2025): λ values greater than 0 indicate that residuals at least partly vary following the phylogenetic structure (Revell, 2010). In Scenarios 1 and 3, the intermediate λ values suggest moderate phylogenetic dependence in the residuals. In contrast, the high λ values observed in Scenarios 2 and 4 indicate stronger covariance structuring of residuals from phylogeny. The higher λ values in scenarios with isolated molars may result from reduced trait precision and uneven sampling across taxa, rather than reflecting true lineage-specific differences.

(2) Observed *versus* expected M2 size

To evaluate whether the observed M2 size aligns with the expectations proposed by Kavanagh et al. (2007), we compared the observed mean M2 size with the expected value, calculated as one-third of the total molar size.

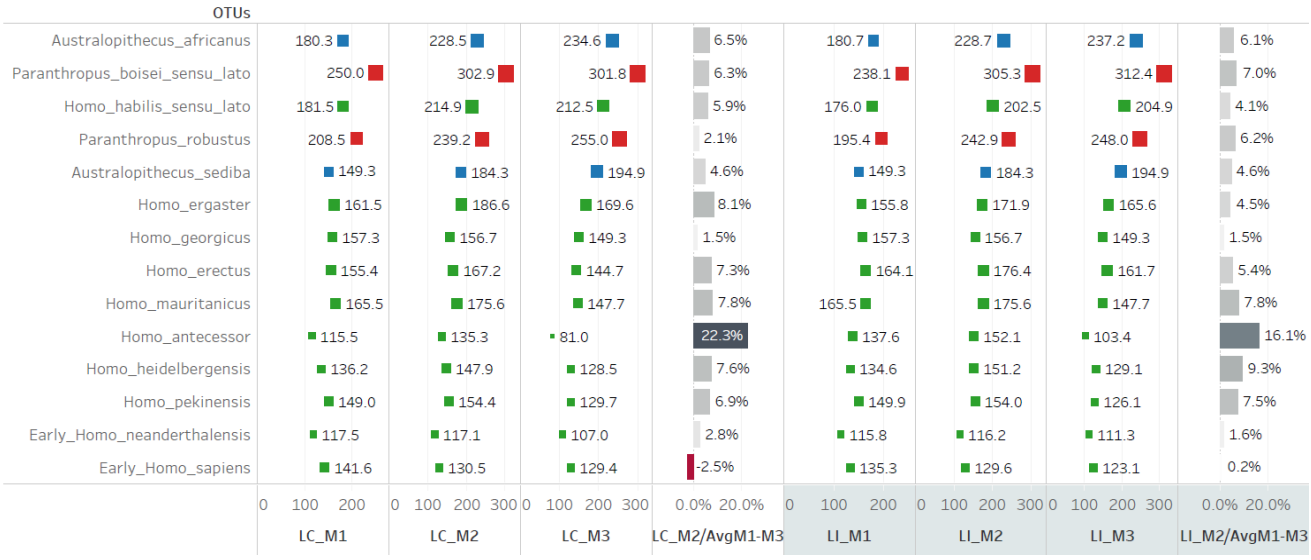

Figure 5. Mean size of molars by OTUs in squares, and the differences between observed and expected M2 sizes for a subset of OTUs in variance bars

(partial, extracted as a continuous portion of the dataset; see Appendix V(a) for full illustration) Square size and horizontal position along the x-axis (0–300) are both proportional to molar size. OTUs are coloured by genus: blue = Australopithecus, red = Paranthropus, green = Homo. Abbreviations: LC_M1 = mean M1 size in the lower consecutive sample; LI_M1 = mean M1 size

in the lower isolated sample; LC_M2/AvgM1–M3 = ratio of M2 size to the average molar size (M1–M3) in the lower consecutive sample.

As shown in Fig. 5, most variance values between observed and expected M2 size fall within the 0–10% range, with a few notable exceptions. *H. antecessor* exhibits the highest deviation in the lower consecutive (LC) sample, where the observed M2 size is 22.3% greater than the expected one-third of total molar size. The pattern reflects a molar size sequence of M1 < M2 > M3, with a strong reduction in LM3 size. Similarly, *H. erectus* shows a substantial amount of variance in the upper consecutive (UC) sample (see Appendix V(a)), where the observed upper M2 size is 11.7% greater than expected, again due to an M1 < M2 > M3 sequence with a pronounced reduction in UM3. In contrast, the variance is lower in the LC sample of *H. erectus*, where LM2 remains the largest molar, but LM3 shows a more gradual size reduction.

On the opposite end of the spectrum, *H. sapiens* (see Appendix V(a)), including Early *H. sapiens* (visible in Fig. 5), are the only OTUs with negative variance in the LC molar samples. Their molar sequence follows M1 > M2 > M3, with a more substantial size decrease from M1 to M2 than from M2 to M3. Accordingly, the observed M2 size in Early *H. sapiens* is 2.5% smaller than the expected value; in *H. sapiens*, it is 1.3% smaller. However, both OTUs show positive variance in the UC sample. For Early *H. sapiens*, the molar size sequence remains M1 < M2 > M3, similar to earlier OTUs. For *H. sapiens*, the sequence transitions to M1 > M2 > M3, similar to the mandible, but the observed M2 size appears larger due to a marked reduction in M3 size.

Aside from a few exceptions where the observed M2 size deviates from the expected by more than 10%, the results are broadly consistent with the expectations described by Kavanagh et al. (2007). While the consecutive molar samples (LC and UC) generally align with this predicted pattern, the isolated molar samples (LI and UI) often conform even more closely. That is, samples with lower consecutive molars tend to exhibit larger deviations from the expected M2 size than those based on lower isolated molars. For instance, *H. ergaster* shows nearly twice the percentage deviation in LC compared to LI, and *H. antecessor* displays a 4-percentage point higher deviation in the LC sample. Although there are some OTUs, such as *P. robustus* that exhibit greater variance in the LI sample (nearly three times that of LC), in most cases, deviations in LI are less pronounced.

A comparison of deviations between consecutive and isolated molar samples across all OTUs (Appendix V(b)) shows that both lower and upper consecutive molars exhibit higher average

deviations than their isolated counterparts. Although the differences in average deviation may appear modest (LC–LI = 0.4%; UC–UI = 0.9%), these values are still meaningful given the relatively narrow range of deviations overall.

Test 2: The better morphological proxy of developmental mechanism: Size *versus* length

(1) Size and length relationship by RMA / PRMA regressions

In the previous section, the PCA result indicated that variables representing molar size and length ratios generally covary. However, as noted by Monson et al. (2022), these metrics have fundamentally different biological interpretations: the size-based IC model is intended to reflect developmental mechanisms but is subject to pleiotropic effects (since BL width incorporates systemic effects of body size and sex (Hlusko et al., 2016)), whereas the length-based MMC could better capture genetic and phylogenetic patterns. By comparing these two approaches, we aim to examine how their biological relevance may differ from a statistical perspective.

PCA results show that the two variables that form the basis of the IC model (M2/M1 and M3/M1 ratios) load mainly on the Dim 1 axis and between the Dim 1–2 axes respectively, whereas M3/M2 aligns closely with Dim 2. As M3/M2 represents the developmental step following M2/M1 in molar formation, their contrasting positions in PCA space i.e., one near Dim1 and the other near Dim 2, together with the developmental order of initiation (M1 before M2: M2/M1; M2 before M3: M3/M2), may capture patterns of variation associated with different molar positions. This observation led to a series of regression analyses comparing size-based *vs.* length-based variables, not only for the standard IC model pairings (M3/M1 *vs.* M2/M1) and the MMC (M3 *vs.* M1), but also for additional combinations such as M2/M1 and M3/M2. By evaluating a broad set of variable pairings, we aim to assess whether the proposed higher potential of length-based metrics to reflect phylogenetic relationships (as expressions of the underlying genetic patterning) holds, and if so, whether it is consistently seen across different molar positions, in order to clarify their applicability for evolutionary and developmental understandings. Table 4 extends the comparisons between molar ratios based on the IC model.

As Monson et al. (2022) noted that the mandibular MMC is more evolutionarily conserved, and since Kavanagh et al. (2007) conducted their experiment of the IC model using mandibular molars,

all analyses in this section (Test 2) were performed on mandibular consecutive molars exclusively for a fair comparison of results.

The IC model (M3/M1 *vs.* M2/M1, Fig. 3) under both RMA (no λ used) and PRMA (λ=0.761) records slope value greater than 1 (RMA slope: 1.593; PRMA slope: 1.713), with significant p-values confirming that the slope is different from isometry. This indicates that the M3/M1 ratio grows disproportionally larger than the M2/M1 ratio, regardless of phylogeny correction. When phylogeny is accounted for, the M3/M1 ratio exhibits more pronounced disproportional increases relative to M2/M1.

In the length-based version (M3MD/M1MD *vs.* M2MD/M1MD), the RMA similarly records a slope of 1.637, significantly different from proportional growth (p=0.009). However, under PRMA, the slope is not significantly different from 1, suggesting the scaling is either approximately proportional or in a very weak relationship. The low R^2 at 0.114 supports the latter, suggesting that the relationship is not clear: only around 11% of the variance in M3MD/M1MD can be explained by M2MD/M1MD. It implies that when taxa are assumed independent, a significant relationship exists; yet in PRMA, where OTUs are considered dependent by phylogeny, the ratio does not scale consistently across OTUs, implying a very weak or even non-existent relationship between variables.

Table 4. IC model and other molar ratio comparisons

	y	*x*	Lambda	Intercept	Slope	R^2	P-value
Size ratio (area)	M3/M1	M2/M1	NA	-0.730	1.593	0.606	0.005
			0.761	-0.928	1.713	0.239	0.015
	M3/M2	M2/M1	NA	-0.076	0.894	0.076	0.618
			0.759	2.634	-1.295	0.006	1.000
	M3/M2	M3/M1	NA	0.333	0.561	0.667	0.000
			0.777	0.032	0.761	0.693	0.047
Length ratio (MD)	M3MD/M1MD	M2MD/M1MD	NA	-0.698	1.637	0.466	0.009
			0.738	-0.442	1.406	0.114	0.131
	M3MD/M2MD	M2MD/M1MD	NA	-0.169	1.070	0.012	0.769
			0.747	2.462	-1.255	0.129	1.000
	M3MD/M2MD	M3MD/M1MD	NA	0.287	0.654	0.639	0.007
			0.766	-0.036	0.902	0.575	0.500

The regressions of M3/M2 *vs.* M2/M1 by RMA returned a slope close to 1, with a high p-value suggesting that the null hypothesis of proportional relationship (slope=1) between *x* and *y* cannot

be rejected. However, when phylogenetic structure is incorporated, the PRMA slope changes to -1.295, reversing the relationship between variables. Fig. 6 explains the phenomenon with two distinct clustering patterns: the upper-right cluster, predominantly earlier hominins intersected by the PRMA slope (orange line), represents a correlation consistent with phylogenetic structuring of residuals; while the middle-left cluster, which contains most *Homo* species intersected only by the RMA slope (green line), suggests an artefactual relationship due to phylogenetic dependence of residuals.

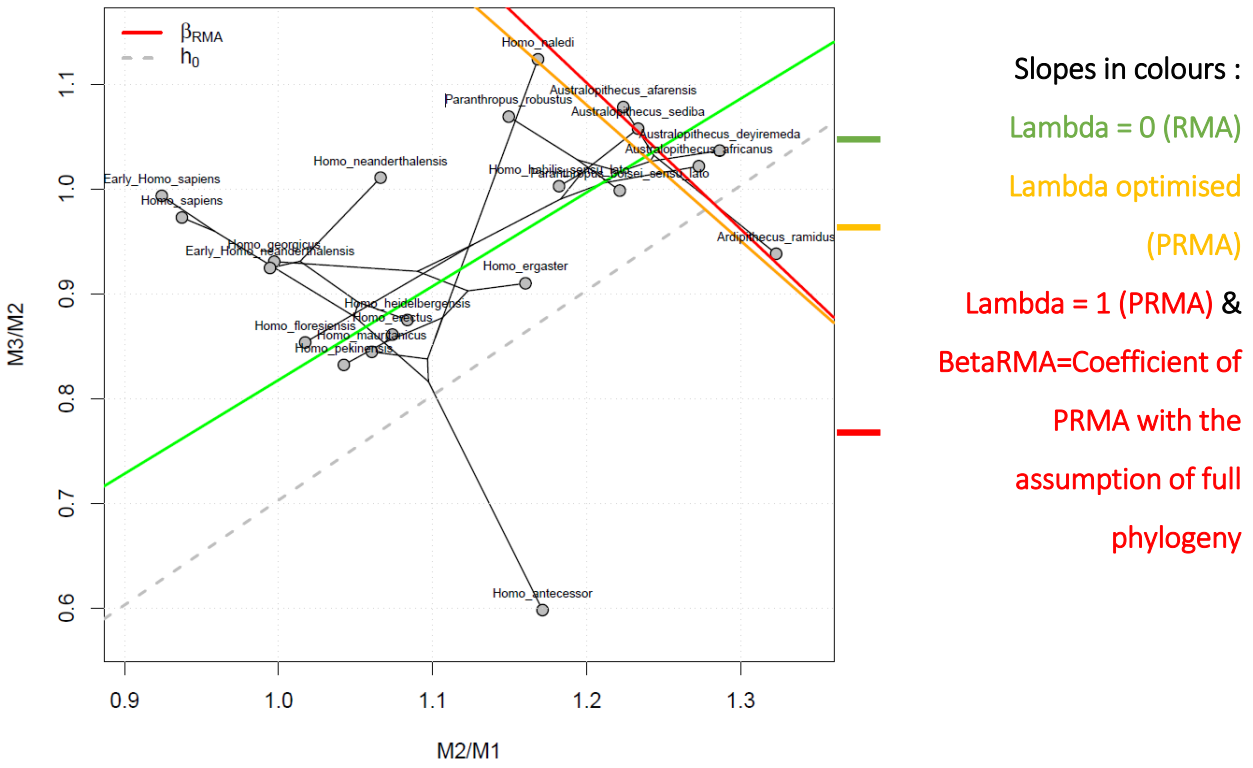

Figure 6. RMA/PRMA graph for M3/M2 versus M2/M1

This pattern mirrors the "worst-case" scenario described by Felsenstein (1985), where ignoring phylogeny can create illusory correlations, caused mainly by differences between unrelated groups rather than reflecting a real developmental or functional connection. Specifically, when two groups, each internally showing little or no correlation, are analysed without accounting for their shared ancestry, methods like RMA can falsely infer a significant trend. In the case of M3/M2 *vs.* M2/M1, the proportional relationship detected by RMA is primarily driven by differences between major phylogenetic groups, rather than by consistent proportional scaling within those groups. Once phylogeny is incorporated, the illusion of proportionality disappears, revealing that the observed

correlation was a statistical artefact of phylogenetic clustering. A similar statistical result is also observed in the length ratio (M3MD/M2MD *vs.* M2MD/M1MD), showing a lack of meaningful correlation between M3/M2 *vs.* M2/M1 ratios.

The PRMA regression of M3/M2 against M3/M1 yields a slope of 0.761. The p-value below 0.05 implies a significant difference from proportional growth (slope$\neq$1). The relationship suggests that M3/M2 grows less than M3/M1 in size, and thereby the size of M2 remains relatively stable while variation in M3 is more pronounced in relation to M1. This finding aligns with the developmental sequence of molar formation, where the last-initiated molar (M3) exhibits greater size variation relative to the first (M1), while the middle molar (M2) remains more consistent. Contrarily, the PRMA of length ratio (M3MD/M2MD *vs.* M3MD/M1MD) returns a slope at 0.902, with the p-value unable to reject the null hypothesis of isometry.

Table 5. MMC model and other absolute measurements comparisons

	y	*x*	Lambda	Intercept	Slope	R^2	P-value
Size measurement (area)	M3	M1	NA	-65.980	1.563	0.790	0.001
			0.998	-13.261	1.360	0.725	0.021
	M2	M1	NA	-24.428	1.322	0.879	0.003
			0.954	2.709	1.251	0.862	0.019
	M3	M2	NA	-37.102	1.182	0.928	0.016
			0.923	-16.834	1.089	0.788	0.433
Length measurement (MD)	M3MD	M1MD	NA	-5.928	1.560	0.701	0.003
			1.000	-1.803	1.330	0.685	0.041
	M2MD	M1MD	NA	-1.068	1.173	0.799	0.140
			0.932	1.027	1.063	0.732	0.617
	M3MD	M2MD	NA	-4.508	1.330	0.876	0.003
			0.922	-3.075	1.249	0.665	0.113

Table 5 extends the comparisons of absolute measurements based on the MMC model. The PRMA regression of the MMC (M3MD *vs.* M1MD) yielded a slope of 1.330, with a p-value <0.05 indicating a statistically significant difference from linear proportionate growth. Fig. 7 displays the distribution of OTUs under the MMC using RMA and PRMA. Except for *H. naledi*, the *Homo* clade is concentrated in the lower-middle part of the slopes, and is largely parallel to the PRMA slope (orange dotted line). While the OTUs are more frequently intersected with the RMA slope (green line), the RMA slope (1.560) suggests that, without phylogenetic correction, M3MD

increases disproportionately relative to M1MD. The PRMA slope, on the other hand, is lower (1.330), indicating that phylogenetic correction moderately reduces the disproportionate scaling.

A similar pattern is observed when comparing size measurements (M3 *vs.* M1), though the difference in intercept between the two pairs of variables is much obvious. This might be due to the differences in measurement units (size *vs.* length). Yet it also illustrates a general trend of significantly higher intercepts in phylogenetic regressions, which reflect an upward shift in the baseline value of *y* when *x* is zero. Notably, in Fig. 7, the PRMA slope (orange line) overlaps the line in red representing full phylogenetic dependence ($\lambda = 1$), implying that the pattern of covariance in the residuals closely matches what is expected under a Brownian motion with the given branch lengths. While this may appear to be a perfect illustration of how the MMC fits with phylogenetic structure, it is also important to note that all regressions performed with absolute measurement variables consistently show very high lambda values.

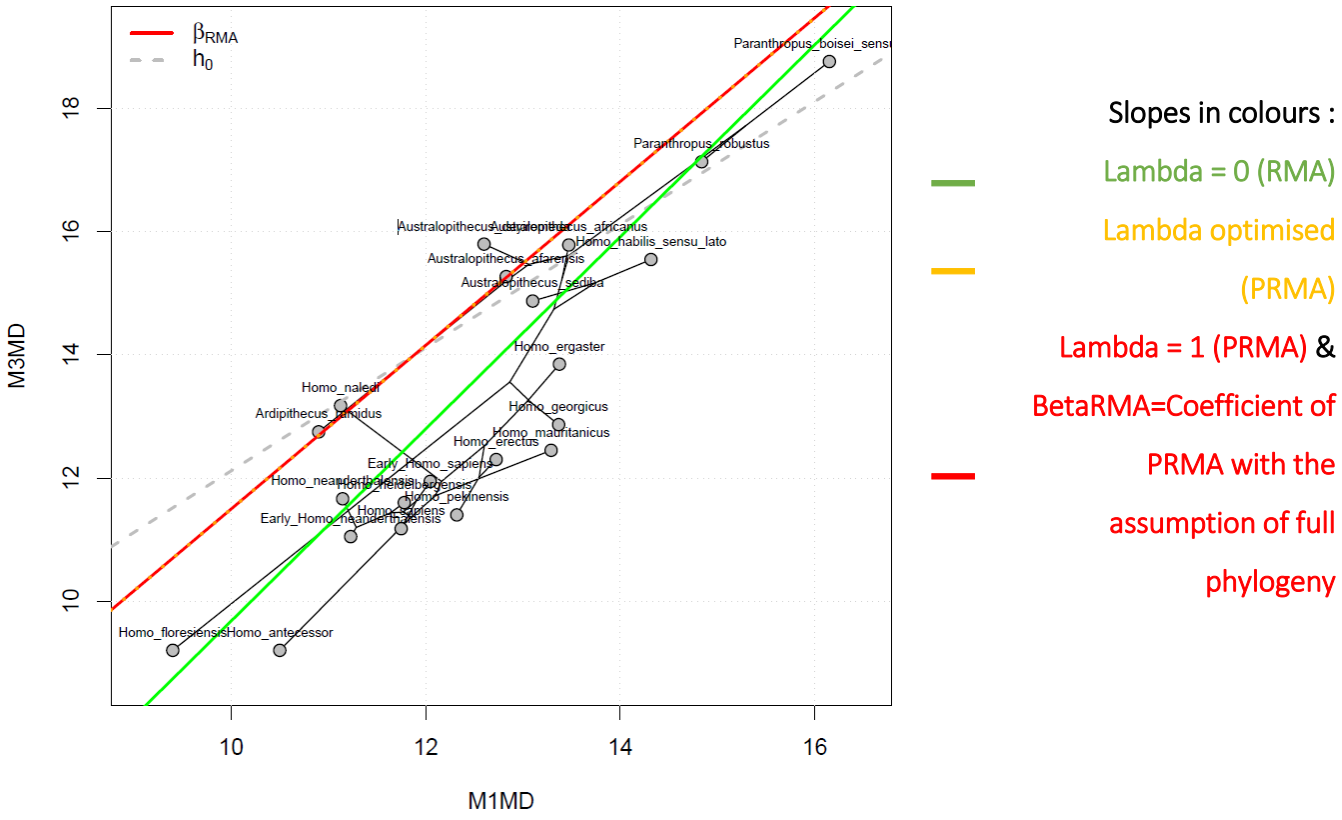

Figure 7. RMA/ PRMA graph for MMC model (M3MD versus M1MD)

M2MD *vs.* M1MD in PRMA yielded a slope of 1.063, close to 1 without a significant p-value, suggesting a proportional relationship between the two variables: M2MD scales linearly with M1MD. In the size-based relationship, the PRMA slope between M2 and M1 size is 1.251 with a significant p-value proving the slope differs from 1, implying M2 area disproportionally increases relative to M1. In the case of M2/M1, the length-based relationship again shows a relatively proportionate relationship compared to the size-based version, supported by a high R^2 at 0.732.

For M3MD vs. M2MD regression, the PRMA slope is 1.249 without significant differences from 1. The same pattern is observed in the size-based relationship, suggesting that with phylogeny, both length and size scale nearly proportionally between M3 and M2.

A comparison of lambda values across variable pairs in Tables 4 and 5 reveals consistent patterns within each table. This implies that the degree to which model residuals covary with phylogenetic structure is similar for both size-based and length-based regressions. The observed differences in λ (approx. 0.7 in Table 4 vs. approx. 0.9 for Table 5) appear to be primarily driven by the unit of comparison: λ is lower for ratio-based models and higher for absolute measurement models. In terms of the strength of the linear relationship, as indicated by R^2 in RMA/PRMA, variable pairs based on size generally yield higher R^2 values compared to length. This shows that size-based relationship tends to show stronger associations between variables.

Comparing the MMC (length-based) to its size-based version, the latter yielded a very similar slope with slightly stronger statistical support, as indicated by a higher R^2 and a lower p-value. This implies that even though the MMC yields a 0.002 higher lambda value, it is due to more residual variance being structured according to phylogeny; whereas the size-based model provides a slope that is statistically more robust and reliable, with datapoints clustering more tightly around the fitted line. From this perspective, the MMC does not display a higher potential over the size-based approach from a statistical perspective in terms of explaining relationships between variables.

(2) Relationship of variables with total molar size by OLS/ PGLS regressions

Since the total molar row size (M1+M2+M3) is the final developmental outcome, its correlation with different molar ratio variables is worth investigating as a window into how the developmental process structures the dentition. By comparing the predictive power of several variables in the two

morphological metrics (length and size), we test which variable better reflects the molar formation process. While some associations with total molar size might arise from scaling effects, they are also likely to capture shared genetic regulation preserved through evolution and thus of greater developmental importance.

M2/M1 size ratio shows a moderate correlation with total molar size in the OLS result (slope=0.000451; R^2=0.290) with statistical support on its significance (p=0.012). Yet, the relationship diminishes and turns insignificant under phylogenetic correction (PGLS), reflected by a lower slope and p-value>0.05. It might be due to the correlation in OLS being "inflated" because the closely related OTUs inherit similar trait values, and tend to deviate from the regression line in the same direction. The association appears to be stronger than what actually exists between M2/M1 ratio and total molar size as a result. When the residuals are corrected under phylogenetic structure in PGLS, the correlation is no longer significant. It reveals that the moderate OLS association was driven by shared ancestry, implying a weak relationship between the M2/ M1 ratio and total molar size.

Table 6. Regression of molar ratios on total molar size (OLS/PGLS)

	y	*x*	Lambda	Intercept	P-value (intercept)	Slope	P-value (slope)	R^2
Size ratio (area)	M2/M1	Total molar row size (M1+ M2+ M3)	NA	0.905	0.0000	0.000451	0.012	0.290
			0.786	1.049	0.0000	0.000313	0.137	0.510
	M3/M1		NA	0.635	0.0001	0.000897	0.002	0.399
			0.665	0.830	0.0003	0.000708	0.037	0.510
	M3/M2		NA	0.759	0.0000	0.000392	0.034	0.216
			-0.129	0.858	0.0000	0.000204	0.180	-0.169
Length ratio (MD)	M2MD/ M1MD		NA	0.991	0.0000	0.000164	0.129	0.117
			0.377	1.045	0.0000	0.000109	0.367	0.197
	M3MD/ M1MD		NA	0.820	0.0000	0.000486	0.004	0.369
			1.023	0.978	0.0000	0.000388	0.048	0.588
	M3MD/ M2MD		NA	0.847	0.0000	0.000287	0.018	0.261
			-0.152	0.843	0.0000	0.000287	0.013	0.023

Unlike M2/M1 ratios (size and length), M3/M1 ratios exhibit strong correlations with total molar size even under phylogenetic correction. PGLS regression of M3/M1 yields a significant positive slope (0.00708; p<0.05; R^2=0.510). Despite a modestly lower slope, the M3MD/M1MD ratio displays a similar pattern: PGLS regression shows the highest predictive power (slope=0.00388) to total molar size among all MD ratios, with robust statistical support. These results indicate that

the link between M3/M1 and total molar size is consistent across OTUs even when phylogenetic structure is considered. It suggests that while M1 and M2 are relatively stable in their development (i.e., less dependence on the total molar size), M3 is more sensitive to overall size, possibly due to its later initiation and longer growth trajectory.

M3/M2 exhibits a weak but statistically significant relationship with total molar size in OLS regression (slope=0.000392; $p<0.05$), but its significance does not persist in PGLS. While it appears that the apparent correlation observed on M3/M2 in the non-phylogenetic model, as with the M2/M1 which might be largely a byproduct of shared ancestry, its negative lambda value in PGLS indicates a negative phylogenetic correlation, meaning that closely related OTUs tend to have oppositely varying phenotypes for this trait (Revell, 2009). The negative R^2 (≈ 0) recorded in PGLS further confirms the very weak link of the M3/M2 ratio with total molar size.

The length-based ratios, on the other hand, yield low slope values with statistical support for their significant difference from 0 ($p<0.05$). However, the low R^2 value in PGLS implies minimal predictive power of the model M3MD/M2MD to total molar size under phylogenetic structure. Together with the negative lambda, the result further suggests a minor developmental association with the total molar size. Overall, the M3/M2-related ratios (both size and length) exhibit a very weak relationship with the final developmental outcome of molar formation, which might reflect the less developmental linkage of later-developing molars with overall molar dimensions.

Among the variables in Table 6, only M3/M1 ratios (size and length) show a strong correlation with the total molar size, even after accounting for phylogeny using PGLS. Although this could be interpreted as support for the MMC (length-based ratio), the size-based version demonstrates a higher slope (nearly twice that of the MMC), with comparatively stronger statistical support (a slightly higher R^2). This suggests that the strong correlation between M3/M1 ratios and the total molar size is not primarily driven by the differences between size and length measurements, but rather by the specific molar position involved: covering the first to the last molar in the developmental sequence, and thus able to capture the full range of molar formation.

(3) Phylogenetic signal of different variables by Blomberg's K

Given the differing outcomes observed in OLS and PGLS regressions with and without phylogenetic correction, we further assessed phylogenetic signal for several variables using Blomberg's K statistics. It helps distinguish whether patterns in molar ratios are predominantly shaped by shared ancestry or reflect a more independent developmental mechanism. This distinction is particularly relevant when comparing size-based *versus* length-based measurements: a strong phylogenetic signal implies influence of lineage-specific evolutionary history, while a weak signal suggests potential independence from phylogeny. Based on Blomberg's K results, we can identify which measurements (size or length) more effectively capture the developmental processes underlying molar morphology.

The result (Table 7) shows that none of the absolute measurements for individual molars (M1, M2, M3 size and length) display significant phylogenetic signal, as indicated by low K-values and non-significant p-values. It means that these traits do not vary significantly according to phylogenetic relationships, i.e. closely related species do not consistently exhibit more similar size or length values than distantly related ones.

Table 7. Phylogenetic signal by variables (Blomberg's K)

Size-based variables			**Length-based variables**		
Variables	Phylogenetic signal K	P-value	Variables	Phylogenetic signal K	P-value
M2/M1	0.628	0.011	M2MD/M1MD	0.495	0.039
M3/M1	0.473	0.043	M3MD/M1MD	0.592	0.020
M3/M2	0.226	0.415	M3MD/M2MD	0.272	0.271
M1	0.216	0.493	M1MD	0.209	0.532
M2	0.218	0.487	M2MD	0.216	0.507
M3	0.249	0.360	M3MD	0.266	0.319

However, the size ratio between M2 and M1 (M2/M1) demonstrates a moderate and statistically significant phylogenetic signal ($K=0.628$, $p<0.05$), and is the strongest among all variables tested. When the closely related OTUs tend to have more similar M2/M1 ratios, the pattern implies that the trait is moderately conserved phylogenetically and its variation is, at least in part, shaped by shared ancestry. This may also be linked to the relationship between M2/M1 and total molar size that becomes non-significant in PGLS after accounting for phylogeny.

M3/M1 ratio exhibits a lower K-value than M2/M1, suggesting that it is less evolutionarily conserved. The M3/M2 ratio has a modest and nonsignificant K value, which implies an absence of phylogenetic signal for this trait. This overall pattern reveals a trend of decreasing evolutionary conservation in molar size ratios according to the sequence of molar initiation: ratios involving earlier-initiated molars display a strong phylogenetic signal.

Nonetheless, the trend does not hold for length-based ratios. Though M2MD/M1MD shows a relatively higher K-value, M3MD/M1MD ratio (corresponding to the MMC) records the highest K among MD ratios. It indicates that the MMC is also influenced and shaped, in part, by shared ancestry. The contMap (Fig. 8) illustrates the evolution of this trait along the phylogeny. The colour gradient of the branches is darker within clades of earlier OTUs, meaning higher similarity in M3MD/M1MD values among closely related lineages. Contrarily, the branches tend to become lighter within the *Homo* clades, reflecting that most of them share similarly low values of the trait due to shared ancestry. However, since its relationship with the total molar size remains significant after phylogenetic correction in PGLS, the slope indicates that not all variation of M3MD/M1MD is attributable only to phylogeny (in contrast to M2/M1). This suggests that, apart from evolutionary conservation among phylogenetic lineages, the MMC is also influenced by developmental processes that operate independently from shared ancestry.

Since Blomberg's K is a univariate measure of phylogenetic signal calculated on the individual variables, it is not directly applicable to a bivariate model like the IC model, which is statistically represented by the relationship between two molar size ratios (M3/M1 and M2/M1). The moderate phylogenetic signal of both M2/M1 and M3/M1 individually indicates that each ratio retains some imprint of shared ancestry. Yet it is important to note that Blomberg's K for a single trait is not equivalent to the lambda value estimated in a regression, as they capture different aspects of phylogenetic structure: the former measures signal within a variable, the latter within the residuals of a relationship between variables. For this reason, K values cannot account for the higher PRMA slope compared to RMA in the IC model (Fig. 3). Although the IC model cannot be directly assessed with Blomberg's K, the fact that both of its component ratios display phylogenetic signal suggests that, the scaling relationship between them preserves, at least in part, the imprint of shared evolutionary history.

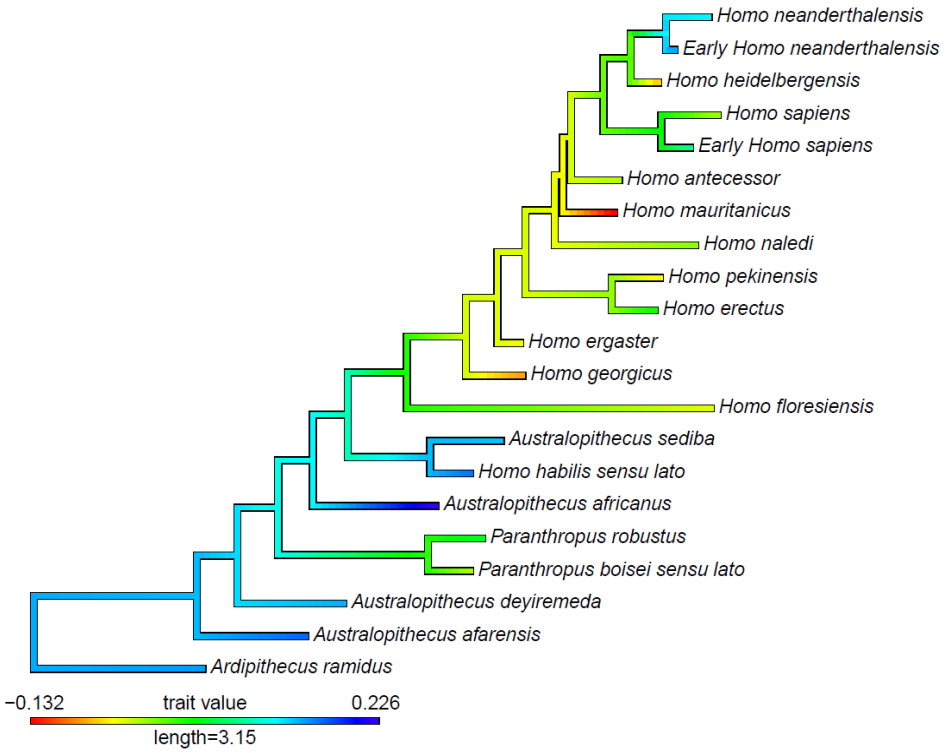

Figure 8. A contMap of the MMC showing trait value projected onto the phylogenetic tree

Lower trait values (lighter colours, red to yellow) correspond to lower M3MD/M1MD ratios, meaning a smaller or even negative M3MD relative to M1MD. Higher trait values (darker colours towards blue) indicate larger M3MD values relative to M1MD.

Throughout this section (Test 2) of comparing size over length, we explored the relationships between molar variables, their associations with total molar size, and their phylogenetic signal, and compared the performance of size-based and length-based measures. Overall, length-based variables generally exhibited lower slopes and weaker relationships with other variables, total molar size, and phylogeny compared to size-based variables. While length-based measures sometimes tended to indicate more proportional scaling, as shown in the relationship between M3MD/M2MD *vs.* M3MD/M1MD, or M2MD *vs.* M1MD, their statistical support was generally limited, as reflected by lower R^2 values and more frequent non-significant correlations. Although the MMC (length-based) metric exhibits strong phylogenetic signal (high λ and K-value), it does not consistently outperform the M3/M1 size-based ratio in capturing phylogenetic patterns, as well as developmental patterns. Size-based measures, by contrast, with more dynamic and stronger associations, demonstrate a greater utility in exploring developmental and evolutionary mechanisms in molar morphology.

Test 3: Spatial capacity: The influence of mandibular width on molar size

While it is found that specific molar positions (M1 and M3) are more closely linked to the final outcome of molar formation, and that size is a better proxy for capturing the dynamics between activation and inhibition in the IC model, we now broaden the scope to consider potential external influences (i.e. outside the molar and its enamel knots): whether the spatial capacity of the mandible influences molar growth. With PGLS regressions, we test whether mandibular width (measured at the M1 position) plays a significant role in determining molar size, beyond the effects of intrinsic activator-inhibitor dynamics. This enables us to assess if the IC operates within a spatial framework constrained by mandibular morphology, or rather independently of it.

Table 8. Molar size regressed on mandibular width at M1 (PGLS)

y	*x*	Lambda	Intercept	P-value (intercept)	Slope	P-value (slope)	R^2
M1size	Mandibular width at M1	0.993	44.262	0.320	6.382	0.006	0.857
M2 size		0.972	1.869	0.965	9.956	0.000	0.095
M3 size		0.961	38.899	0.512	8.544	0.007	0.913
M1-M3 avg		0.979	36.061	0.462	7.922	0.004	0.906

While the size of M1 would be expected to be the most influenced by the mandibular width at its own position, the result (Table 8) shows that M3, the most distal molar, exhibits the strongest positive association with mandibular width at M1. With a slope of 8.544, M3 size increases most sharply as mandibular width at M1 increases, statistically supported by a low p-value and high R^2 of 0.913, where the latter indicates that ~91% of the variation in M3 size is explained by variation in mandibular width at M1. It suggests that M3 size is particularly dependent on, and sensitive to, the space available for its development. Fig. 9a presents a steep, upward PGLS slope of M3 against mandibular width at M1. The slope is higher than that observed for M1 (Fig. 9b), but slightly lower than that of M2 (Appendix VI). However, the phylomorphospace of M3 is the most widely dispersed, which shows greater variability, whereas M1 and M2 are more tightly clustered along the respective slope.

Although M1 follows closely with a slightly lower slope (6.382), as shown in Fig. 9b, and a modestly lower R^2 (0.857), the relationship remains strongly statistically significant. It confirms that mandibular width is also a major determinant of M1 size, but with less variability across OTUs.

(a) M3 size *vs.* mandibular width at M1 (b) M1 size *vs.* mandibular width at M1

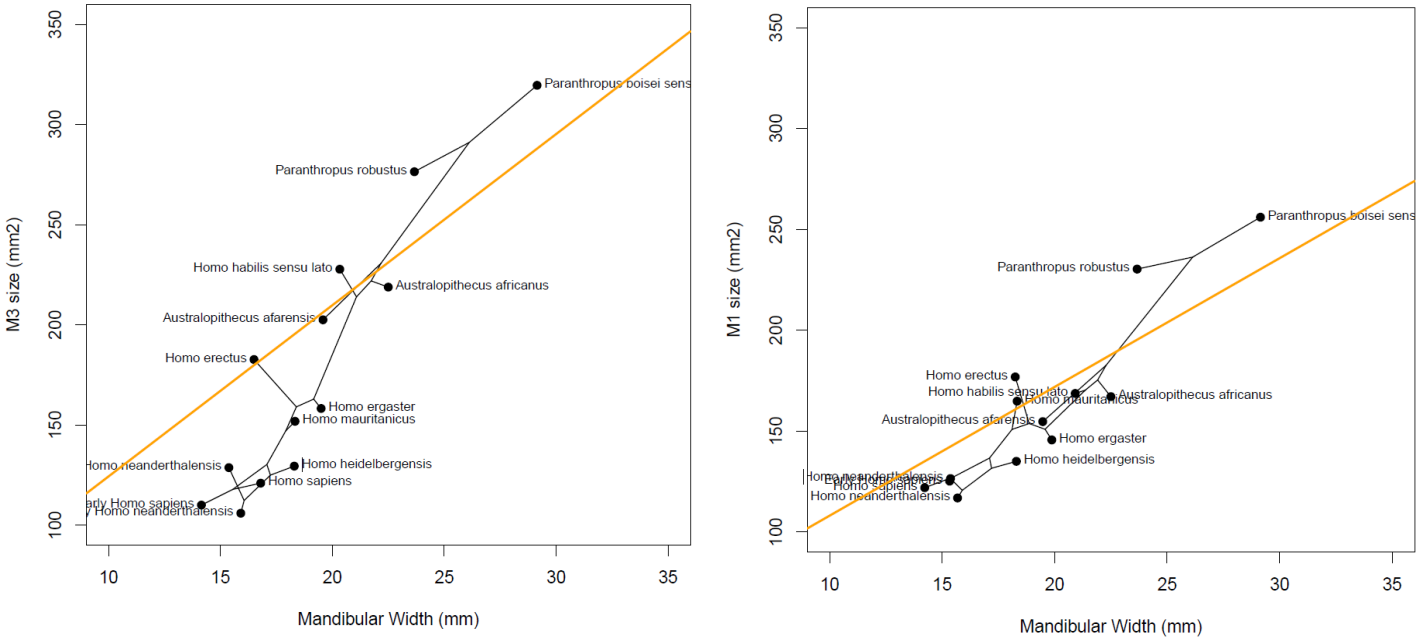

Figure 9. PGLS regression graphs of individual molar size versus mandibular width at M1 (M2 see Appendix VI)

M2, positioned and initiated midway in the molar sequence, presents a high and significant slope but with an extremely low R^2, unlike M1 and M3. It implies minimal explanatory power of mandibular width for its size. Although the statistical relationship cannot be rejected, the weak fit suggests that M2 size is less influenced by the space available at the M1 position. While none of the intercepts are statistically significant, M2's notably lower intercept might reflect a relatively independent growth compared to M1 and M3.

Taxonomically, *Paranthropus* consistently plots above the slope, while most of the *Homo* fall below. The early OTUs from the Pliocene to Early Pleistocene, including *Australopithecus*, *H. habilis*, and *H. erectus*, tend to occupy the middle area intersecting the slope. Notably, M3 displays the most pronounced downward displacement of the more recent *Homo* below the slope, suggesting that in these lineages, narrower mandibular width at M1 would cause greater M3 size reduction. It might suggest a developmental constraint on M3 due to a stronger space limitation in recent *Homo* compared to earlier OTUs.

The overall result indicates that, across the molar row, the first and the last molars are highly determined by the space available for growth, with the effect being particularly pronounced for the

last molar initiated (M3). The finding that mandibular width predicts the size of both M1 and M3 implies that the total molar row size might be, to a large extent, "pre-determined" according to the spatial capacity offered by the mandible (at M1 position). M3, as the last molar to develop, its size is limited by the space remaining after M1 and M2 have formed. This hypothesis is supported by the PGLS regression of the average M1-M3 size (which represents overall molar row size) against mandibular width (Table 8) with a high slope value (7.922) and strong statistical support ($p<0.05$; $R^2=0.906$).

The high variability of M3 accords with Kavanagh et al. (2007)'s description that, due to the ratcheting nature of inhibitory signaling, a change in inhibition affects more the relative size of M3 compared to M2. On the contrary, M2 shows only a weak link with mandibular width at the M1 position, suggesting that its size might be influenced more by inhibitory effects from M1 than by space availability. This further implies that although M1 size is strongly dependent on mandibular width, the inhibitory signal it transmits to M2 is largely independent of spatial constraints.

Test 4: Mandible *versus* Maxilla: The influence of jaw type on molar size

In Test 1, the PRMA regressions of M3/M1 on M2/M1 (the IC model) yielded different results for the lower consecutive (LC) and upper consecutive (UC) samples, implying that the developmental dynamics in the maxilla might differ from those in the mandible. In this part, we widen the scope to a broader anatomical scale to compare jaw types. The purpose is to examine how differences in molar location by jaws may influence the developmental patterns of molar size across evolutionary history.

Table 9. Allometries of molars by jaw types

Allometry to total size	*y*	*x*	Lambda	Intercept	P-value (Intercept)	Slope	P-value (slope)	R^2
Mandibular consecutive (LC) molars	M1 size	Mandibular total molar size (LC)	0.974	-0.231	0.593	0.837	0.000	0.943
	M2 size		-0.105	-0.884	0.002	0.974	0.000	0.943
	M3 size		0.204	-2.446	0.000	1.220	0.000	0.941
Maxillary consecutive (UC) molars	M1 size	Maxillary total molar size (UC)	0.818	-0.201	0.719	0.845	0.000	0.910
	M2 size		-0.624	-1.290	0.000	1.037	0.000	0.983
	M3 size		-1.020	-3.013	0.000	1.308	0.000	0.557

The allometric analysis of molar size relative to total molar size (Table 9) reveals the developmental patterns of the upper and lower jaw. Both mandibular and maxillary M1s show slopes below 1 (mandibular slope=0.837; maxillary slope=0.845), indicating negative allometry: M1sizes decrease as total molar size increases. M2s' slopes, on the other hand, are very close to 1 (mandibular slope=0.974; maxillary slope=1.037), suggesting near-isometric scaling, where M2 sizes grow proportionally to the total molar size. M3s record the highest slopes above 1, with a mandibular slope of 1.220 and the maxillary one reaching 1.308. The result indicates positive allometry, that a larger total molar row size is associated with a relatively larger M3. Although the R^2 for the maxillary M3 is lower, the low p-value supports its statistical significance.

In general, this pattern reflects a scaling trend following the molar initiation sequence: shifting from the strongest inverse relationship with the total molar size in the earliest-forming molars, to the increasingly positive scaling responses in the later (and the latest-) forming molars. Although a similar trend is observed in both mandible and maxilla, it is also found that across all positions, mandibular molars have slightly lower slopes than those on the maxilla. It implies a relatively lower allometric coefficient and a weaker scaling response to total molar size within the mandible compared to the maxilla.

To further investigate the differences in molar scaling dynamics, we examined n=27 individuals (representing 10 OTUs) in our dataset who preserve both consecutive upper and lower molars. For better comparability, the mean absolute size of each molar within an OTU was expressed relative to the size of M1: the M1 size was set arbitrarily and for easy comparisons as 1000, mainly due to its role as the first-formed molar and the first in the molar row, with potential inhibitory effects on subsequent molars. Therefore, using M1 as the reference scale enables a direct comparison of size changes in later molars under the same scale.

Table 10. Upper and lower consecutive molar size in scales

OTUs	LM1 : LM2 : LM3	UM1 : UM2 : UM3
Australopithecus afarensis	1000 : 1184 : 1378	1000 : 1206 : 1195
Australopithecus africanus	1000 : 1202 : 1226	1000 : 1186 : 1203
Homo habilis sensu lato	1000 : 1174 : 1212	1000 : 1105 : 1058
Paranthropus robustus	1000 : 1099 : 1219	1000 : 1006 : 1034
Australopithecus sediba	1000 : 1270 : 1345	1000 : 1128 : 1171
Homo georgicus	1000 : 963 : 753	1000 : 941 : 690

Early *Homo neanderthalensis*	1000 : 993 : 992	1000 : 919 : 800
Early *Homo sapiens*	1000 : 942 : 930	1000 : 896 : 854
Homo naledi	1000 : 1213 : 1334	1000 : 1202 : 1188
Homo neanderthalensis	1000 : 1076 : 1083	1000 : 1015 : 865

The scaled results (Table 10) show a more pronounced reduction in M3 size in the maxilla compared to the mandible. This tendency is apparent even in early hominins, as evidenced by *A. afarensis*: while mandibular molars increase in size from M1 to M3, the maxillary molars show a slight decline from M2 to M3 (assuming UM1 is 100.0 mm^2, UM2 increases to 120.6 mm^2, and UM3 drops slightly to 119.5 mm^2). Although the pattern of maxillary reduction relative to the mandible is not observed in other OTUs of genus *Australopithecus* or *Paranthropus*, it is consistent across the genus *Homo*. In *H. habilis*, UM3 is slightly smaller, while LM3 size continues to increase. This pattern is also observed on *H. neanderthalensis*, though with a smaller LM3 increment and a greater UM3 reduction; in Early *H. sapiens*, both upper and lower molar series decrease in size from M1 to M3, but the reduction is much higher in the maxilla. In general, the mandibles more often exhibit distal enlargement, or subtler M3 reduction, whereas the maxilla tends toward more pronounced distal size reduction in M3.

The differences in molar size development between jaw types might partly account for the different PRMA regression results obtained from lower consecutive and upper consecutive molar samples. For the maxillary sample (UC), the PRMA intercept is -1.099 (0.098 more negative than -1) and the slope is 1.933 (0.067 below 2), both are closer to the standard IC model than those of the mandibular sample (LC). In Fig. 10, the PRMA slope (orange line) is parallel to the IC model slope (blue line), indicating a close fit to the IC theoretical expectations in the maxilla.

The more negative intercept in the maxilla implies that, when the M2/M1 ratio is small (i.e. M2 relatively reduced), the M3/M1 ratio starts from an even lower baseline than in the mandible. The slope, which is very close to the IC model, indicates a stronger positive association between the two ratios in the maxilla: a sharper increase in M3/M1 as M2/M1 rises. This pattern is consistent with the higher allometric coefficient for maxillary M3 relative to total molar size (Table 9): as total size increases, maxillary M3 enlarges more, but as total size decreases (e.g., in recent hominins), M3 contracts more sharply, contributing to its pronounced reduction in the maxilla compared to the mandible (Table 10).

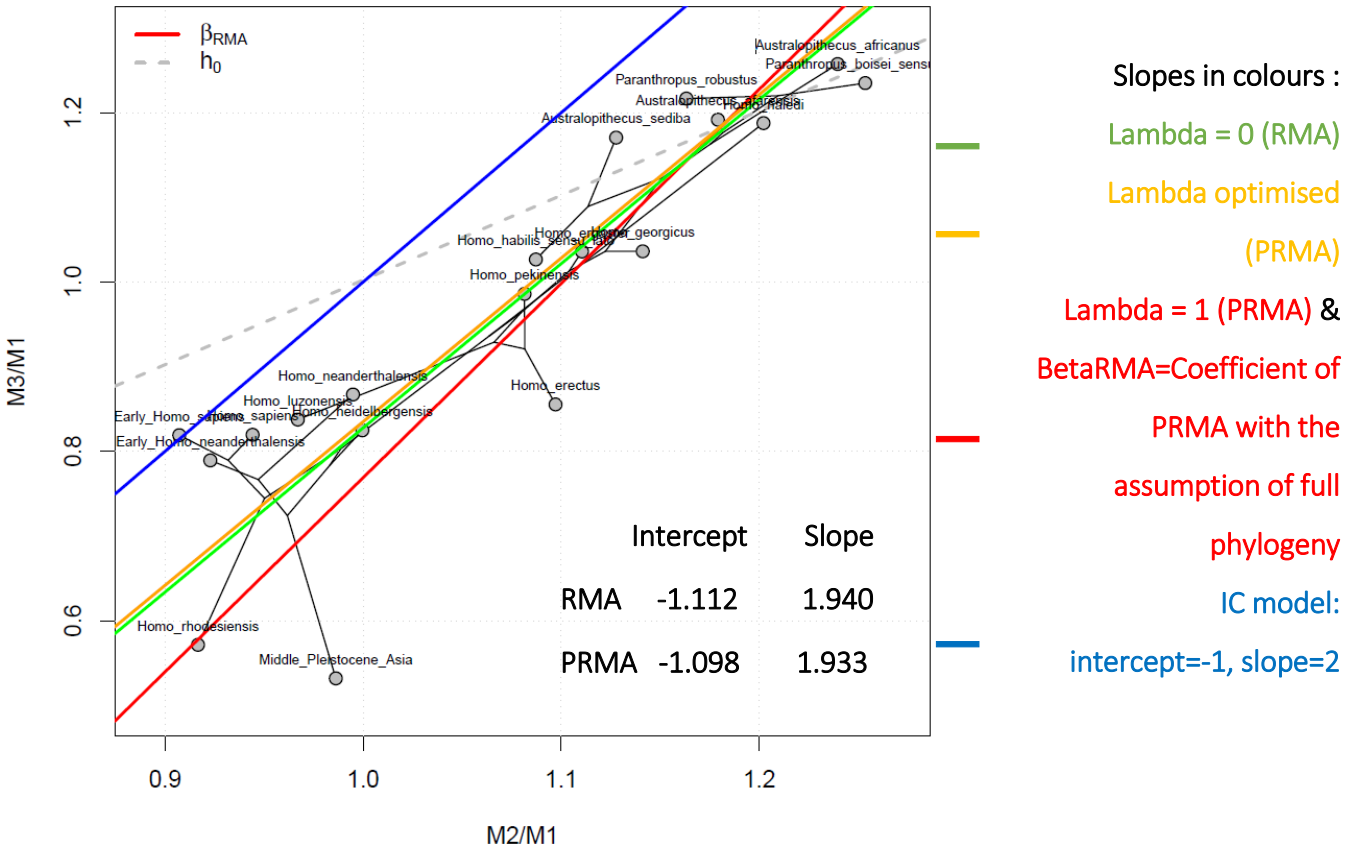

Figure 10. RMA/PRMA regression on consecutive maxillary molars

Although the IC model does not explicitly involve the total molar size, but only proportional scaling between molars in the row, the two are related. While M2/M1 is not a direct measure of total molar size, it reflects part of the proportional distribution of crown area within the row, and is mathematically linked to total molar size through its shared denominator with M3/M1. Total molar size, in turn, emerges as the cumulative outcome of the developmental cascade, making M3's allometric response to total molar size an extension of the M3/M1 dynamics. In Test 3 (Table 8), the strong association of M3 with mandibular width at M1 indicates that total molar size is constrained by spatial capacity at the site of development. Despite the absence of maxillary space measurement in this study, a similar allometric coefficient of M3 in both jaws logically suggests that M3/M1 tracks M2/M1 closely under comparable (but not in the same degree) developmental space limitations.

Test 5: Patterning cascade model at a micro-scale: Cusp size development

While the IC model allows statistical testing of the molar sizing patterns, no standardised statistical model currently exists for quantifying cusp size development under the patterning cascade framework, although its role in influencing cusp presence or absence is documented. Nonetheless, investigating the relationship between cusp size and crown size (molar size) offers a valuable micro-scale perspective on the developmental mechanism. Unlike mandibular width at M1, which is one of the several possible definitions measuring "space" at the molar level, crown size represents a direct and universally consistent measure of spatial capacity at the cusp level. This makes it a suitable context for testing whether patterning cascade dynamics operate together with spatial factors to determine cusp size.

(1) PCA for cusp-related variables by molar position

The PCA plots by each molar (Fig.11 and Appendix VII) show a consistent pattern of variable distribution across M1-M3. In all plots, Dimension 1 accounts for over 50% of the total variance and captures the clustering of crown area ("size") with the size of protoconid ("Prd") and cusp 6, indicating that both cusps covary strongly with respective molar size. While the relative positions of variables vary slightly among molars (e.g. M2 shows the widest spread of variables, whereas M3 has the most tightly clustered variables along the Dim 1 axis), the overall pattern is broadly similar. Dimension 2, on the other hand, explains roughly one quarter of the variance (~25%), primarily captures variation in the size of cusp 7, again with minor positional shifts among molars: cusp 7 in M1 loads toward the left of Dim 2 axis; that of M2 is in the same direction but slightly closer to the axis; cusp 7 in M3 nearly overlapping Dim 2 and slightly to the its right. The cusp number variables are positioned between Dim 1 and 2. The distinct separation of cusp 7 and cusp number from the main cluster defined by molar size, protoconid and cusp 6 suggests that they (cusp 7 and cusp number), to a certain extent, develop independently of the molar size.

(a) Variables of M2

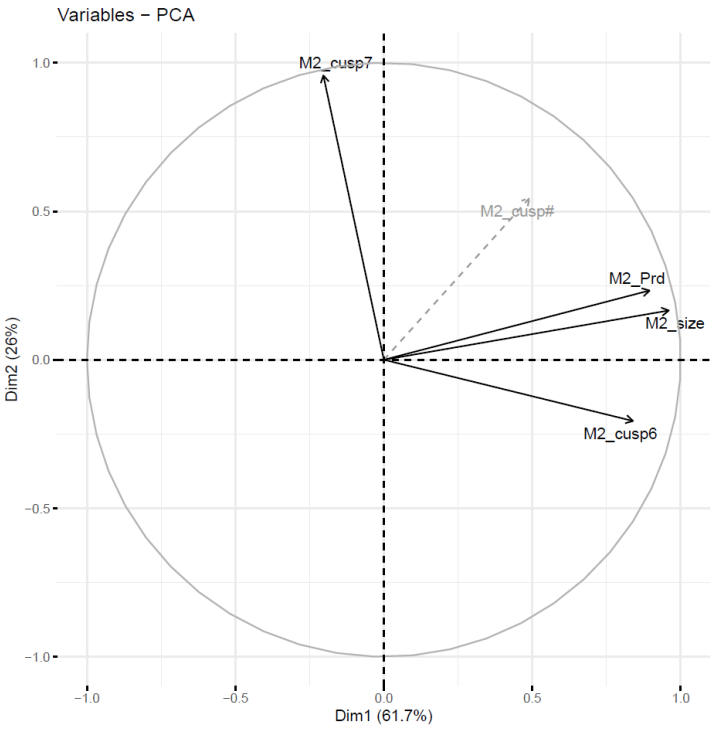

(b) Variables of M3

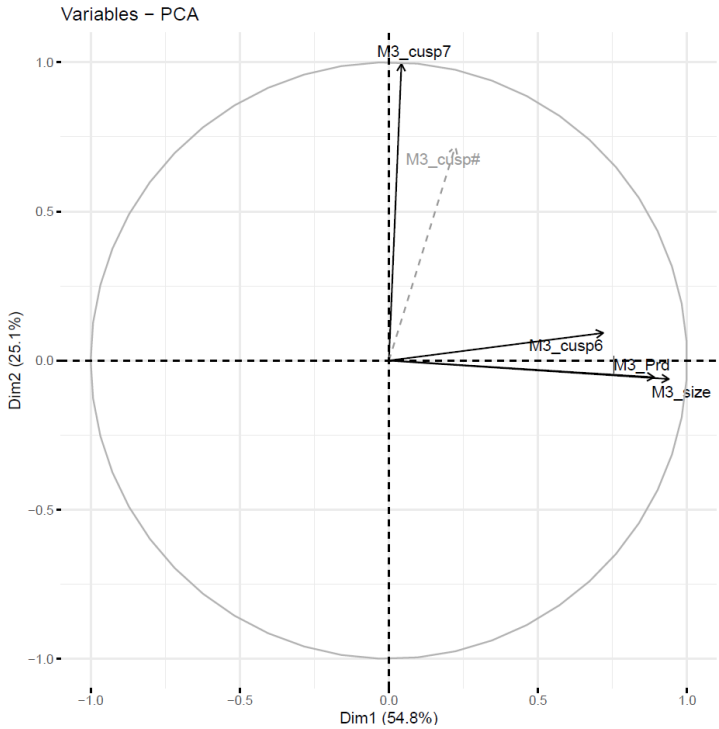

Figure 11. PCA of cusp-related variables by molars (PCA of M1 variables see Appendix VII)

Variables in black: active variables; variables in grey: supplementary variables. Abbreviations: M2_size = crown size of M2; M2_Prd = protoconid size; M2_cusp6/7 = accessory cusp size; M2_cusp# = number of cusps on the occlusal surface. The same abbreviations apply to M3.

The PCA results show that, rather than grouping by molar position, cusp variables tend to cluster by cusp type. It means that the cusp is more strongly correlated with its homologue across molars (visual illustration of clustering see Appendix VIII). This pattern suggests that the formation of each type of cusp is largely governed by its developmental process, with only minor variations seeming to be influenced by molar position. Across all molars, the protoconid consistently clusters closely with the crown size, positioned slightly apart from cusp 6. It indicates that molar size covaries more tightly with the protoconid than with accessory cusps, i.e. cusp 6 and cusp 7. It is also consistent with the cusp formation sequence, in which the protoconid is the first cusp to form and its size is strongly tied to the molar size, similar to the pattern that M1 size is closely related to the total molar size at the molar level. However, since the developmental timing of cusp 6 and cusp 7 is under study, it is not certain if they follow different formation rules. Yet their developments correlate with the molar size will be explored in this part of the analysis.

(2) Protoconid size *versus* molar size

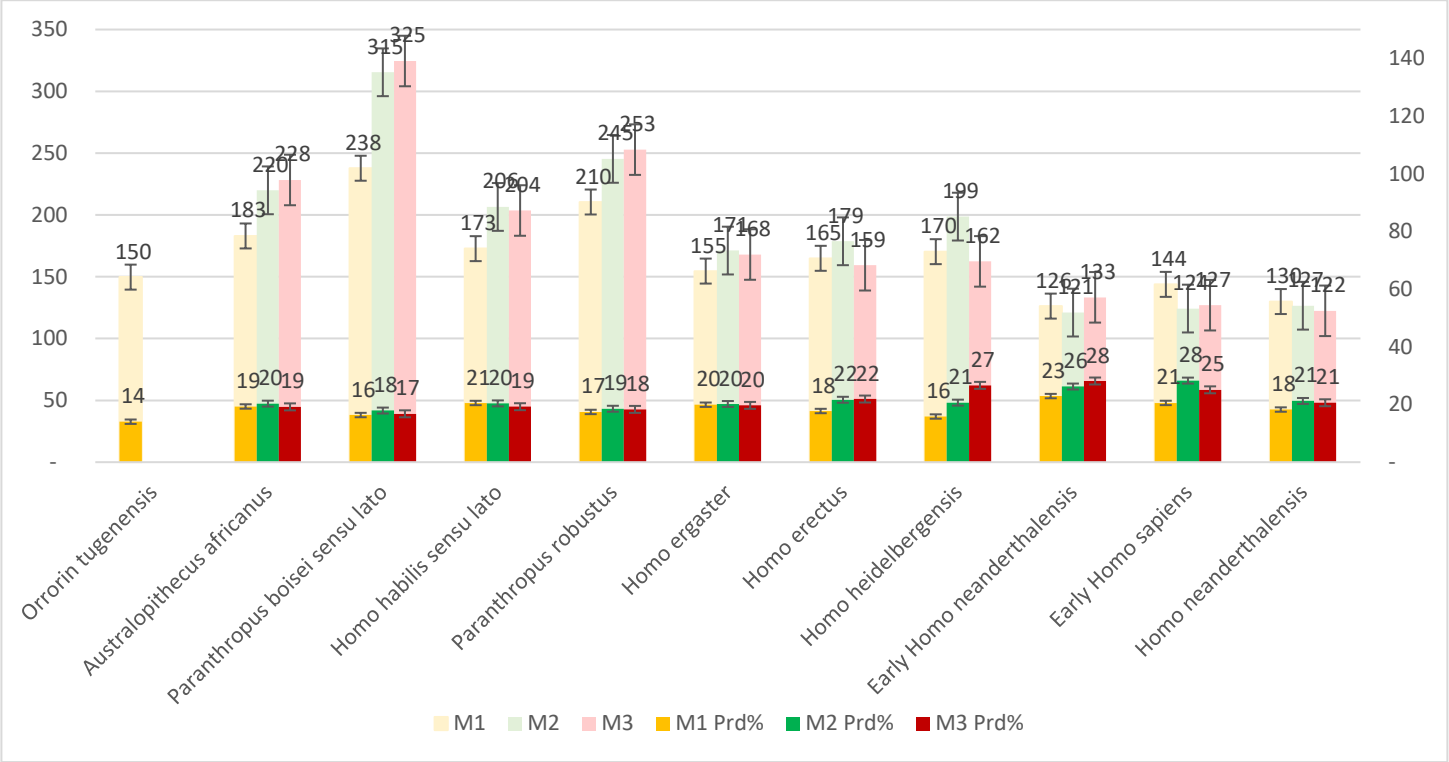

Figure 12. Relative protoconid size versus molar size by OTUs (absolute protoconid size and sample size details see Appendix IX (a))

Across OTUs in Fig. 12, only our samples of *H. neanderthalensis* have the same absolute molar size sequence of M1>M2>M3 as *H. sapiens*, which Bermúdez de Castro (2022) reported to have a reverse-increasing sequence of the relative protoconid size, i.e. M1<M2<M3. However, the relative protoconid sizes of *H. neanderthalensis* do not follow the pattern found on *H. sapiens*: M2 and M3 show almost the same protoconid proportions despite a reduction in M3 crown size. The mirrored trend seen in *H. sapiens*, where molar size gradually decreases from M1 to M3 while relative protoconid size progressively increases, is absent across OTUs in Fig. 12. In general, changes in relative protoconid size do not consistently oppose changes in molar size across positions. For example, early hominins from *A. africanus* to *P. robustus* (except *H. habilis* from the genus *Homo*) exhibit an absolute molar size sequence of M1<M2<M3, but that of relative protoconid size is M1<M2>M3. Among these taxa, the relative protoconid size varies only slightly from 17% to 20% across positions, with M2 being just around 1 percentage point larger than M1 and M3. The result suggests that protoconid size varies closely with molar size in the earlier

evolutionary stage, maintaining consistent relative proportions across positions. This also explains the tight clustering of absolute protoconid size and molar size in the PCAs (Fig. 11): when a consistent proportion of protoconid to the crown size is maintained, its absolute size increases or decreases in direct proportion to changes in molar size.

The 17% - 20% relative size range persists until *H. erectus*, which marks a shift to 22% in M2 and M3. Since then, protoconid proportions increase rapidly, particularly in M3, reaching 28% in Early *H. neanderthalensis*, driven largely by reductions in molar size. In Early *H. sapiens*, relative protoconid size in M3 decreases, yet that of M2 rises to 28%. These two OTUs thus exhibit the highest relative protoconid sizes across molars due to the marked reductions in molar crown size. However, in later *H. neanderthalensis*, relative protoconid size returns to a lower range (18-21%) similar to earlier hominins.

Table 11. Regression of absolute protoconid size on molar size (PGLS)

	y	*x*	Lambda	Intercept	P-value (intercept)	Slope	P-value (slope)	R^2
M1	Absolute	Molar	0.786	13.670	0.101	0.088	0.059	0.665
M2	protoconid	size	-0.528	17.315	0.000	0.121	0.000	0.789
M3	size		-0.430	17.315	0.000	0.114	0.000	0.155

Under phylogenetic correction, M2 exhibits the strongest association between protoconid size and molar size, with the highest slope (0.121), a low p-value and high R^2 (0.789). Fig. 13(a) shows that the OTUs are tightly clustered along the PGLS slope, reflecting the strong predictive power of the slope. M3 follows with a slightly lower slope (0.114) and much weaker explanatory power of the model (R^2 =0.155) despite a low p-value. The more extended distribution of OTUs in the phylomorphospace (Fig. 13b) reflects greater variability in this relationship.

M1 shows a contrasting pattern: the slope is markedly lower (0.088), with the high p-value indicating no significant difference from zero. This suggests little to no association between M1 protoconid size and M1 molar size. The intercept of M1 is also lower than those of M2 and M3, with a high p-value again suggesting the intercept is not significantly different from zero when molar size is zero. Statistically, this means that the predicted *y*-value is not distinguishable from zero when *x*=0. While it could biologically mean the absence of a protoconid when there is no molar at all, under the assumption that M1 develops alongside M2 and M3, the notably lower

intercept might instead reflect a different developmental relationship between M1 protoconid size and M1 molar size compared to those of M2 and M3.

(a) PGLS on M2 protoconid *vs.* molar size

(b) PGLS on M3 protoconid *vs.* molar size

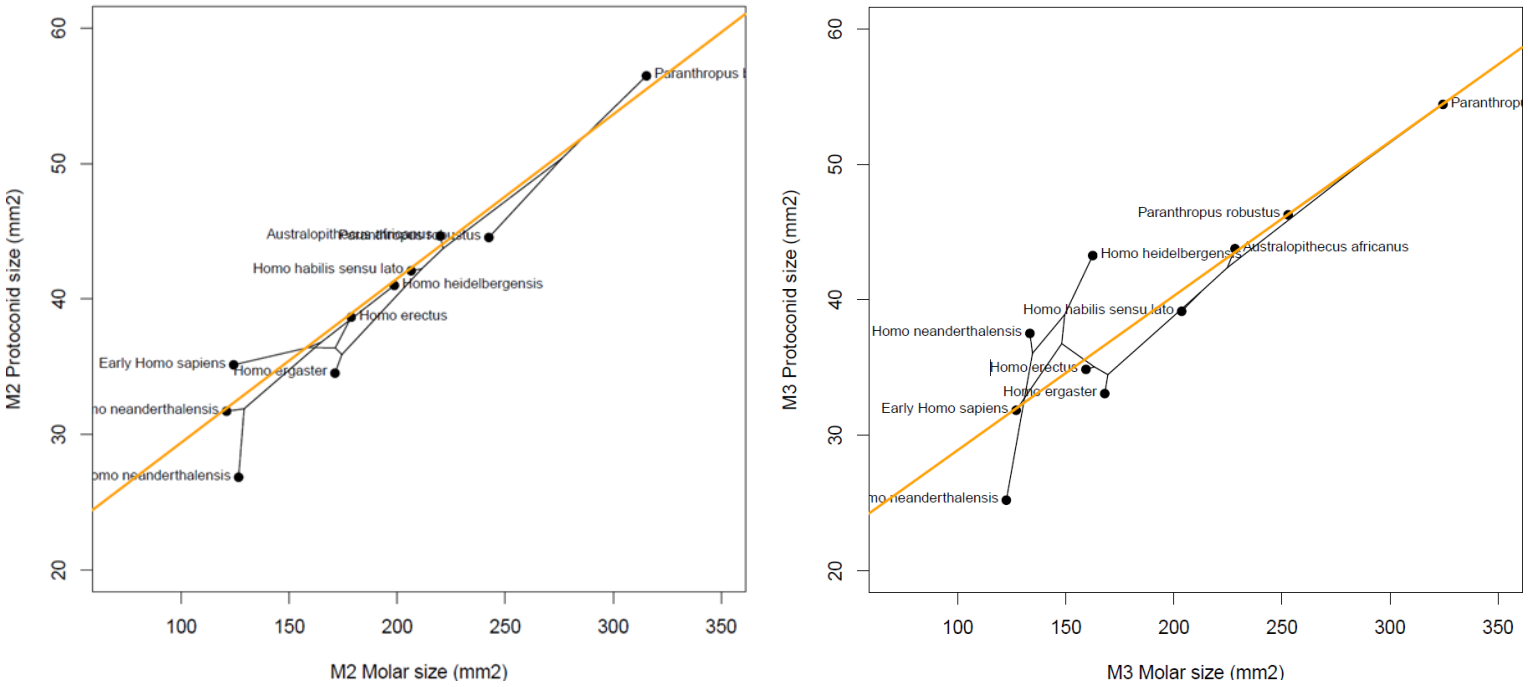

Figure 13. PGLS regression on M2 and M3 protoconid versus molar size (M1: Appendix IX (b))

Jernvall and Jung (2000) suggested that cusp patterning begins as early as a day after the formation of the tooth cap. This cap stage is a very early developmental phase in which the tip of the tooth bud folds and forms a cap-like structure. It is the stage when the primary enamel knot develops, shaping the future base of the tooth crown and initiating cusp patterning. These processes happen well before cusps are morphologically visible and before crown formation is complete (see Appendix X for illustration). Although Jernvall and Jung (2000) did not specify a particular species, the formation process they described is likely to be applicable broadly to primate tooth development and is therefore relevant to our hominin samples.

The different intercept of M1 obtained in PGLS might be viewed in light of this developmental framework. As the first molar to initiate, the first cusp (i.e. protoconid) begins its development very early, possibly much earlier than in M2 and M3. The relatively low intercept for M1 might suggest a weaker baseline relationship between protoconid size and molar size, although this hypothesis cannot be directly tested with our dataset (since with permanent molars, the

morphology of M1 at the initiation stage lies outside the range we examine, and it is also difficult to document due to the very limited availability of specimens at this developmental stage). The relative insensitivity of M1 protoconid size to variation in molar size is consistent with its role in initiating the inhibitory cascade, in which it influences the development of subsequent molars (and cusps). M2 and M3 protoconids, on the other hand, appear more responsive to later developmental events, with their sizes relatively closely linked to the changes in molar size and space, or developmental constraints, that act later in the molar formation sequence.

(3) Cusp 6 size *versus* molar size

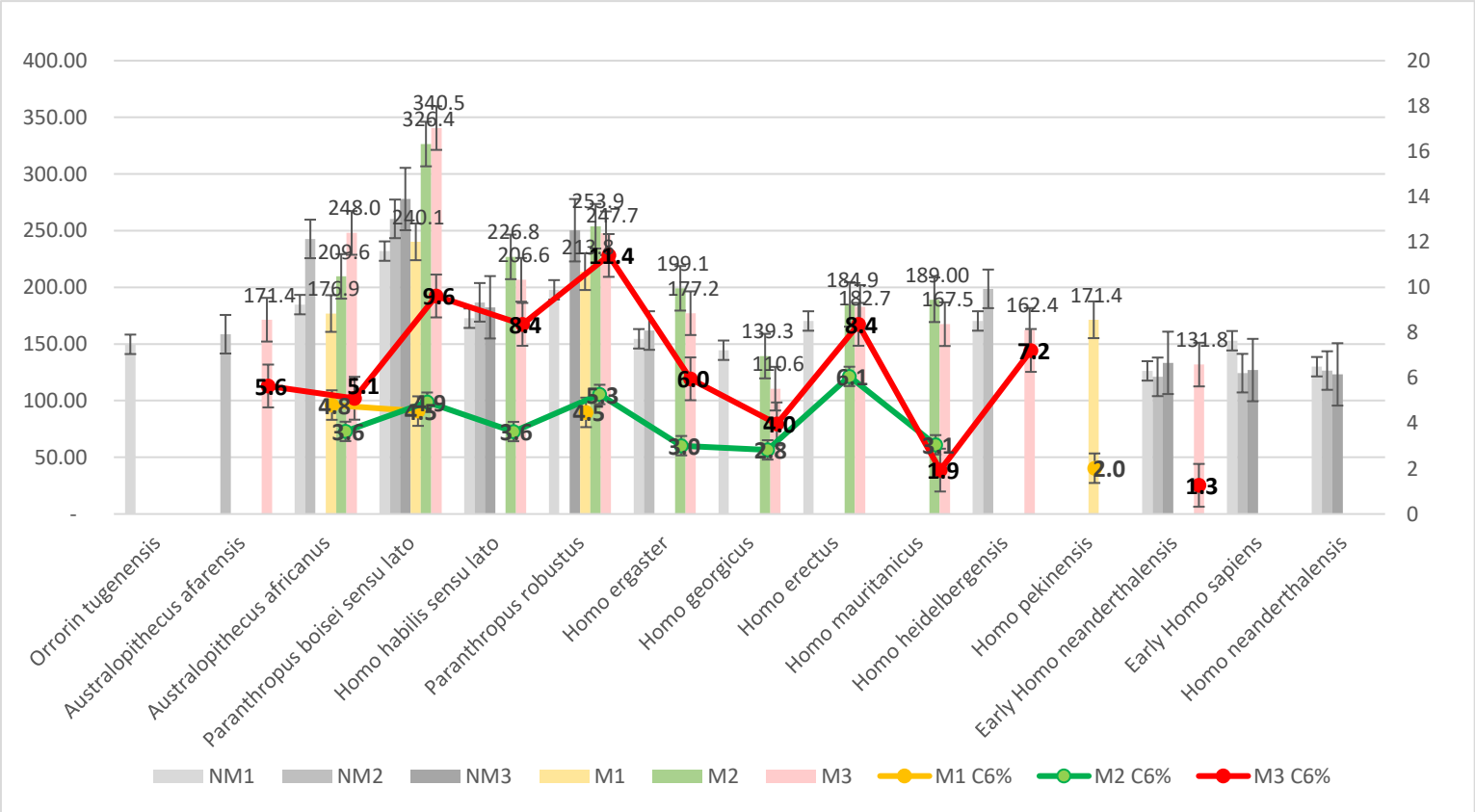

Figure 14. Relative cusp 6 size versus molar size by OTUs (molar size and sample size details see Appendix XI (a))

Legend: "N" refers to no, NM1/NM2/NM3 columns correspond to size of molar with cusp 6 absence

Fig. 14 shows that the relative size of cusp 6 varies much more than that of the protoconid. Only four OTUs have specimens with cusp 6 presence on M1, making the yellow M1 line barely visible. The limited occurrence of cusp 6 in M1 might be partly due to a small sample size, but might also reflect that cusp 6 is generally rare on M1.

Cusp 6 is more frequently expressed on M2, with proportions to molar size (relative size) ranging from 2.8% to 6.1%. The green trend line for M2 is comparatively stable, peaks in *H. erectus* and ends in *H. mauritanicus*.

M3 displays both the highest frequency and the greatest variability in relative cusp 6 size, from 1.3 % in Early *H. neanderthalensis* to 11.4 % in *P. robustus*. Unlike the relatively stable M2, the red line representing M3 shows more fluctuations: *Australopithecus* averages around 5%, *Paranthropus* reaches the highest values (*P. boisei*=9.6%; *P. robustus*=11.4%), and *Homo* spans the widest range, from 1.3% (Early *H. neanderthalensis*) to 8.4% (*H. habilis* and *H. erectus*). It is noteworthy that while *Paranthropus* and *H. erectus* both show high relative cusp 6 sizes in M2 and M3, variation in M2 is far narrower than in M3.

In general, as shown in Fig. 14, molars with cusp 6 tend to be larger in size than those without. This pattern is consistent with Skinner and Gunz's (2010) observation in chimpanzees' molars: the larger molars exhibit a higher frequency of cusp 6, because the larger size of the molar reduces spatial constraints on secondary enamel knot formation, and therefore results in short and widely spaced distal dentine horns that enable more space for additional cusps to initiate.

Table 12. Regression of absolute cusp 6 size on molar size (PGLS)

	y	*x*	Lambda	Intercept	P-value (intercept)	Slope	P-value (slope)	R^2
M1	Absolute cusp 6 size	Molar size	1.322	-2.130	0.337	0.050	0.000	0.489
M2			-0.605	-4.985	0.026	0.066	0.000	0.543
M3			-0.253	-13.442	0.002	0.138	0.000	0.726

The PGLS regressions result (Table 12) reveals a gradient in cusp 6's dependence on molar size increasing from M1 to M3. Cusp 6 in M3 displays the strongest association, with the highest slope (0.138), reflected by the "longest" phylomorphospace produced by the widely dispersed OTUs along the slope (Fig. 15 (b)), and also supported by a low p-value and the highest R^2 (0.726). M2 exhibits a moderate relationship (slope = 0.066; R^2 = 0.543) with less variability (Fig. 15(a)), while M1 shows the weakest association (slope = 0.050; R^2 = 0.489). The generally lower slopes and R^2 values of M1 and M2 suggest that their size of cusp 6 is less consistently predicted by the respective molar size compared to M3.

The regression intercepts become increasingly negative from M1 to M3. M1's intercept is not significant, indicating that the predicted cusp 6 size is not distinguishable from zero when the molar size approaches zero, might be due to the rarity of cusp 6 on M1 and therefore no defined developmental baseline is captured. The significant negative intercepts of M2 and M3 imply that a hypothetically small molar would predict a biologically implausible negative cusp size. The pattern suggests the potential existence of a developmental "threshold": for cusp 6, according to Skinner and Gunz's (2010), its formation requires sufficient molar crown size and cusp spacing between dentine horns to allow the initiation of an additional cusp (cusp 6). Such a threshold effect is conceptually similar to the "quasi-continuous" mode of variation or "threshold dischotomy" described by Hunter et al. (2010) for morphogenesis regarding the expression of Carabelli's cusp.

(a) PGLS on M2 cusp6 *vs.* molar size

(b) PGLS on M3 cusp6 *vs.* molar size

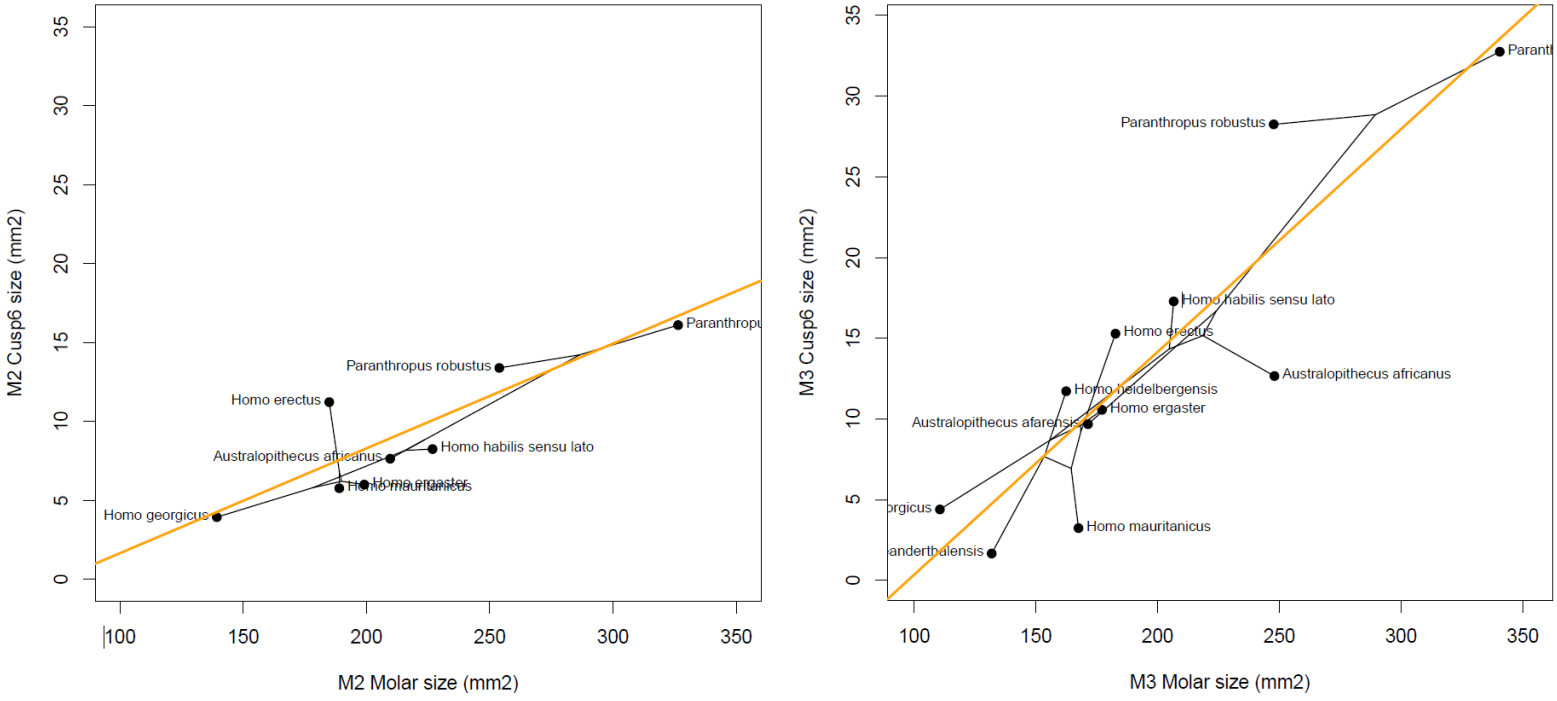

Figure 15. PGLS regression on M2 and M3 cusp 6 versus molar size (M1: Appendix XI(b))

Among the talonid cusps, the hypoconulid is frequently the smallest cusp and is considered to be the last to initiate (Davies et al., 2021). Bermúdez de Castro et al. (2022) also suggested that the sizes of distal talonid cusps are influenced by the trigonid cusps through the patterning cascade mechanism. Considering the distal position and accessory nature of cusp 6, which makes it generally relatively smaller than hypoconulid (in the ASUDAS system, only 2 out of 6 grades in

Cusp 6 describe the size of C6 as slightly/ markedly larger than cusp 5 (Scott and Irish, 2017)), it is reasonable to hypothesize that cusp 6 is also a late-forming cusp, probably the last cusp formed. As a distal accessory cusp arises between existing dentine horns, its initiation would depend on crown size and the spatial condition set by earlier cusps. This hypothesis is consistent with its high variability in M3, where the cumulative effects of developmental cascades are strongest. According to Jernvall (2000), small changes in early cusp initiation can be amplified through the cascade, transmitting the greater effects in later-developing cusps. Cusp 6 of M3, being the distal accessory cusp in the distal molar, is therefore expected to be particularly sensitive to the cumulative processes. This explains its higher variabilities across OTUs.

(4) Cusp 7 size *versus* molar size

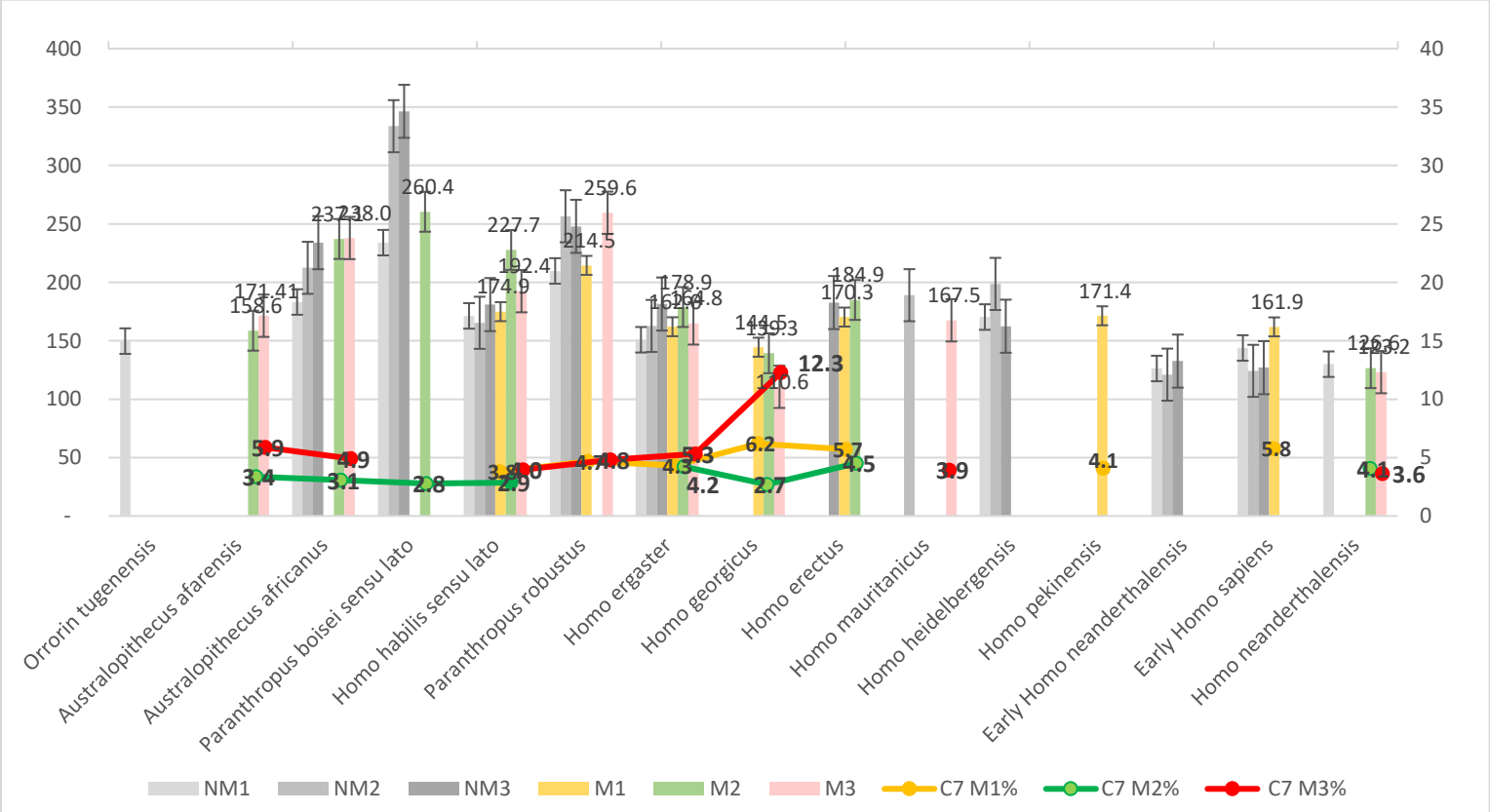

Figure 16. Relative cusp 7 size versus molar size by OTUs (molar size and sample size details see Appendix XII (a))

Legend: "N" refers to no, NM1/NM2/NM3 columns correspond to size of molar with cusp 7 absence

The relative size of cusp 7 is less variable compared to that of cusp 6. Fig. 16 shows comparatively stable patterns across molars. M1 has a slightly higher frequency of OTUs in cusp 7 expression

than cusp 6, with the cusp 7 proportion ranging from 3.8% (*H. habilis*) to 6.2% (*H. georgicus*) of molar size. M2 displays a similarly steady trend, but with a narrower range (2.8% to 4.5%), spanning less than 2 percentage points. The relative size of cusp 7 in M3 begins at nearly 6% in *A. afarensis*, maintains between 4%-5% through *H. ergaster* (5.3%), and then falls below 4% in *H. mauritanicus* and *H. neanderthalensis*. No obvious size difference is observed between molars with and without cusp 7, unlike what is seen with cusp 6.

The unusually high value of relative cusp 7 size in *H. georgicus* (12.3%) appears to be an outlier, potentially reflecting measurement uncertainty rather than true biological variation. The M3 corresponds to specimen D5099 LRM3, an isolated molar later assigned to the Dmanisi mandible D2735 by Margvelashvili et al. (2016) based on its fit within the mandibular dental alveoli. While cusp 7 was identifiable on the 3D model, the fissure boundaries were partially obscured by slight occlusal wear (Appendix XIII). Following the protocol of projecting fissures by their direction before they became attenuated, some additional area might have been assigned to cusp 7, leading to a modest overestimation. Excluding this case, cusp 7 proportions in M3 range between 3.6% and 5.9%, close to the range of M1.

Table 13. Regression of absolute cusp 7 size on molar size (PGLS)

	y	*x*	Lambda	Intercept	P-value (intercept)	Slope	P-value (slope)	R^2
M1	Absolute cusp 7 size	Molar size	-0.344	4.900	0.284	0.020	0.453	0.956
M2			-0.340	3.115	0.118	0.018	0.098	0.977
M3			-5.861	4.486	0.103	0.030	0.031	-0.066
M3	(Excl. *H. georgicus)*		0.467	-1.118	0.692	0.054	0.010	0.770

The PGLS regression results reveal a general weak association between the absolute size of cusp 7 and molar size, consistent with the earlier PCA results (Fig. 11 and Appendix VII), where cusp 7 followed a markedly different developmental trajectory. Among the three molars, only M3 shows a slope with a significant p-value (0.031) and a relatively higher slope (0.030) compared to those of M1 and M2. Yet the negative R^2 ($-0.066 \approx 0$) indicates a poor model fit in spite of the statistical significance. As shown in Fig. 17(a), the regression slope intersects only a subset of OTUs in the upper-right corner, with the phylomorphospace of M3 strongly pulled by *H. georgicus*, and makes the other OTUs scattered perpendicularly to the slope. It illustrates a weak explanatory power of the model.

When *H. georgicus* is excluded, the regression result becomes less abnormal and a better fit of the model: the slope increases (0.054), supported by a significant p-value and a high R^2 (0.770). As shown in Fig. 17(b), the OTUs cluster more tightly along the PGLS slope. This suggests that although cusp 7 generally exhibits a weak developmental link to molar size, M3, contrarily, shows a positive correlation and closer scaling with the molar size. Despite relatively high R^2 values, the slopes of M1 and M2 are non-significant, indicating that cusp 7 varies largely independently of molar size in the first and second molar position. Intercepts of M1-M3 are generally positive (except the adjusted M3 regression without *H. georgicus*), yet their low statistical support implies that no concrete baseline between the development of cusp 7 and molar size is captured.

(a) PGLS on M3 cusp7 *vs.* molar size

(b) PGLS on M3 cusp7 *vs.* molar size (*H. georgicus* excluded)

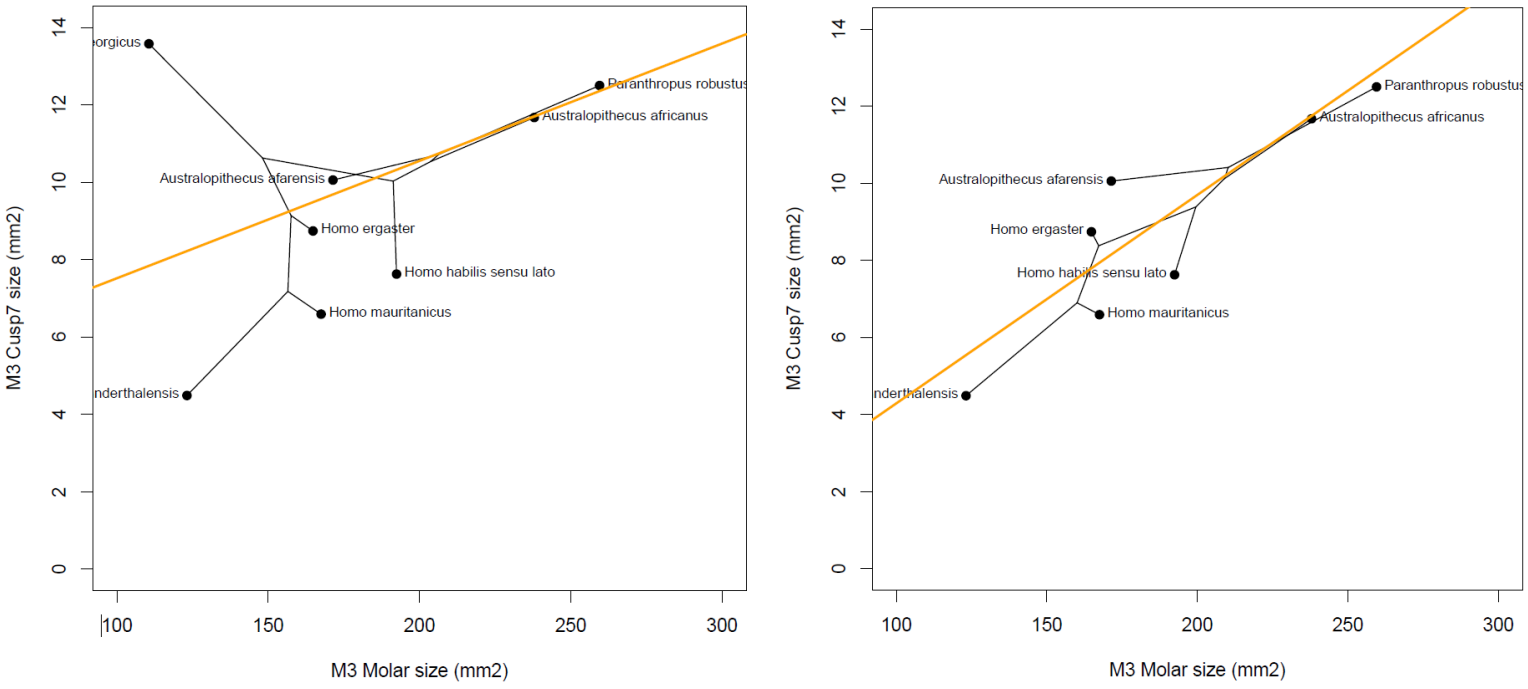

Figure 17. PGLS regression on M3 (with and without H. georgicus) cusp 7 versus molar size (M1 & M2: Appendix XII (b) & (c))

The much weaker association of cusp 7 with molar size compared to cusp 6 suggests that, although both of them are accessory cusps, the development pathways differ. Cusp 6, positioned distally, is typically linked to the later stage of overall cusp patterning, whereas cusp 7 develops along the lingual ridge between trigonid (mesial and earlier-forming) and talonid (distal, later-forming), metaconid and entoconid. While it is believed that the entoconid is typically initiated later than the

metaconid (Davies et al., 2021; Smith et al., 2007; Mahoney, 2008), it remains uncertain whether cusp 7 follows the same mesial-to-distal initiation sequence as the main cusps. Given its intermediate location, cusp 7 might initiate after the protoconid but before cusp 6, and its development might be more sensitive to spatial constraints imposed by surrounding main cusps within the overall crown architecture. The relatively stronger and significant slope of M3 likely reflects the cumulative effect of both molar and cusp cascading processes, which amplifies the scaling effect of molar size on cusp 7 expression.

DISCUSSION

The inhibitory cascade (IC) model

Effects of sampling strategies

In Test 1, we compared the four sampling approaches of the IC model with PRMA regressions. For mandibular samples, the consecutive molars (LC) sample produced slope and intercept values much closer to those predicted by the IC model, compared to those of the isolated molars (LI) sample. A similar pattern was observed in the maxillary samples. The result indicates that statistically, consecutive samples align more closely with both the developmental baseline (intercept) and the linear relationship between the IC model variables (M3/M1 *vs.* M2/M1). While being closer to the IC model slope and intercept is not inherently good or bad, the weaker fit of isolated samples likely reflects the fact that aggregating isolated molars without referencing their adjacent molars does not allow for taking into account properly the relative size relationships. Contrarily, consecutive samples retain the developmental context by producing results that more directly reflect the structure predicted by the IC model. This highlights not only the obvious discrepancies in results caused by different sampling strategies, but also that when the developmental pattern is preserved, hominin molar development shows, to a certain extent, higher consistency with the IC model. That could also explain why Evans et al. (2016) and D'Addona et al. (2024), who used isolated molar samples of fossil hominins, did not find their samples fit with the IC model. Boughner et al. (2021) and Bermúdez de Castro et al. (2021) used consecutive molar samples, but they were only within a single species. Since earlier studies analysed either isolated molars or consecutive molars within single species, our analysis, based on consecutive molars across multiple hominin species, provides a perspective in which the IC model may show higher consistency than in isolated molar samples that were commonly used in earlier studies.

At the same time, the lambda (λ) values reported in the PRMA regressions on isolated molar samples were unexpectedly high, with both mandibular and maxillary samples exceeding 0.9. Although λ in phylogenetic regressions itself does not measure phylogenetic signal, it does reflect the degree to which the regression optimises when the residuals are modelled as following the phylogenetic covariance structure, e.g. values close to 1 indicate a strong phylogenetic component in the fit. In Table 3, consecutive molar samples show lower lambda values at 0.761 (LC) and 0.595 (UC), indicating weaker covariance structuring of the residuals from the phylogeny compared to those of the respective isolated samples.

The reasons for these differences in λ values between sampling approaches are uncertain, but we can propose several hypotheses (which are not necessarily mutually exclusive): (1) isolated molar samples (LI and UI) combine molars not belonging to the same specimens might artificially inflate variation; (2) phylogenetic structure differs between samples, since more OTUs were included in the isolated samples, expanding the referencing phylogenetic trees compared to the ones corresponding to the consecutive molars samples; (3) there are undeniable possibilities that isolated molars might sometimes be misattributed taxonomically due to limited diagnostic features, particularly the absence of adjacent molars that would otherwise provide referencing points; and (4) consecutive molars align more closely with the expected developmental scaling and thus require less phylogenetic structuring, whereas isolated molars might be farer from the developmental scaling and thus push the model to optimise λ upward.

As further verified by Test 2 Part 2, simply increasing the sample size by including more isolated molars in the samples does not clarify relative size relationships. Instead, it might add noise and dilute species-specific patterns. This risk is particularly evident in OTUs represented by small or very small samples. For instance, *H. antecessor* is represented in the lower consecutive (LC) sample by one single specimen (n=1), whose "unusually" small M3 (81 mm², compared to M1 (115.5 mm²) and especially M2 (135.3 mm²)) drives its outlying position in the regression (Fig. 3 and Fig. 5). Adding more isolated molars to this OTU could dilute its distinctive characteristics and thereby mask potential lineage-specific signals.

However, in precisely such cases of very limited representation, isolated molars can, on the other hand, counterbalance the disproportionate influence of "atypical" individuals. Through aggregating more specimens, more "general" molar proportions might be generated, and therefore

appear closer to expectations from shared ancestry. This likely explains the higher lambda values observed in isolated molar samples: by diluting individual variation, the data align more closely with phylogenetic structure, but at the cost of blurring distinctive morphological signals. While isolated molars might sometimes enhance phylogenetic signal (particularly in OTUs represented by very small samples), consecutive specimens remain the more reliable basis for capturing the developmental logic of molar proportions in general.

The IC model *versus* the MMC: length or size?

Test 2 reveals no greater ability performance of length (MD) over size (i.e. computed area of the crown surface) observed as a proxy for modelling molar relationships, with length generally exhibits weaker associations across ratios, absolute measurements, and total molar size. For the IC model (Table 4), the original size-based version yielded a strong slope and a higher R^2 value between variables compared to the length-based version, along with a slightly better fit of residuals to phylogeny (as indicated by the lambda value). Similarly, for the MMC (Table 5) that emphasises length measurements, the size-based version also demonstrated higher slopes and R^2 values, despite a modestly lower lambda. While the better performance of size in the IC model is expected (since it was originally defined in terms of size), the absence of stronger performance by length in the MMC (which explicitly emphasises length ratios) is more surprising, since the result suggests that length does not significantly outperform size.

Hlusko et al. (2016) and Monson et al. (2022) argued that taxonomic differences in MMC may represent underlying genetic variance, thereby reflecting the genetic architecture driving phenotypic variation. However, our analyses do not support this for MD length. Neither phylogenetic signal tests (Blomberg's K) on univariate traits nor lambda values from bivariate residual structures indicated an outstanding ability of length to reflect these evolutionary relationships. Conceptually, if a phenotype is more directly patterned by genotype, one would expect clearer alignment with phylogeny, as these would manifest statistical tendencies towards inheritance. In our hominin sample, however, this tendency was not observed: length consistently "underperformed" relative to size in these regards, suggesting that it is not particularly effective at reflecting phylogenetic relationships or in capturing the developmental–genetic architecture underlying molar morphologies.

Given the challenges of experimental validation (e.g., culturing primate molars) and the limitation of tracing traits through early hominin pedigrees (which do not exist in reality), the statistical patterns consistently prove that size-based measures may provide a more reliable proxy for inferring evolutionary and developmental dynamics in hominins.

The IC model *versus* the MMC: M1, M3… and M2?

Test 2 also highlights that the explanatory potential of the MMC lies less in the measurement metric (length *vs.* size), but more in the specific molar positions it involves (i.e. M1 and M3). By focusing on only M1 and M3, the MMC may be able to explain most of the variability of the molar row (Monson et al., 2022; Lucas et al., 1986), but this simplification might come at the cost of omitting the developmental role of M2.

The M2/M1 ratio exhibits the strongest phylogenetic signal among all ratios and variables tested (Blomberg's K=0.628, p=0.011), which points to its evolutionary conservation across hominin lineages. On the other hand, the PGLS regression of M2/M1 against total molar size (Table 6) displays only an insignificant association under phylogenetic correction. It suggests that the M2/M1 stability reflected by the high K-value implies inheritance from a common ancestry rather than independent variation with molar size. The conserved nature is consistent with the central position of M2 in the inhibitory cascade, where it maintains a proportional relationship to the molar row (i.e. almost isometry to total molar size).

Results in Test 3 reinforce this interpretation. While M1 and M3 show strong positive correlations with mandibular width (R^2 of M1= 0.857; R^2 of M3=0.913), M2 shows only a weak association (R^2 = 0.095). The results might seem contradictory: if space availability, effectively, or to a larger extent, determines the total molar size, how could M2, which scales nearly isometrically with the total molar size, be weakly associated with the available space? A plausible explanation is that the size of M2 is not directly constrained by the external space; instead is secondarily regulated through the inhibitory cascade: M1 sets the initial baseline relative to available space, and M2 is then patterned in proportion to M1, usually around one-third of the total molar area. By this, the proportionality of M2 to total molar size is usually stably maintained through developmental signaling rather than directly by spatial constraints.

Allometric results in Test 4 further support these dynamics. M1 scales with negative allometry that reflects its relative stability as the earliest-initiated molar and the baseline setter of the cascade model. M3 contrastingly displays strong positive allometry, which highlights its developmental sensitivity to total molar size and the cumulative inhibitory effects. M2 scales close to isometry, consistent with its role as an intermediate element: while not strongly dependent on space, it transmits inhibitory signals downstream to M3, helping translate the total molar size into a final balance of proportions.

If M2 is excluded, it might risk overlooking a crucial element of molar development. While the M3/M1 ratio captures broad variation from the starting and ending points of the molar row and correlates strongly with total molar size, it misses the conserved intermediate role of M2, which is central to the inhibitory cascade mechanism. By incorporating all three molars, the IC model therefore provides a more complete account of the developmental and evolutionary dynamics of the molar row.

The IC model on hominins

Despite the broad agreement with the IC model, Test 2 shows a weaker statistical fit of the IC model compared to the MMC, in terms of the variance explained (R^2) and the model residual fit to phylogeny (λ). The differences might reflect the higher number of measurements involved in the IC model: it requires both M3/M1 and M2/M1 size ratios, which depend on six MD x BL measurements across M1-M3, whereas the MMC, like a very simplified version of the IC model, relies on only two values (M1MD and M3MD). With more parameters, there is a lower probability that the data will align neatly with the model. In the LC sample, the PRMA slope in Fig. 3 runs broadly parallel to the standard IC slope, yet the low R^2 (which reflects a loose clustering of data points, i.e. OTUs, around the fitted PRMA line, implying a weak linear relationship) suggest that the hominin mandibular molars are in line with the IC model rather qualitatively.

Notably, this weaker fit is not universal: the UC sample (maxillary molars) produces a slope that matches the standard IC prediction more closely, as shown in Test 1 and Test 4. It statistically suggests that, based on the maxillary molars, hominin molar development largely follows the inhibitory cascade mechanism. Also, when placed in the broader comparative context of mammals using consecutive maxillary molar data from Billet and Bardin (2021), hominin species cluster

much closer to the standard IC slope (blue line) than most other mammals (Fig. 18), despite a slight deviation of their own slope.

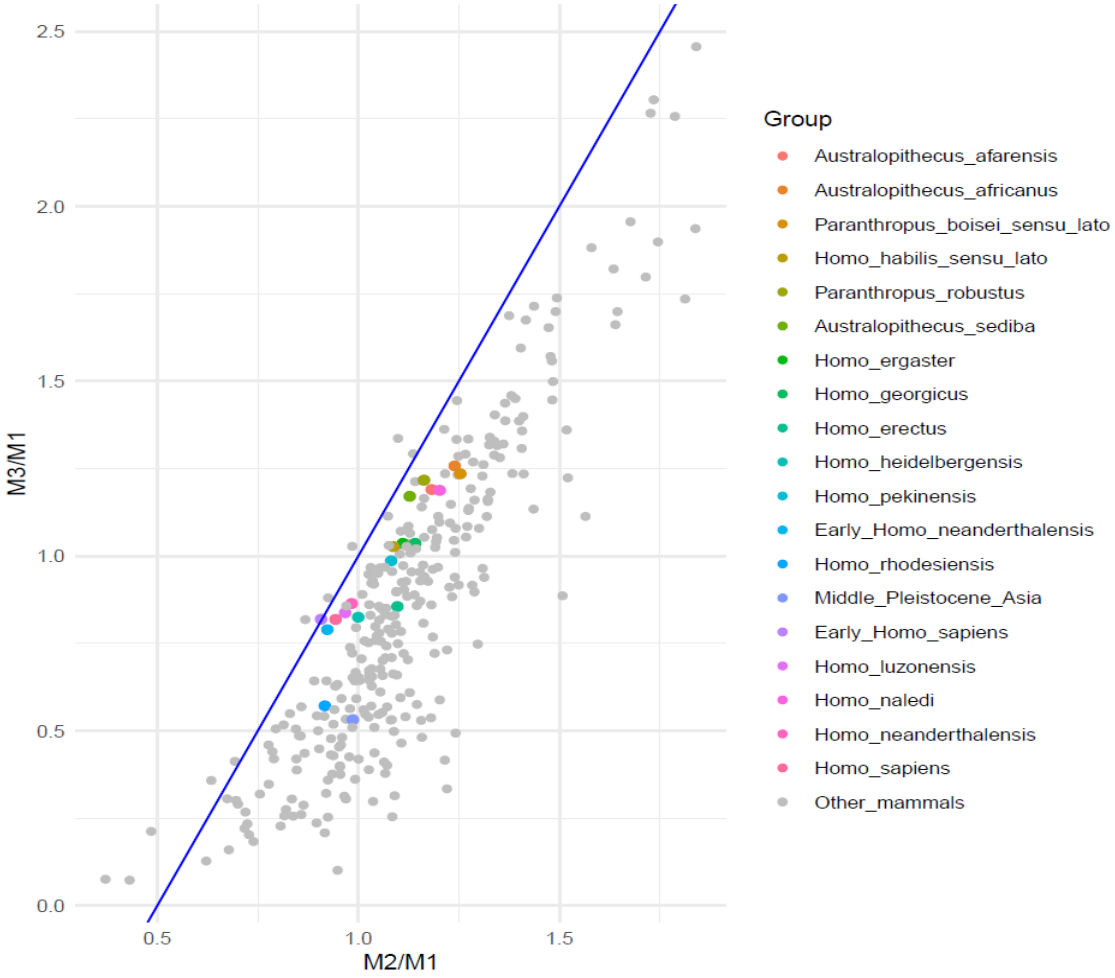

Figure 18. A compilation of our upper consecutive molar data of hominins and the upper consecutive molar data of other mammals from Billet and Bardin (2021)

Illustrates how hominin upper molars cluster along the IC slope (blue line) compared with those of other mammals

This answers directly to the first question raised in this report: humans, and hominins in general, conform to the IC mechanism in the same way as other mammals, and, in fact, their alignment with the model is even stronger than in other taxa. One might argue that mandibular and maxillary molars develop under different dynamics (as shown in our result) and might not be directly applicable to the maxilla, especially since the IC model was first demonstrated on mouse mandibular molars. However, it is worth recalling that the original experimental molars used to prove the inhibitory cascade were grown from *in vitro* tooth germs separated from jaw tissues

(Kavanagh et al., 2007), and therefore outside the mandibular developmental environment. That means, the molar development suggested by the IC model should be minimally affected by the spatial constraint from the jaws.

Mandible *versus* maxilla

The absence of maxillary width measurements in this study limits a direct comparison of spatial influence on molar size between the maxilla and mandible. It therefore remains uncertain whether spatial constraints operate in the maxilla the same way as in the mandible. Nonetheless, Test 4 (Table 9) shows that maxillary molars exhibit slightly higher allometric slopes with total molar size than mandibular molars, suggesting a generally greater sensitivity of maxillary molars to total molar size, particularly for M3. The differences in allometry might relate to the timing of molar formation: in humans, mandibular molars generally complete crown formation and erupt (or finish eruption) slightly earlier than maxillary molars (White et al., 2012), implying that later-forming molars might be more responsive to variations in total molar size. While such timing disparities could explain the subtle allometric contrasts observed, they are too weak to account for the pronounced M3 reduction or obviously closer fit of maxillary molars to the IC model.

The divergence between jaws might reflect a broader developmental integration. Billet and Bardin (2021) proposed that maxillary molar allometry is linked to craniofacial growth by sharing the same mechanism. The maxillary integration with the neurocranium could foster a spatiotemporal linkage between jaw growth and molar formation. When M3 forms last and in the most posterior position of the maxilla, its growth might be more sensitive to jaw size: larger jaws could support relatively larger posterior molars, whereas smaller jaws might be associated with greater M3 reduction. Since the growing jaw's biomechanics actively constrain the shape of the molar (Renvoisé et al., 2017), potentially the smaller M3 might have resulted from a more compressed posterior palate of the maxilla, due to stronger limitation on the posterior maxilla itself for its role in accommodating cranial development. Mandible, being less tightly integrated with the cranium, is considered to be less influenced by the cranial-facial development, and thus shows a much subtler reduction of M3 size compared to the maxilla.

Whether or not this hypothesis is correct, it is unlikely that maxillary molars develop independently of space availability. Evidence of positive correlations between maxillary dimensions and M3 development (Marchiori et al., 2019) suggests that spatial factors do influence the upper jaw

molars, though to a different extent than in the mandible (as shown in Test 3). Although the IC model was originally established *in vitro* independently from jaw influence, it was also verified *in vivo* across 29 murine rodent species (Kavanagh et al., 2007). It indicates that the IC model, developed independently of jaw considerations, is nonetheless able to predict molar proportions *in vivo*, even in the presence of jaw influence. While rodents presumably experience some jaw influences, such as spatial constraints, the strength of those constraints relative to inhibitory signaling is unclear. In hominins, the closer alignment of maxillary molars with IC predictions compared to the mandibular molars suggests that either the spatial effects play a stronger role in the upper jaw than in the mandible, or that maxillary molars are further shaped by higher-level developmental processes tied to craniofacial growth. If space and inhibition operated equally across both jaws, it would be expected that mandibular molars show a more similar degree of fit to the model. Their divergence highlights the possibility that molar development is shaped by multiple layers of developmental control, from local cascade dynamics to jaw-specific spatial effects and broader craniofacial/ anatomical integration.

Patterning cascade model on cusps

The earliest cusp: protoconid

Test 5 demonstrates that the protoconid cusp is highly stable across hominins. Its absolute size varies proportionally to molar size, while its relative size remains largely consistent across OTUs throughout evolution, especially in M1. In early hominins, the protoconid size was especially stable, as shown in Fig. 13 (a-b) and Appendix IX (b): the early OTUs cluster tightly along the upper-right part of the PGLS slopes for M1-M3. Subtle differences in dynamics, however, appear within the genus *Homo*, especially more recent OTUs including *H. heidelbergensis*, Early *H. neanderthalensis* and Early *H. sapiens*. For example, *H. heidelbergensis* shows protoconid size below the slope in M1, on the slope in M2, and above the slope in M3; whereas Early *H. sapiens* generally plots above the slopes for M1 and M2 but aligns with the slope for M3. While these shifts possibly reflect differences in how protoconid growth interacts with the overall molar size development, the underlying mechanisms remain unclear. It might also simply result from the very limited sample size available for these OTUs (Appendix IX(a)), which could bias the observed patterns due to the limited representativeness.

In general, the results indicate that the protoconid cusp of hominins did not develop as fixed absolute size (e.g. M2 protoconid absolute area ≈ M3 protoconid absolute area), as observed by Bermúdez de Castro (2022) on modern humans. Instead, they scaled proportionally with crown size. Given that the protoconid formation is governed by the molecular control of the primary enamel knot (rather than secondary enamel knots that govern other cusps) and forms very early, its growth appears tightly integrated with crown development. In this sense, the size of the protoconid is not passively determined by crown size; instead, both protoconid cusp and molar crown develop in parallel under shared developmental controls. The co-developmental process also explains the proportional stability of the protoconid in relation to molar size across species.

The distal accessory cusp: cusp 6

Test 5 demonstrates that cusp 6 develops through a distinct process from the protoconid. Like other cusps that form after the protoconid, it arises under the regulation of secondary enamel knots after the crown base has been established. As an accessory cusp, it originates outside the inhibition zones of the earlier cusp. Its distal position, forming after both the trigonid and talonid cusps, determines that its size is strongly dependent on the remaining crown area, i.e. occupying space not already claimed by earlier-forming cusps. It seems to be the exact opposite of the protoconid, which co-develops with the crown under the control of the primary enamel knot.

As shown by the results, the variability of cusp 6 is not uniform across molars. It is most pronounced in M3, relatively stable in M2, and less evident in M1. This mirrors the pattern of developmental dynamics also observed in the protoconid: the first cusp to form (protoconid) is characterised by its stability, most evident in the first molar (M1), whereas the last cusp to form (cusp 6) is characterised by its variability, which is maximised in the last molar (M3). This pattern not only supports Jernvall's (2000) observation that small differences in early development can be amplified to produce large variation in later-forming structures, but also highlights the influence of molar position on cusp patterning. While each molar develops its cusps through a succession of primary and secondary enamel knots in the cascading dynamics, the molars themselves are initiated sequentially along the row. In the case of cusp 6 on M3, the cumulative developmental signals from both earlier cusp and earlier molars are maximised, and therefore produce the highest variability.

The protoconid and cusp 6 together represent the two ends of the developmental spectrum: fixed early by the primary enamel knot, the protoconid reflects stability, whereas cusp 6, shaped by the cascading influence of both cusp-level and molar-level sequences, reflects cumulative variability. Although space is necessary for cusp 6 to form, the "space" is not an independent determinant. Instead, it is the outcome of a slightly upper-level developmental process, i.e. sequential molar initiation, rather than local cusp cascading on crown occlusal alone.

The lingual accessory cusp: cusp 7

In contrast to the clear trajectories of the protoconid and cusp 6 reconstructed in Test 5, the developmental pattern of cusp 7 is less evident. As shown in Fig. 16, none of the molar positions (M1-M3) display a particularly pronounced pattern in relative cusp 7 size. At first glance, cusp 7 appears to scale proportionally with molar size, resembling the apparent stability of the protoconid. However, unlike the protoconid, cusp 7 forms under the governance of secondary enamel knots, outside the inhibition zones of earlier cusps, similar to cusp 6. It is therefore surprising that cusp 7 shows far less variability than cusp 6.

There might be several factors that contribute to this visual stability. First, cusp 7's location between the trigonid and talonid may constrain its development more tightly than distal accessory cusps. Second, cusp 7 is generally small in size, and smaller structures tend to show reduced proportional variability compared to larger cusps such as the protoconid (≈20% of crown area) or cusp 6 (ranges 1.3–11.4% of crown area). Third, the limited number of specimens with cusp 7 presence largely reduces sample size and may bias representation.

Despite the visual stability in relative size (Fig. 16), cusp 7 does not share the same developmental integration with crown growth as the protoconid. The PGLS results in Table 13 confirm a generally weak association between cusp 7 and molar size. However, a significant relationship was detected in M3 at the same time ($p=0.031$; $p=0.010$ with *H. georgicus* excluded). This, on one hand, could reflect a false positive arises from the large number of tests performed, a risk that would ideally be controlled for by multiple-test corrections such as Bonferroni (Dunn, 1961). Yet on the other hand, the high slope of M3 cusp 7 (0.054 without *H. georgicus*) and its strong explanatory power ($R^2 = 0.770$) suggest the association is unlikely to arise from chance alone. In this view, the significant slope may indicate that cumulative effects which influence the last molar might also extend to cusp 7, partially resembling the variability pattern of cusp 6. It reinforces the possibility

that small developmental differences might get amplified and reflected in the last-formed molar: M3.

The timing of cusp 7 initiation within the sequential cusp initiation process is not clearly understood. It may form between the completion of the trigonid and the initiation of the talonid, or after both complexes are established. Its mixed features, i.e. low variability resembling the protoconid, combined with a tendency toward cumulative effects in M3 resembling cusp 6, make cusp 7 an important cusp to understand the intermediate stage of accessory cusp development. For the intermediate stage between protoconid and cusp 6, there are several other main cusps (i.e., metaconid, entoconid, hypoconid and hypoconulid for lower molars) also formed under the regulation of the secondary enamel knots and are initiated midway through the whole cusp patterning process. They are worth studying too because comparative analyses of these main cusps alongside cusp 7 would be particularly informative, as they may reveal whether cusp 7 arises within a broader developmental pattern of mid-sequence cusp formation, or a distinct accessory pathway. While this study did not investigate other main cusps apart from the protoconid, such comparisons would probably provide empirical insights for reconstructing the full sequence of cusp formation and its relationship to molar size.

Accessory cusps overall and phylogeny

Although the sequence and formation mechanism of cusp 7 cannot be fully explained by our data – since its weak association with molar size does not fully align with expectations from the patterning cascade, contradicts to the assumption that accessory cusp development should be influenced by the size and spacing of earlier cusps - it is likely due to limited sample size, as well as our limited understanding of the "space" between earlier forming cusps, thus should not be taken as evidence that the cascade is inadequate to explain variation in cusp 7.

For cusps with clearer positions in the developmental sequence, the cascade model performs more consistently. Although the possibility that some cusps are not strictly homologous across species and specimens cannot be excluded (where homologous refers to two structures represents corresponding parts of organism built according to the same body plan (Wagner, 1989)), the observed patterns align with developmental expectations: the stability of the protoconid, particularly in M1, and the marked variability of cusp 6 and cusp 7, particularly in M3, are in line with Davies et al. (2021)'s observation that accessory cusps are not individually patterned between

cusps. It also points to a broader level of cascading pattern between molars, where molars themselves are influenced by the development of earlier molars in the row, to produce variation of cusp size expression between molar positions.

In Test 5, no OTU or clade consistently exhibited a distinct pattern in accessory cups, such as consistently large or small cusp 6 or cusp 7. It might, on one hand, be again due to the limited sampling; yet on the other hand, it accords with Davies et al. (2021)'s argument that accessory cusps are not good phylogenetic markers. It is because their presence and size are shaped by multiple arrangements between cusp size and spacing, rather than being directly determined by unique genetic programs. As Jernvall and Jung (2000) suggested, all cusps that arise from the secondary enamel knots express the same set of genes, with the formation process repeating until the cusps are all patterned. Trait differences might therefore indirectly be determined by more gene-related factors such as crown size and cusp spacing, which in turn modulate the likelihood of accessory cusp formation (Davies et al., 2021).

Although some taxa may show a higher tendency for particular accessory cusps, the PGLS regressions on each molar and accessory cusp (with mostly negative λ values) indicate that model residuals do not follow phylogenetic structure. Instead, OTUs that deviate from the regression slopes tend to show accessory cusp sizes vary independently of the phylogeny. This provides indirect additional support for the conclusion that accessory cusps are not reliable traits for both taxonomic differentiation and phylogenetic reconstruction.

Cusp number

Only limited results on cusp number were obtained in this study due to sample limitations. In several specimens, molars exhibited a clearly defined cusp 6 or cusp 7, but were heavily worn elsewhere on the occlusal surface, which makes reliable counts of the total cusp number impossible. As a result, usable data were very limited, and segmenting traits by cusp number further reduced usable observations. Moreover, cusp number is an ordinal variable ranging only from 4 to 7, making it unsuitable for regression against continuous variables such as molar size or cusp size.

The PCA revealed that cusp number, as the outcome of sequential cusp formation regulated by the secondary enamel knot (including cusp 6 and cusp 7), clusters most closely with cusp 7, rather than with cusp 6, protoconid, or molar size. It suggests that variation in cusp count might be more

strongly linked to the presence and relative development of cusp 7 than to molar size itself. One might expect that larger molars would simply accommodate more cusps due to the increased occlusal space. However, the results indicate this might not be consistently the case. In our results, larger molars express cusp 6 more often, which contributes one additional cusp to the count. Yet once present, it seems that the cusp 6 tends to take up space and scale with the molar size, rather than driving additional cusp formation. There might be more than one interpretation for this observation.

Interpretation of cusp 6 is also complicated by its different definitions in the literature (Wood, 1983, 1991; Skinner and Gunz, 2010; Davies, 2021). Much of our cusp size data was compiled from the monograph of Wood (1991), where cusp 6 size was treated as a single trait regardless of whether one or two adjacent distal accessory cusps were present; in cases of a "double" cusp 6, the total area was incorporated as one measurement. Under this definition, the relationship reflected in the PCA result is straightforward: larger crowns accommodate larger cusp 6, with little indication of a direct link between cusp 6 size and cusp number. By contrast, Skinner and Gunz (2010) found on the EDJ of chimpanzees' molars that the "double" cusp 6 reflects an additional cusp formed by a small dentine horn adjacent to the main cusp 6, generated through the same iterative developmental process as the primary accessory cusp. This interpretation implies that the larger "cusp 6" values in our dataset may sometimes represent two cusps rather than one enlarged cusp.

While our data cannot separate these cases, the way cusp 6 is defined, again, raises the issue of whether our cusp 6 measurements always refer to homologous structures: in some cases, it may denote a single cusp and in others a combined area of two adjacent distal cusps. Nonetheless, both outcomes, in fact, follow the same developmental logic of the patterning cascade: larger molars with more space allow the initiation of accessory cusps, which may manifest in either as an enlarged cusp 6 or as an additional cusp next to it. In this sense, even if cusp 6 is not strictly homologous across cases, the variation we capture still reflects the cascading pattern that later-forming distal cusps show greater variability in size and number as space in the molar crown increases. It also does not contradict the result in Test 5 that after the cumulative effect of the cascading, the last molar (M3) shows higher variability in terms of space provided between cusps, and as a result allows more distal cusps (or/ instead of larger cusp 6) initiated in the distal part of

the crown. As for the PCA result, the independence shown between cusp 6 size and cusp number may therefore reflect a limitation of how cusp 6 was defined and measured, rather than an absence of developmental association.

The stronger association of cusp number with cusp 7 size, on the other hand, suggests that cusp 7 formation may be tied to overall cusp count, due to some unknown mechanism. The following implications are also uncertain, as the mechanisms governing cusp 7 formation are unresolved. Future studies with larger samples and data on additional main cusps might clarify whether cusp number influences cusp sizes or *vice versa*, and may potentially provide deeper insights into patterning cascade dynamics on cusp formation.

Size determination of molars

To answer our central research question: how do the developmental mechanisms determine hominin molar size? Our results suggest that the inhibitory cascade mechanism should be understood not as a standalone rule, but instead as a component of a complex and hierarchical system that also incorporates spatial constraints. The final molar morphology is the result of the interaction between an intrinsic patterning sequence and the broader anatomical environment where the sequence operates.

At the local level, where the inhibitory cascade lies, the sequence of initiation is established for the molars along the jaw (M1- M3) and for the cusps within each crown, governed by the primary and secondary enamel knots. The order of initiation provides a fundamental rule that determines relative proportions, and thus explains the stability of early-formed structures (e.g., M1 and the protoconid), and, contrarily the high variability of late-formed ones (e.g., M3 and cusp 6).

However, the cascading sequential process does not operate in a vacuum. Our analyses show that sequential dynamics alone do not fully explain variation in size; rather, they are modulated by the spatial context of the surrounding anatomy. At the cusps level, the crown area mostly sets the surface within which the developmental sequence operates, explaining how larger crowns allow the initiation or enlargement of an accessory cusp. At the molar level, jaw dimensions define the physical boundaries of the entire row, with a wider mandible supporting larger molars overall. In this way, anatomy provides the scaling framework that channels the output of the patterning cascade into individual morphology.

These spatial influences themselves arise from a broader developmental organisation. The distinct pathways of the maxilla and mandible, particularly the tighter integration of the maxilla with cranial growth, likely explain the differences in molar proportions between the upper and lower jaw, as well as their different degree of alignment with the IC model. Therefore, the jaw-level (and/or craniofacial-level) process adds further layers of regulation above the local cascade.

Taken together, molar size determination in hominins is best understood as a developmental hierarchy: broader anatomical development shapes jaw architecture, jaw dimensions set spatial boundaries, and the inhibitory cascade operates within these constraints to produce final proportions of molars and then of cusps. In this sense, the balance of activator and inhibitor signals in the cascade mechanism should not be seen as a final determinant but as a developmental "midpoint," integrating higher-level influences before producing the final dental phenotype.

CONCLUSION

This study reframes hominin molar size determination as a hierarchical process and positions the inhibitory cascade (IC) model as a mid-level rule whose explanatory power of hominin molar development lies in its integration with broader anatomical contexts.

By deconstructing the IC model, we demonstrate that molar size represents the minimum level to which the cascade can be meaningfully expressed, as it reflects the motions of primary and secondary enamel knots in establishing the crown base as an integrated developmental field. Further subdivision into linear dimensions (e.g. MD length) would result in a loss of developmental coherence.

In this hierarchy, developmental outcomes at each level - from enamel knots that establish local cascades, to jaws that define spatial limits, to the broader anatomical organisation that possibly integrates teeth within skeletal growth - are constrained and shaped by the context of the next, and ultimately produce the final morphology.

However, the integration of the IC model's sequential structure with spatial dynamics is only partially resolved. Based on the evidence from mandibular width and previous studies on maxillary spatial constraints on humans, we deduced the high possibility that upper molars are subject to stronger spatial regulation, potentially related to craniofacial development. Yet this speculation

could not be tested in this study directly due to the absence of maxillary width measurements, which are difficult to quantify. Also, the development mechanism of cusp 7 remains unclear due to the limitations in sample representations and the scope of the study. Further studies with larger comparative datasets, with measures of maxillary available space and additional main cusp measurements, are suggested to clarify the developmental processes occurring mid-sequence during cusp initiations (which possibly mirrors the process in the midway of molar initiation correlated to M2).

Finally, while this study focuses on proximate mechanisms, it is important to note that these developmental processes only set the stage. As Darwin (1871) emphasised, variation affords the raw materials for natural selection, and the diversity of molar size and proportion we observed in hominins reflects not only developmental rules but also the ecological and adaptive pressures that shaped them.

BIBLIOGRAPHY

Bailey S.E., Pilbrow V.C., Wood B.A. 2004. Interobserver error involved in independent attempts to measure cusp base areas of *Pan* M1s. *Journal of Anatomy* 205, 323–331.

Bermúdez de Castro, J.M., Modesto-Mata, M., Martín-Francés, L., García-Campos, C., Martínez De Pinillos, M., Martinón-Torres, M., 2021. Testing the inhibitory cascade model in the Middle Pleistocene Sima de los Huesos (Sierra de Atapuerca, Spain) hominin sample. *Journal of Anatomy* 238, 173–184.

Bermúdez de Castro, J.M., García-Campos, C., Sarmiento, S., Martinón-Torres, M., 2022. The protoconid: a key cusp in lower molars. Evidence from a recent modern human population. *Annals of Human Biology* 49, 145–151.

Billet, G., Bardin, J., 2021. Segmental Series and Size: Clade-Wide Investigation of Molar Proportions Reveals a Major Evolutionary Allometry in the Dentition of Placental Mammals. *Systematic Biology* 70, 1101–1109.

Blomberg, S.P., Garland, T., Ives, A.R., 2003. Testing For Phylogenetic Signal In Comparative Data: Behavioral Traits Are More Labile. *Evolution* 57, 717–745.

Boughner, J.C., Marchiori, D.F., Packota, G.V., 2021. Unexpected variation of human molar size patterns. *Journal of Human Evolution* 161, 103072.

Brakefield, P.M., 2011. Evo-devo and accounting for Darwin's endless forms. *Phil. Trans. R. Soc. B* 366, 2069–2075.

Clarke, M.R.B., 1980. The reduced major axis of a bivariate sample. *Biometrika* 67, 441–446.

D'Addona L.A., Bernal V., Gonzalez P.N. 2024. Variation in molar size and proportions in the hominid lineage: an inter- and intraspecific approach. *Integrative Organismal Biology* 6(1), obae041.

Darwin, C., 1871. *On the origin of species*. D. Appleton and Co., New York.

Davies, T.W., Alemseged, Z., Gidna, A., Hublin, J.-J., Kimbel, W.H., Kullmer, O., Spoor, F., Zanolli, C., Skinner, M.M., 2021. Accessory cusp expression at the enamel-dentine junction of hominin mandibular molars. *PeerJ* 9, e11415.

Dean, C., Zanolli, C., Le Cabec, A., Tawane, M., Garrevoet, J., Mazurier, A., Macchiarelli, R., 2020. Growth and development of the third permanent molar in Paranthropus robustus from Swartkrans, South Africa. *Sci Rep 10*, 19053.

Dembo, M., Radovčić, D., Garvin, H.M., Laird, M.F., Schroeder, L., Scott, J.E., Brophy, J., Ackermann, R.R., Musiba, C.M., De Ruiter, D.J., Mooers, A.Ø., Collard, M., 2016. The evolutionary relationships and age of Homo naledi: An assessment using dated Bayesian phylogenetic methods. *Journal of Human Evolution* 97, 17–26.

Dunn, O.J., 1961. Multiple Comparisons among Means. *Journal of the American Statistical Association* 56, 52–64.

Evans, A.R., Daly, E.S., Catlett, K.K., Paul, K.S., King, S.J., Skinner, M.M., Nesse, H.P., Hublin, J.-J., Townsend, G.C., Schwartz, G.T., Jernvall, J., 2016. A simple rule governs the evolution and development of hominin tooth size. *Nature* 530, 477–480.

Felsenstein, J., 1985. Phylogenies and the Comparative Method. *The American Naturalist* 125, 1–15.

Hershkovitz, I., May, H., Sarig, R., Pokhojaev, A., Grimaud-Hervé, D., Bruner, E., Fornai, C., Quam, R., Arsuaga, J.L., Krenn, V.A., Martinón-Torres, M., De Castro, J.M.B., Martín-Francés,

Hlusko, L.J., Schmitt, C.A., Monson, T.A., Brasil, M.F., Mahaney, M.C., 2016. The integration of quantitative genetics, paleontology, and neontology reveals genetic underpinnings of primate dental evolution. *Proc. Natl. Acad. Sci. U.S.A.* 113, 9262–9267.

Hunter, J.P., Guatelli-Steinberg, D., Weston, T.C., Durner, R., Betsinger, T.K., 2010. Model of Tooth Morphogenesis Predicts Carabelli Cusp Expression, Size, and Symmetry in Humans. *PLoS ONE* 5, e11844.

Hershkovitz, I., May, H., Sarig, R., Pokhojaev, A., Grimaud-Hervé, D., Bruner, E., Fornai, C., Quam, R., Arsuaga, J.L., Krenn, V.A., Martinón-Torres, M., De Castro, J.M.B., Martín-Francés, L., Slon, V., Albessard-Ball, L., Vialet, A., Schüler, T., Manzi, G., Profico, A., Di Vincenzo, F., Weber, G.W., Zaidner, Y., 2021. A Middle Pleistocene *Homo* from Nesher Ramla, Israel. *Science* 372, 1424–1428.

Hillson, S., 2014. Tooth Development in Human Evolution and Bioarchaeology, 1st ed. Cambridge University Press.

Huxley, J.S., 1924. Constant Differential Growth-Ratios and their Significance. *Nature* 114, 895–896.

Huxley, J.S., Teissier, G., 1936. Terminology of Relative Growth. *Nature* 137, 780–781.

Ives, A., 2018. rr2: R2s for Regression Models. *CRAN: Contributed Packages*.

Ives, A.R., 2019. R^{2}s for Correlated Data: Phylogenetic Models, LMMs, and GLMMs. *Systematic Biology* 68, 234–251.

Jernvall, J., 2000. Linking development with generation of novelty in mammalian teeth. Proc. Natl. *Acad. Sci. U.S.A.* 97, 2641–2645.

Jernvall, J., Jung, H., 2000. Genotype, phenotype, and developmental biology of molar tooth characters. *Am. J. Phys. Anthropol*. 113, 171–190.

Kavanagh K., Evans A., Jernvall J. 2007. Predicting evolutionary patterns of mammalian teeth from development. *Nature* 449, 427–432.

Kilmer, J.T., Rodríguez, R.L., 2017. Ordinary least squares regression is indicated for studies of allometry. *J of Evolutionary Biology* 30, 4–12

Liu, W., Athreya, S., Xing, S., Wu, X., 2022. Hominin evolution and diversity: a comparison of earlier-Middle and later-Middle Pleistocene hominin fossil variation in China. Phil. Trans. R. Soc. B 377, 20210040.

Lucas, P.W., Corlett, R.T., Luke, D.A., 1986. Postcanine tooth size and diet in anthropoid primates. *zmorph_anthropol* 76, 253–276.

Mahoney, P., 2008. Intraspecific variation in M1 enamel development in modern humans: implications for human evolution. *Journal of Human Evolution* 55, 131–147.

Marchiori, D.F., Packota, G.V., Boughner, J.C., 2019. Initial third molar development is delayed in jaws with short distal space: An early impaction sign? *Archives of Oral Biology* 106, 104475.

Margvelashvili A., Zollikofer C.P.E., Lordkipanidze D., Tafforeau P., Ponce de León M.S. 2016. Comparative analysis of dentognathic pathologies in the Dmanisi mandibles. *American Journal of Physical Anthropology* 160(2), 229–253.

Mongle C.S., Pugh K.D., Strait D.S., et al. 2022. Modelling hominin evolution requires accurate hominin data. *Nature Ecology & Evolution* 6, 1090–1091.

Monson, T.A., Brasil, M.F., Mahaney, M.C., Schmitt, C.A., Taylor, C.E., Hlusko, L.J., 2022. Keeping 21st Century Paleontology Grounded: Quantitative Genetic Analyses and Ancestral State Reconstruction Re-Emphasize the Essentiality of Fossils. *Biology* 11, 1218.

Noerwidi S. 2020. Hominin diversity in the western Indonesian archipelago during the Quaternary: a dental record perspective. Thèse de doctorat. Muséum national d'histoire naturelle, Paris ; Universitat Rovira i Virgili, Tarragone.

Palmer A.R., Strobeck C. 1992. Fluctuating asymmetry as a measure of developmental stability: implications of non-normal distributions and power of statistical tests. *Acta Zoologica Fennica* 191, 57–72.

Pan, L., Zanolli, C., Martinón-Torres, M., Bermúdez De Castro, J.M., Martín-Francés, L., Xing, S., Liu, W., 2022. Early Pleistocene hominin teeth from Gongwangling of Lantian, Central China. *Journal of Human Evolution* 168, 103212.

Paradis, E., Blomberg, S., Bolker, B., Brown, J., Claramunt, S., Claude, J., Cuong, H.S., Desper, R., Didier, G., Durand, B., Dutheil, J., Ewing, R., Gascuel, O., Guillerme, T., Heibl, C., Ives, A., Jones, B., Krah, F., Lawson, D., Lefort, V., Legendre, P., Lemon, J., Louvel, G., Marotta, F., Marcon, E., McCloskey, R., Nylander, J., Opgen-Rhein, R., Popescu, A.-A., Royer-Carenzi, M., Schliep, K., Strimmer, K., De Vienne, D., 2002. ape: Analyses of Phylogenetics and Evolution. *CRAN: Contributed Packages*.

Pearse, W.D., Davies, T.J., Wolkovich, E.M., 2025. How to Define, Use, and Interpret Pagel's λ (Lambda) in Ecology and Evolution. *Global Ecol Biogeogr* 34.

Renvoisé, E., Kavanagh, K.D., Lazzari, V., Häkkinen, T.J., Rice, R., Pantalacci, S., Salazar-Ciudad, I., Jernvall, J., 2017. Mechanical constraint from growing jaw facilitates mammalian dental diversity. *Proc. Natl. Acad. Sci. U.S.A.* 114, 9403–9408.

Revell L.J. 2024. *phytools* 2.0: an updated R ecosystem for phylogenetic comparative methods (and other things). *PeerJ* 12, e16505.

Revell, L.J., 2012. Phylogenetic Tools for Comparative Biology: Phylogenetic signal with K and λ [WWW Document], n.d. URL https://blog.phytools.org/2012/03/phylogenetic-signal-with-k-and.html (accessed 9.8.25).

Revell, L.J., 2010. Phylogenetic signal and linear regression on species data: Phylogenetic regression. *Methods in Ecology and Evolution* 1, 319–329.

Revell, L.J., 2009. Re: [R-sig-phylo] negative lambda in gls with corPagel? [WWW Document], n.d. URL https://www.mail-archive.com/r-sig-phylo@r-project.org/msg00321.html (accessed 8.6.25).

Richards G.D., Jabbour R.S., Guipert G., Defleur A. 2025. Early Neanderthal mandibular remains from Baume Moula-Guercy (Soyons, Ardèche). *The Anatomical Record* 308(3), 892–929.

Pinheiro, J., R Core Team, Bates, D., 1999. nlme: Linear and Nonlinear Mixed Effects Models. CRAN: Contributed Packages.

Rocatti G., Perez S.I. 2019. The evolutionary radiation of hominids: a phylogenetic comparative study. *Scientific Reports* 9, 15267.

Roseman, C.C., Delezene, L.K., 2019. The Inhibitory Cascade Model is Not a Good Predictor of Molar Size Covariation. *Evol Biol* 46, 229–238.

Salazar-Ciudad, I., Jernvall, J., 2002. A gene network model accounting for development and evolution of mammalian teeth. *Proc. Natl. Acad. Sci. U.S.A.* 99, 8116–8120.

Scott, G.R., Irish, J.D., 2017. *Human Tooth Crown and Root Morphology: The Arizona State University Dental Anthropology System*, 1st ed. Cambridge University Press.

Skinner, M.M., Gunz, P., 2010. The presence of accessory cusps in chimpanzee lower molars is consistent with a patterning cascade model of development. *Journal of Anatomy* 217, 245–253.

Smith, T.M., Reid, D.J., Dean, M.C., Olejniczak, A.J., Martin, L.B., 2007. Molar development in common chimpanzees (Pan troglodytes). *Journal of Human Evolution* 52, 201–216.

Villmoare B., Kimbel W.H., Seyoum C., et al. 2015. Early *Homo* at 2.8 Ma from Ledi-Geraru, Afar, Ethiopia. *Science* 347, 1352–1355.

Wagner, G.P., 1989. The Biological Homology Concept. *Annu. Rev. Ecol. Syst*. 20, 51–69.

White, T.D., Black, M., Folkens, P.A., 2012. *Human osteology*, Third edition. ed. Elsevier Academic Press, Amsterdam Boston Heidelberg.

Wiens, J.J., 2005. Can Incomplete Taxa Rescue Phylogenetic Analyses from Long-Branch Attraction? *Systematic Biology* 54, 731–742.

Wood, B.A., Abbott, S.A., 1983. Analysis of the dental morphology of Plio-pleistocene hominids. I. Mandibular molars: crown area measurements and morphological traits. *J Anat* 136, 197–219.

Wood, B.A., Abbott, S.A., Graham, S.H., 1983. Analysis of the dental morphology of Plio-Pleistocene hominids. II. Mandibular molars--study of cusp areas, fissure pattern and cross sectional shape of the crown. *J Anat* 137 (Pt 2), 287–314.

Wood, B.A., Engleman, C.A., 1988. Analysis of the dental morphology of Plio-Pleistocene hominids. V. Maxillary postcanine tooth morphology. *J Anat* 161, 1–35.

Wood, B., 1991. *Koobi Fora research project: researches into geology, palaeontology, and human origins. 4. Hominid cranial remains.* Clarendon Press.

Xing, S., Martinón-Torres, M., Deng, C., Shao, Q., Wang, Y., Luo, Y., Zhou, X., Pan, L., Ge, J., Bermúdez De Castro, J.M., Liu, W., 2021. Early Pleistocene hominin teeth from Meipu, southern China. *Journal of Human Evolution* 151, 102924.

APPENDIX I. Sources of dental metric data

Bailey, S., Glantz, M., Weaver, T.D., Viola, B., 2008. The affinity of the dental remains from Obi-Rakhmat Grotto, Uzbekistan. Journal of Human Evolution 55, 238–248. https://doi.org/10.1016/j.jhevol.2008.03.004

Bailey, S.E., 2004. A morphometric analysis of maxillary molar crowns of Middle-Late Pleistocene hominins. Journal of Human Evolution 47, 183–198. https://doi.org/10.1016/j.jhevol.2004.07.001

Bailey, S.E., Hublin, J.-J., 2006. Dental remains from the Grotte du Renne at Arcy-sur-Cure (Yonne). Journal of Human Evolution 50, 485–508. https://doi.org/10.1016/j.jhevol.2005.11.008

Becam, G., Chevalier, T., 2019. Neandertal features of the deciduous and permanent teeth from Portel-Ouest Cave (Ariège, France). American Journal of Physical Anthropology 168, 45–69. https://doi.org/10.1002/ajpa.23719

Becam, G., Verna, C., Gómez-Robles, A., Gómez-Olivencia, A., Albessard, L., Arnaud, J., Frelat, M.A., Madelaine, S., Schwab, C., Souday, C., Turq, A., Balzeau, A., 2019. Isolated teeth from La Ferrassie: Reassessment of the old collections, new remains, and their implications. American Journal of Physical Anthropology 169, 132–142. https://doi.org/10.1002/ajpa.23798

Benazzi, S., Viola, B., Kullmer, O., Fiorenza, L., Harvati, K., Paul, T., Gruppioni, G., Weber, G.W., Mallegni, F., 2011a. A reassessment of the Neanderthal teeth from Taddeo cave (southern Italy). Journal of Human Evolution 61, 377–387. https://doi.org/10.1016/j.jhevol.2011.05.001

Benazzi, S., Viola, B., Kullmer, O., Fiorenza, L., Harvati, K., Paul, T., Gruppioni, G., Weber, G.W., Mallegni, F., 2011b. A reassessment of the Neanderthal teeth from Taddeo cave (southern Italy). Journal of Human Evolution 61, 377–387. https://doi.org/10.1016/j.jhevol.2011.05.001

Berger, L.R., Parkington, J.E., 1995. A new pleistocene hominid-bearing locality at Hoedjiespunt, South Africa. American Journal of Physical Anthropology 98, 601–609. https://doi.org/10.1002/ajpa.1330980415

Bermúdez de Castro, J.-M., Martinón-Torres, M., Gómez-Robles, A., Prado, L., Sarmiento, S., 2007. Comparative analysis of the Gran Dolina-TD6 (Spain) and Tighennif (Algeria) hominin mandibles. Bulletins et mémoires de la Société d'Anthropologie de Paris 19, 149–167. https://doi.org/10.4000/bmsap.4623

Bermúdez de Castro, J.M., Rosas, A., Nicola´s, M.E., 1999. Dental remains from Atapuerca-TD6 (Gran Dolina site, Burgos, Spain). Journal of Human Evolution 37, 523–566. https://doi.org/10.1006/jhev.1999.0323

Bermúdez, F.J., Martínez de Pinillos, M., Medina-Lara, F., Barroso-Medina, C., Cabral-Mesa, A.L., Santiago-Pérez, A., Ortiz, J.E., Sánchez-Palencia, Y., Saos, T., Grégoire, S., Pois, V., Vialet, A.,

Monge, G., Moigne, A.-M., Caparrós, M., de Torres, T., Bermúdez de Castro, J.M., Barroso-Ruiz, C., 2022. A human lower third molar from the Acheulean site of Cueva del Ángel (Lucena, Córdoba, Spain). American Journal of Biological Anthropology n/a. https://doi.org/10.1002/ajpa.24677

Billy, G., 1982. Les dents humaines de la grotte du Coupe-Gorge à Montmaurin. Bulletins et Mémoires de la Société d'Anthropologie de Paris 9, 211–225. https://doi.org/10.3406/bmsap.1982.9761

Blinkhorn, J., Zanolli, C., Compton, T., Groucutt, H.S., Scerri, E.M.L., Crété, L., Stringer, C., Petraglia, M.D., Blockley, S., 2021. Nubian Levallois technology associated with southernmost Neanderthals. Sci Rep 11, 2869. https://doi.org/10.1038/s41598-021-82257-6

Blumenberg, B., Lloyd, A.T., 1983. Australopithecus and the origin of the genus Homo: Aspects of biometry and systematics with accompanying catalog of tooth metric data. Biosystems 16, 127–167. https://doi.org/10.1016/0303-2647(83)90033-3

Braga, J., Grine, F.E., 2024. New craniodental fossils of Paranthropus robustus from Kromdraai, South Africa (2014–2017 excavations). Journal of Human Evolution 188, 103481. https://doi.org/10.1016/j.jhevol.2023.103481

Brown, F., Harris, J., Leakey, R., Walker, A., 1985. Early Homo erectus skeleton from west Lake Turkana, Kenya. Nature 316, 788–792. https://doi.org/10.1038/316788a0

Brunet, M., Guy, F., Pilbeam, D., Lieberman, D.E., Likius, A., Mackaye, H.T., Ponce de León, M.S., Zollikofer, C.P.E., Vignaud, P., 2005. New material of the earliest hominid from the Upper Miocene of Chad. Nature 434, 752–755. https://doi.org/10.1038/nature03392

Brunet, M., Guy, F., Pilbeam, D., Mackaye, H.T., Likius, A., Ahounta, D., Beauvilain, A., Blondel, C., Bocherens, H., Boisserie, J.-R., De Bonis, L., Coppens, Y., Dejax, J., Denys, C., Duringer, P., Eisenmann, V., Fanone, G., Fronty, P., Geraads, D., Lehmann, T., Lihoreau, F., Louchart, A., Mahamat, A., Merceron, G., Mouchelin, G., Otero, O., Campomanes, P.P., De Leon, M.P., Rage, J.-C., Sapanet, M., Schuster, M., Sudre, J., Tassy, P., Valentin, X., Vignaud, P., Viriot, L., Zazzo, A., Zollikofer, C., 2002. A new hominid from the Upper Miocene of Chad, Central Africa. Nature 418, 145–151. https://doi.org/10.1038/nature00879

Carbonell, E., Bermúdez de Castro, J.M., Parés, J.M., Pérez-González, A., Cuenca-Bescós, G., Ollé, A., Mosquera, M., Huguet, R., van der Made, J., Rosas, A., Sala, R., Vallverdú, J., García, N., Granger, D.E., Martinón-Torres, M., Rodríguez, X.P., Stock, G.M., Vergès, J.M., Allué, E., Burjachs, F., Cáceres, I., Canals, A., Benito, A., Díez, C., Lozano, M., Mateos, A., Navazo, M., Rodríguez, J., Rosell, J., Arsuaga, J.L., 2008. The first hominin of Europe. Nature 452, 465–469. https://doi.org/10.1038/nature06815

Chen, F., Welker, F., Shen, C.-C., Bailey, S.E., Bergmann, I., Davis, S., Xia, H., Wang, H., Fischer, R., Freidline, S.E., Yu, T.-L., Skinner, M.M., Stelzer, S., Dong, Guangrong, Fu, Q., Dong, Guanghui,

Wang, J., Zhang, D., Hublin, J.-J., 2019. A late Middle Pleistocene Denisovan mandible from the Tibetan Plateau. Nature 569, 409–412. https://doi.org/10.1038/s41586-019-1139-x

Ciochon, R., Long, V.T., Larick, R., González, L., Grün, R., de Vos, J., Yonge, C., Taylor, L., Yoshida, H., Reagan, M., 1996. Dated co-occurrence of Homo erectus and Gigantopithecus from Tham Khuyen Cave, Vietnam. Proceedings of the National Academy of Sciences 93, 3016–3020. https://doi.org/10.1073/pnas.93.7.3016

Clarke, R.J., 2012. A Homo habilis maxilla and other newly-discovered hominid fossils from Olduvai Gorge, Tanzania. Journal of Human Evolution, Five Decades after Zinjanthropus and Homo habilis: Landscape Paleoanthropology of Plio-Pleistocene Olduvai Gorge, Tanzania 63, 418–428. https://doi.org/10.1016/j.jhevol.2011.11.007

Condemi, S., 2001. Les néandertaliens de La Chaise: Abri Bourgeois-Delaunay. Comité des travaux historiques et scientifiques-CTHS.

Condemi, S., 1992. Les hommes fossiles de Saccopastore et leurs relations phylogénétiques, CNRS éditions. ed.

Curnoe, D., Tobias, P.V., 2006. Description, new reconstruction, comparative anatomy, and classification of the Sterkfontein Stw 53 cranium, with discussions about the taxonomy of other southern African early *Homo* remains. Journal of Human Evolution 50, 36–77. https://doi.org/10.1016/j.jhevol.2005.07.008

Daujeard, C., Falguères, C., Shao, Q., Geraads, D., Hublin, J.-J., Lefèvre, D., Graoui, M.E., Rué, M., Gallotti, R., Delvigne, V., Queffelec, A., Arous, E.B., Tombret, O., Mohib, A., Raynal, J.-P., 2020. Earliest African evidence of carcass processing and consumption in cave at 700 ka, Casablanca, Morocco. Sci Rep 10, 4761. https://doi.org/10.1038/s41598-020-61580-4

de Lumley, M.A., 2023. Les dents. Généralités. Les dents définitives. Les dents déciduales ou temporaires, in: de Lumley, M.-A. (Ed.), Les restes humains du Pléistocène moyen de la Caune de l'Arago. Caune de l'Arago. Tautavel-en-Roussillon, Pyrénées-Orientales, France. pp. 249–398.

de Lumley, M.A., 1973. Anténéandertaliens et Néandertaliens du bassin méditerranéen occidental européen. Univ. de Provence-Laboratoire de paléontologie humaine et de préhistoire.

Delezene, L.K., Skinner, M.M., Bailey, S.E., Brophy, J.K., Elliott, M.C., Gurtov, A., Irish, J.D., Moggi-Cecchi, J., De Ruiter, D.J., Hawks, J., Berger, L.R., 2023. Descriptive catalog of Homo naledi dental remains from the 2013 to 2015 excavations of the Dinaledi Chamber, site U.W. 101, within the Rising Star cave system, South Africa. Journal of Human Evolution 180, 103372. https://doi.org/10.1016/j.jhevol.2023.103372

Demeter, F., Shackelford, L., Westaway, K., Barnes, L., Duringer, P., Ponche, J.-L., Dumoncel, J., Sénégas, F., Sayavongkhamdy, T., Zhao, J.-X., Sichanthongtip, P., Patole-Edoumba, E., Dunn, T., Zachwieja, A., Coppens, Y., Willerslev, E., Bacon, A.-M., 2017. Early Modern Humans from Tam

Pà Ling, Laos: Fossil Review and Perspectives. Current Anthropology 58, S527–S538. https://doi.org/10.1086/694192

Demeter, F., Zanolli, C., Westaway, K.E., Joannes-Boyau, R., Duringer, P., Morley, M.W., Welker, F., Rüther, P.L., Skinner, M.M., McColl, H., Gaunitz, C., Vinner, L., Dunn, T.E., Olsen, J.V., Sikora, M., Ponche, J.-L., Suzzoni, E., Frangeul, S., Boesch, Q., Antoine, P.-O., Pan, L., Xing, S., Zhao, J.-X., Bailey, R.M., Boualaphane, S., Sichanthongtip, P., Sihanam, D., Patole-Edoumba, E., Aubaile, F., Crozier, F., Bourgon, N., Zachwieja, A., Luangkhoth, T., Souksavatdy, V., Sayavongkhamdy, T., Cappellini, E., Bacon, A.-M., Hublin, J.-J., Willerslev, E., Shackelford, L., 2022. A Middle Pleistocene Denisovan molar from the Annamite Chain of northern Laos. Nat Commun 13, 2557. https://doi.org/10.1038/s41467-022-29923-z

Détroit, F., Mijares, A.S., Corny, J., Daver, G., Zanolli, C., Dizon, E., Robles, E., Grün, R., Piper, P.J., 2019. A new species of Homo from the Late Pleistocene of the Philippines. Nature 568, 181–186. https://doi.org/10.1038/s41586-019-1067-9

Garralda, M.-D., Vandermeersch, B., 2000. Les Néandertaliens de la grotte de Combe-Grenal (Domme, Dordogne, France) / The Neanderthals from Combe-Grenal cave (Domme, Dordogne, France). Paléo, Revue d'Archéologie Préhistorique 12, 213–259. https://doi.org/10.3406/pal.2000.1603

Gómez-Olivencia, A., López-Onaindia, D., Sala, N., Balzeau, A., Pantoja-Pérez, A., Arganda-Carreras, I., Arlegi, M., Rios-Garaizar, J., Gómez-Robles, A., 2020. The human remains from Axlor (Dima, Biscay, northern Iberian Peninsula). American Journal of Physical Anthropology 172, 475–491. https://doi.org/10.1002/ajpa.23989

Gómez-Robles, A., de Castro, J.M.B., Martinón-Torres, M., Prado-Simón, L., 2011. Crown size and cusp proportions in Homo antecessor upper first molars. A comment on Quam et al. 2009. Journal of Anatomy 218, 258–262. https://doi.org/10.1111/j.1469-7580.2010.01324.x

Grine, F.E., 2012. Observations on Middle Stone Age human teeth from Klasies River Main Site, South Africa. Journal of Human Evolution 63, 750–758. https://doi.org/10.1016/j.jhevol.2012.08.005

Grine, F.E., 2000. Middle Stone Age human fossils from Die Kelders Cave 1, Western Cape Province, South Africa. Journal of Human Evolution 38, 129–145. https://doi.org/10.1006/jhev.1999.0353

Grine, F.E., 1989. New hominid fossils from the Swartkrans formation (1979–1986 excavations): Craniodental specimens. American Journal of Physical Anthropology 79, 409–449. https://doi.org/10.1002/ajpa.1330790402

Grine, F.E., Leakey, M.G., Gathago, P.N., Brown, F.H., Mongle, C.S., Yang, D., Jungers, W.L., Leakey, L.N., 2019. Complete permanent mandibular dentition of early Homo from the upper Burgi Member of the Koobi Fora Formation, Ileret, Kenya. Journal of Human Evolution 131, 152–175. https://doi.org/10.1016/j.jhevol.2019.03.017

Guy, F., Boistel, R., Lenoir, N., Bonis, L.D., 2015. A Middle Pleistocene fossil hominin maxilla from the Republic of Djibouti (East Africa). Anthropological Science advpub, 150624. https://doi.org/10.1537/ase.150624

Haile-Selassie, Y., Gibert, L., Melillo, S.M., Ryan, T.M., Alene, M., Deino, A., Levin, N.E., Scott, G., Saylor, B.Z., 2015. New species from Ethiopia further expands Middle Pliocene hominin diversity. Nature 521, 483–488. https://doi.org/10.1038/nature14448

Haile-Selassie, Y., Melillo, S.M., Ryan, T.M., Levin, N.E., Saylor, B.Z., Deino, A., Mundil, R., Scott, G., Mulugeta Alene, Gibert, L., 2016. Dentognathic remains of Australopithecus afarensis from Nefuraytu (Woranso-Mille, Ethiopia): Comparative description, geology, and paleoecological context. Journal of Human Evolution 100, 35–53. https://doi.org/10.1016/j.jhevol.2016.08.003

Hawks, J., Elliott, M., Schmid, P., Churchill, S.E., Ruiter, D.J. de, Roberts, E.M., Hilbert-Wolf, H., Garvin, H.M., Williams, S.A., Delezene, L.K., Feuerriegel, E.M., Randolph-Quinney, P., Kivell, T.L., Laird, M.F., Tawane, G., DeSilva, J.M., Bailey, S.E., Brophy, J.K., Meyer, M.R., Skinner, M.M., Tocheri, M.W., VanSickle, C., Walker, C.S., Campbell, T.L., Kuhn, B., Kruger, A., Tucker, S., Gurtov, A., Hlophe, N., Hunter, R., Morris, H., Peixotto, B., Ramalepa, M., Rooyen, D. van, Tsikoane, M., Boshoff, P., Dirks, P.H., Berger, L.R., 2017. New fossil remains of *Homo naledi* from the Lesedi Chamber, South Africa. eLife 6, e24232. https://doi.org/10.7554/eLife.24232

Henrion, J., Maureille, B., Beauval, C., Vanderesse, N., Hublin, J.-J., Hardy, M., 2025. The Grotte du Bison Neandertals (Arcy-sur-Cure, France). Journal of Human Evolution 199, 103631. https://doi.org/10.1016/j.jhevol.2024.103631

Hershkovitz, I., May, H., Sarig, R., Pokhojaev, A., Grimaud-Hervé, D., Bruner, E., Fornai, C., Quam, R., Arsuaga, J.L., Krenn, V.A., Martinón-Torres, M., de Castro, J.M.B., Martín-Francés, L., Slon, V., Albessard-Ball, L., Vialet, A., Schüler, T., Manzi, G., Profico, A., Di Vincenzo, F., Weber, G.W., Zaidner, Y., 2021. A Middle Pleistocene Homo from Nesher Ramla, Israel. Science 372, 1424–1428. https://doi.org/10.1126/science.abh3169

Hershkovitz, I., Smith, P., Sarig, R., Quam, R., Rodríguez, L., García, R., Arsuaga, J.L., Barkai, R., Gopher, A., 2011. Middle pleistocene dental remains from Qesem Cave (Israel). American Journal of Physical Anthropology 144, 575–592. https://doi.org/10.1002/ajpa.21446

Hershkovitz, I., Weber, G.W., Fornai, C., Gopher, A., Barkai, R., Slon, V., Quam, R., Gabet, Y., Sarig, R., 2016. New Middle Pleistocene dental remains from Qesem Cave (Israel). Quaternary International, State of the art of the multidisciplinary research at the Middle Pleistocene Qesem Cave, Israel, 2015 398, 148–158. https://doi.org/10.1016/j.quaint.2015.08.059

Hershkovitz, I., Weber, G.W., Quam, R., Duval, M., Grün, R., Kinsley, L., Ayalon, A., Bar-Matthews, M., Valladas, H., Mercier, N., Arsuaga, J.L., Martinón-Torres, M., Bermúdez de Castro, J.M., Fornai, C., Martín-Francés, L., Sarig, R., May, H., Krenn, V.A., Slon, V., Rodríguez, L., García, R., Lorenzo, C., Carretero, J.M., Frumkin, A., Shahack-Gross, R., Bar-Yosef Mayer, D.E., Cui, Y., Wu, X., Peled, N., Groman-Yaroslavski, I., Weissbrod, L., Yeshurun, R., Tsatskin, A., Zaidner,

Y., Weinstein-Evron, M., 2018. The earliest modern humans outside Africa. Science 359, 456–459. https://doi.org/10.1126/science.aap8369

Hillson, S.W., Parfitt, S.A., Bello, S.M., Roberts, M.B., Stringer, C.B., 2010. Two hominin incisor teeth from the middle Pleistocene site of Boxgrove, Sussex, England. Journal of Human Evolution 59, 493–503. https://doi.org/10.1016/j.jhevol.2010.06.004

Hlusko, L.J., Carlson, J.P., Guatelli-Steinberg, D., Krueger, K.L., Mersey, B., Ungar, P.S., Defleur, A., 2013. Neanderthal teeth from moula-guercy, Ardèche, France. American Journal of Physical Anthropology 151, 477–491. https://doi.org/10.1002/ajpa.22291

Holt, B., Aggott, Z., Vicino, G., Semprebon, G., 2012. A human tooth from the Mousterian site of Arma delle Manie (Liguria, Italy). Bull. Mus. anthropol. préhist. Monaco 43–46.

Howells, W.W., 1974. Metric trends in hominid dental evolution. By Milford H. Wolpoff. xii + 244 pp., tables, bibliography. Studies in Anthropology No. 2, Case Western Reserve University Press, Cleveland. 1971. $5.95(paper). American J Phys Anthropol 40, 451–452. https://doi.org/10.1002/ajpa.1330400317

Hublin, J.-J., Ben-Ncer, A., Bailey, S.E., Freidline, S.E., Neubauer, S., Skinner, M.M., Bergmann, I., Le Cabec, A., Benazzi, S., Harvati, K., Gunz, P., 2017. New fossils from Jebel Irhoud, Morocco and the pan-African origin of Homo sapiens. Nature 546, 289–292. https://doi.org/10.1038/nature22336

Hublin, J.-J., Verna, C., Bailey, S., Smith, T., Olejniczak, A., Sbihi-Alaoui, F.Z., Zouak, M., 2012. Dental Evidence from the Aterian Human Populations of Morocco, in: Hublin, Jean-Jacques, McPherron, S.P. (Eds.), Modern Origins: A North African Perspective. Springer Netherlands, Dordrecht, pp. 189–204. https://doi.org/10.1007/978-94-007-2929-2_13

Indriati, E., Antón, S.C., 2008. Earliest Indonesian facial and dental remains from Sangiran, Java: a description of Sangiran 27. Anthropological Science 116, 219–229. https://doi.org/10.1537/ase.070814

Irish, J.D., Hemphill, B.E., de Ruiter, D.J., Berger, L.R., 2016. The apportionment of tooth size and its implications in Australopithecus sediba versus other Plio-pleistocene and recent African hominins. American Journal of Physical Anthropology 161, 398–413. https://doi.org/10.1002/ajpa.23039

Jianing, H., 2000. Preliminary study on the teeth of Jinniushan archaichomo sapiens. Acta Anthropologica Sinica 19, 216.

Kaifu, Y., Kono, R.T., Sutikna, T., Saptomo, E.W., Jatmiko, Awe, R.D., Baba, H., 2015. Descriptions of the dental remains of *Homo floresiensis*. Anthropol. Sci. 123, 129–145. https://doi.org/10.1537/ase.150501

Kimbel, W.H., Johanson, D.C., Rak, Y., 1997. Systematic assessment of a maxilla of Homo from Hadar, Ethiopia. American Journal of Physical Anthropology 103, 235–262. https://doi.org/10.1002/(SICI)1096-8644(199706)103:2<235::AID-AJPA8>3.0.CO;2-S

Kimbel, W.H., Johanson, D.C., Rak, Y., 1994. The first skull and other new discoveries of Australopithecus afarensis at Hadar, Ethiopia. Nature 368, 449–451. https://doi.org/10.1038/368449a0

Kimbel, W.H., Rak, Y., Johanson, D.C., 2004. The Skull of Australopithecus afarensis. Oxford University Press.

King, T., Compton, T., Rosas, A., Andrews, P., Yepiskoposyan, L., Asryan, L., 2016. Azokh Cave Hominin Remains, in: Fernández-Jalvo, Y., King, T., Yepiskoposyan, L., Andrews, P. (Eds.), Azokh Cave and the Transcaucasian Corridor, Vertebrate Paleobiology and Paleoanthropology. Springer International Publishing, Cham, pp. 103–116. https://doi.org/10.1007/978-3-319-24924-7_5

Kramer, A., Djubiantono, T., Aziz, F., Bogard, J.S., Weeks, R.A., Weinand, D.C., Hames, W.E., Michael Elam, J., Durband, A.C., Agus, 2005. The first hominid fossil recovered from West Java, Indonesia. Journal of Human Evolution 48, 661–667. https://doi.org/10.1016/j.jhevol.2005.01.005

Leakey, M.G., Feibel, C.S., McDougall, I., Ward, C., Walker, A., 1998. New specimens and confirmation of an early age for Australopithecus anamensis. Nature 393, 62–66. https://doi.org/10.1038/29972

Leakey, M.G., Spoor, F., Dean, M.C., Feibel, C.S., Antón, S.C., Kiarie, C., Leakey, L.N., 2012. New fossils from Koobi Fora in northern Kenya confirm taxonomic diversity in early Homo. Nature 488, 201–204. https://doi.org/10.1038/nature11322

Liu, W., Schepartz, L.A., Xing, S., Miller-Antonio, S., Wu, X., Trinkaus, E., Martinón-Torres, M., 2013. Late Middle Pleistocene hominin teeth from Panxian Dadong, South China. Journal of Human Evolution 64, 337–355. https://doi.org/10.1016/j.jhevol.2012.10.012

Liu, X., Shen, G., Tu, H., Lu, C., Granger, D.E., 2015. Initial 26Al/10Be burial dating of the hominin site Bailong Cave in Hubei Province, central China. Quaternary International, The Jaramillo Subchron and the Early-Middle Pleistocene transition in continental records from a multidisciplinary perspective 389, 235–240. https://doi.org/10.1016/j.quaint.2014.10.028

López-Onaindia, D., Lozano, M., Gómez-Robles, A., Arrizabalaga, A., Subirà, M.E., 2023. Neanderthal teeth from Lezetxiki (Arrasate, Iberian Peninsula): New insights and reassessment. American Journal of Biological Anthropology 180, 745–760. https://doi.org/10.1002/ajpa.24694

Lordkipanidze, D., Ponce de León, M.S., Margvelashvili, A., Rak, Y., Rightmire, G.P., Vekua, A., Zollikofer, C.P.E., 2013. A Complete Skull from Dmanisi, Georgia, and the Evolutionary Biology of Early Homo. Science 342, 326–331. https://doi.org/10.1126/science.1238484

Macchiarelli, R., Bondioli, L., Falk, D., Faupl, P., Illerhaus, B., Kullmer, O., Richter, W., Said, H., Sandrock, O., Schäfer, K., Urbanek, C., Viola, B.T., Weber, G.W., Seidler, H., 2004. Early Pliocene Hominid Tooth from Galili, Somali Region, Ethiopia. Coll. Antropol.

Maddux, S.D., Ward, C.V., Brown, F.H., Plavcan, J.M., Manthi, F.K., 2015. A 750,000 year old hominin molar from the site of Nadung'a, West Turkana, Kenya. Journal of Human Evolution 80, 179–183. https://doi.org/10.1016/j.jhevol.2014.11.004

Martín-Francés, L., de Castro, J.M.B., de Pinillos, M.M., Martinón-Torres, M., Arsuaga, J.L., Bertrand, B., Vialet, A., 2022. Middle Pleistocene hominin teeth from Biache-Saint-Vaast, France. Archaeol Anthropol Sci 14, 215. https://doi.org/10.1007/s12520-022-01680-6

Martinón-Torres, M., Bermúdez de Castro, J.M., Gómez-Robles, A., Prado-Simón, L., Arsuaga, J.L., 2012. Morphological description and comparison of the dental remains from Atapuerca-Sima de los Huesos site (Spain). Journal of Human Evolution 62, 7–58. https://doi.org/10.1016/j.jhevol.2011.08.007

Martinón-Torres, M., Bermúdez de Castro, J.M., Martínez de Pinillos, M., Modesto-Mata, M., Xing, S., Martín-Francés, L., García-Campos, C., Wu, X., Liu, W., 2019. New permanent teeth from Gran Dolina-TD6 (Sierra de Atapuerca). The bearing of Homo antecessor on the evolutionary scenario of Early and Middle Pleistocene Europe. Journal of Human Evolution 127, 93–117. https://doi.org/10.1016/j.jhevol.2018.12.001

Martinón-Torres, M., Spěváčková, P., Gracia-Téllez, A., Martínez, I., Bruner, E., Arsuaga, J.L., Bermúdez de Castro, J.M., 2013. Morphometric analysis of molars in a Middle Pleistocene population shows a mosaic of 'modern' and Neanderthal features. Journal of Anatomy 223, 353–363. https://doi.org/10.1111/joa.12090

Melillo, S.M., Gibert, L., Saylor, B.Z., Deino, A., Alene, M., Ryan, T.M., Haile-Selassie, Y., 2021. New Pliocene hominin remains from the Leado Dido'a area of Woranso-Mille, Ethiopia. Journal of Human Evolution 153, 102956. https://doi.org/10.1016/j.jhevol.2021.102956

Moggi-Cecchi, J., Grine, F.E., Tobias, P.V., 2006. Early hominid dental remains from Members 4 and 5 of the Sterkfontein Formation (1966–1996 excavations): Catalogue, individual associations, morphological descriptions and initial metrical analysis. Journal of Human Evolution 50, 239–328. https://doi.org/10.1016/j.jhevol.2005.08.012

Morales, J.I., Cebrià, A., Soto, M., Rodríguez-Hidalgo, A., Hernando, R., Moreno-Ribas, E., Lombao, D., Rabuñal, J.R., Martín-Perea, D.M., García-Tabernero, A., Allué, E., García-Basanta, A., Lizano, E., Marquès-Bonet, T., Talamo, S., Tassoni, L., Lalueza-Fox, C., Fullola, J.M., Rosas, A., 2023. A new assemblage of late Neanderthal remains from Cova Simanya (NE Iberia). Frontiers in Earth Science 11.

Ni, X., Ji, Q., Wu, W., Shao, Q., Ji, Y., Zhang, C., Liang, L., Ge, J., Guo, Z., Li, J., Li, Q., Grün, R., Stringer, C., 2021. Massive cranium from Harbin in northeastern China establishes a new Middle Pleistocene human lineage. Innovation 2. https://doi.org/10.1016/j.xinn.2021.100130

P. James Macaluso, J., 2010. Variation in dental remains from Dmanisi, Georgia. Anthropological Science 118, 31–40. https://doi.org/10.1537/ase.090501

Pan, L., Zanolli, C., Martinón-Torres, M., Bermúdez de Castro, J.M., Martín-Francés, L., Xing, S., Liu, W., 2022. Early Pleistocene hominin teeth from Gongwangling of Lantian, Central China. Journal of Human Evolution 168, 103212. https://doi.org/10.1016/j.jhevol.2022.103212

Radović, P., Lindal, J., Mihailović, D., Roksandic, M., 2019. The first Neanderthal specimen from Serbia: Maxillary first molar from the Late Pleistocene of Pešturina Cave. Journal of Human Evolution 131, 139–151. https://doi.org/10.1016/j.jhevol.2019.03.018

Raynal, J.-P., Sbihi-Alaoui, F.-Z., Mohib, A., El Graoui, M., Lefèvre, D., Texier, J.-P., Geraads, D., Hublin, J.-J., Smith, T., Tafforeau, P., Zouak, M., Grün, R., Rhodes, E.J., Eggins, S., Daujeard, C., Fernandes, P., Gallotti, R., Hossini, S., Schwarcz, H.P., Queffelec, A., 2011. Contextes et âge des nouveaux restes dentaires humains du Pléistocène moyen de la carrière Thomas I à Casablanca (Maroc). Bulletin de la Société préhistorique française 108, 645–669.

Rodríguez García, L., García González, R., Sanz Borràs, M., Daura Luján, J., Quam, R.M., Fullola Pericot, J.M., Arsuaga Ferreras, J.L., Rodríguez García, L., García González, R., Sanz Borràs, M., Daura Luján, J., Quam, R.M., Fullola Pericot, J.M., Arsuaga Ferreras, J.L., 2011. A Neanderthal Lower Incisor from Cova del Gegant: (Sitges, Barcelona, Spain). Boletín de la Real Sociedad Española de Historia Natural. Sección geológica 105.

Roksandic, M., Radović, P., Lindal, J., Mihailović, D., 2022. Early Neanderthals in contact: The Chibanian (Middle Pleistocene) hominin dentition from Velika Balanica Cave, Southern Serbia. Journal of Human Evolution 166, 103175. https://doi.org/10.1016/j.jhevol.2022.103175

Semaw, S., Rogers, M.J., Simpson, S.W., Levin, N.E., Quade, J., Dunbar, N., McIntosh, W.C., Cáceres, I., Stinchcomb, G.E., Holloway, R.L., Brown, F.H., Butler, R.F., Stout, D., Everett, M., 2020. Co-occurrence of Acheulian and Oldowan artifacts with Homo erectus cranial fossils from Gona, Afar, Ethiopia. Science Advances 6, eaaw4694. https://doi.org/10.1126/sciadv.aaw4694

Senut, B., Pickford, M., Gommery, D., Mein, P., Cheboi, K., Coppens, Y., 2001. First hominid from the Miocene (Lukeino Formation, Kenya). Comptes Rendus de l'Académie des Sciences - Series IIA - Earth and Planetary Science 332, 137–144. https://doi.org/10.1016/S1251-8050(01)01529-4

Simpson, S.W., Kleinsasser, L., Quade, J., Levin, N.E., McIntosh, W.C., Dunbar, N., Semaw, S., Rogers, M.J., 2015. Late Miocene hominin teeth from the Gona Paleoanthropological Research Project area, Afar, Ethiopia. Journal of Human Evolution 81, 68–82. https://doi.org/10.1016/j.jhevol.2014.07.004

Spoor, F., Leakey, M.G., Gathogo, P.N., Brown, F.H., Antón, S.C., McDougall, I., Kiarie, C., Manthi, F.K., Leakey, L.N., 2007. Implications of new early Homo fossils from Ileret, east of Lake Turkana, Kenya. Nature 448, 688–691. https://doi.org/10.1038/nature05986

Stynder, D.D., Moggi-Cecchi, J., Berger, L.R., Parkington, J.E., 2001. Human mandibular incisors from the late Middle Pleistocene locality of Hoedjiespunt 1, South Africa. Journal of Human Evolution 41, 369–383. https://doi.org/10.1006/jhev.2001.0488

Suwa, G., Asfaw, B., Beyene, Y., White, T.D., Katoh, S., Nagaoka, S., Nakaya, H., Uzawa, K., Renne, P., WoldeGabriel, G., 1997. The first skull of Australopithecus boisei. Nature 389, 489–492. https://doi.org/10.1038/39037

Suwa, G., Asfaw, B., Haile-Selassie, Y., White, T., Katoh, S., Woldegabriel, G., Hart, W.K., Nakaya, H., Beyene, Y., 2007. Early Pleistocene Homo erectus fossils from Konso, southern Ethiopia. Anthropological Science 115, 133–151. https://doi.org/10.1537/ase.061203

Thoma, A., Vallois, H.V., 1977. Les dents de l'Homme de Rabat. Bulletins et Mémoires de la Société d'Anthropologie de Paris 4, 31–58. https://doi.org/10.3406/bmsap.1977.1861

Tillier, A., 2014. New Middle Palaeolithic Hominin Dental Remains from Qafzeh, Israel. Paléorient 40, 13–24.

Tillier, A., Arensburg, B., Belfer-Cohen, A., Vandermeersh, B., 2011. Early Hominid Remains from Hayonim Cave (Israel) in the Context of the Late Middle and Upper Pleistocene Record from the Near East. Paléorient 37, 47–63.

Tobias, P.V., 1991. Olduvai Gorge IV: The skulls, endocasts and teeth of Homo habilis. Cambridge University Press.

Tobias, P.V., 1971. Human skeletal remains from the cave of Hearths, Makapansgat, Northern Transvaal. American Journal of Physical Anthropology 34, 335–367. https://doi.org/10.1002/ajpa.1330340305

Trinkaus, E., 1983. The Shanidar Neandertals. Academic Press, London.

Trinkaus, E., Walker, M.J., 2017. The People of Palomas: Neandertals from the Sima de las Palomas del Cabezo Gordo, Southeastern Spain. Texas A&M University Press.

van den Bergh, G.D., Kaifu, Y., Kurniawan, I., Kono, R.T., Brumm, A., Setiyabudi, E., Aziz, F., Morwood, M.J., 2016. Homo floresiensis-like fossils from the early Middle Pleistocene of Flores. Nature 534, 245–248. https://doi.org/10.1038/nature17999

Vandermeersch, B., 1981. Les Hommes fossiles de Qafzeh, Cahier de paléontologie (paléoanthropologie). CNRS Editions, 15 quai Anatole France, Paris.

Verna, C., 2006. Les restes humains moustériens de la Station Amont de la Quina - (Charente, France) : contexte archéologiqe et constitution de l'assemblage : étude morphologique et métrique des restes crânio-faciaux : apport à l'étude de la variation néandertalienne (These de doctorat). Bordeaux 1.

Vialet, A., Modesto-Mata, M., Martinón-Torres, M., Pinillos, M.M. de, Castro, J.-M.B. de, 2018. A reassessment of the Montmaurin-La Niche mandible (Haute Garonne, France) in the context of European Pleistocene human evolution. PLOS ONE 13, e0189714. https://doi.org/10.1371/journal.pone.0189714

Villa, G., Giacobini, G., 1996. Neandertal Teeth from Alpine Caves of Monte Fenera (piedmont, Northern Italy): Description of the Remains and Microwear Analysis. Anthropologie (1962-) 34, 55–67.

Voisin, J.-L., Condemi, S., Wolpoff, M.H., Frayer, D.W., 2012. A new online database (http://anthropologicaldata.free.fr/) and a Short Reflection About the Productive Use of Compiling Internet Data. PaleoAnthropology 241, 244.

Ward, C.V., Manthi, F.K., Plavcan, J.M., 2013. New fossils of Australopithecus anamensis from Kanapoi, West Turkana, Kenya (2003–2008). Journal of Human Evolution 65, 501–524. https://doi.org/10.1016/j.jhevol.2013.05.006

Ward, C.V., Plavcan, J.M., Manthi, F.K., 2020. New fossils of Australopithecus anamensis from Kanapoi, West Turkana, Kenya (2012–2015). Journal of Human Evolution, Kanapoi: The Paleobiology of a Pliocene Site in the Turkana Basin, Kenya 140, 102368. https://doi.org/10.1016/j.jhevol.2017.07.008

Westaway, K.E., Louys, J., Awe, R.D., Morwood, M.J., Price, G.J., Zhao, J. -x, Aubert, M., Joannes-Boyau, R., Smith, T.M., Skinner, M.M., Compton, T., Bailey, R.M., van den Bergh, G.D., de Vos, J., Pike, A.W.G., Stringer, C., Saptomo, E.W., Rizal, Y., Zaim, J., Santoso, W.D., Trihascaryo, A., Kinsley, L., Sulistyanto, B., 2017. An early modern human presence in Sumatra 73,000–63,000 years ago. Nature 548, 322–325. https://doi.org/10.1038/nature23452

White, T.D., 1980. Additional fossil Hominids from Laetoli, Tanzania: 1976–1979 specimens. American Journal of Physical Anthropology 53, 487–504. https://doi.org/10.1002/ajpa.1330530405

White, T.D., 1977. New fossil hominids from Laetolil, Tanzania. Am. J. Phys. Anthropol. 46, 197–229. https://doi.org/10.1002/ajpa.1330460203

White, T.D., Asfaw, B., DeGusta, D., Gilbert, H., Richards, G.D., Suwa, G., Clark Howell, F., 2003. Pleistocene Homo sapiens from Middle Awash, Ethiopia. Nature 423, 742–747. https://doi.org/10.1038/nature01669

White, T.D., Suwa, G., Asfaw, B., 1994. Australopithecus ramidus, a new species of early hominid from Aramis, Ethiopia. Nature 371, 306–312. https://doi.org/10.1038/371306a0

White, T.D., Suwa, G., Simpson, S., Asfaw, B., 2000. Jaws and teeth of Australopithecus afarensis from Maka, Middle Awash, Ethiopia. American Journal of Physical Anthropology 111, 45–68. https://doi.org/10.1002/(SICI)1096-8644(200001)111:1<45::AID-AJPA4>3.0.CO;2-I

Wolpoff, M.H., 1979. The Krapina dental remains. American Journal of Physical Anthropology 50, 67–113. https://doi.org/10.1002/ajpa.1330500110

Wolpoff, M.H., 1969. Metric trends in hominid dental evolution. University of Illinois at Urbana-Champaign.

Wood, B., 1991. Koobi Fora research project: researches into geology, palaeontology, and human origins. 4. Hominid cranial remains. Clarendon Press.

Wu, X.-J., Pei, S.-W., Cai, Y.-J., Tong, H.-W., Li, Q., Dong, Z., Sheng, J.-C., Jin, Z.-T., Ma, D.-D., Xing, S., Li, X.-L., Cheng, X., Cheng, H., de la Torre, I., Edwards, R.L., Gong, X.-C., An, Z.-S., Trinkaus, E., Liu, W., 2019. Archaic human remains from Hualongdong, China, and Middle Pleistocene human continuity and variation. Proceedings of the National Academy of Sciences 116, 9820–9824. https://doi.org/10.1073/pnas.1902396116

Xing, S., Martinón-Torres, M., Bermúdez de Castro, J.M., 2019. Late Middle Pleistocene hominin teeth from Tongzi, southern China. Journal of Human Evolution 130, 96–108. https://doi.org/10.1016/j.jhevol.2019.03.001

Xing, S., Martinón-Torres, M., Deng, C., Shao, Q., Wang, Y., Luo, Y., Zhou, X., Pan, L., Ge, J., Bermúdez de Castro, J.M., Liu, W., 2021. Early Pleistocene hominin teeth from Meipu, southern China. Journal of Human Evolution 151, 102924. https://doi.org/10.1016/j.jhevol.2020.102924

Xing, S., Sun, C., Martinón-Torres, M., Bermúdez de Castro, J.M., Han, F., Zhang, Y., Liu, W., 2016. Hominin teeth from the Middle Pleistocene site of Yiyuan, Eastern China. Journal of Human Evolution 95, 33–54. https://doi.org/10.1016/j.jhevol.2016.03.004

Zaim, Y., Ciochon, R.L., Polanski, J.M., Grine, F.E., Bettis, E.A., Rizal, Y., Franciscus, R.G., Larick, R.R., Heizler, M., Aswan, Eaves, K.L., Marsh, H.E., 2011. New 1.5 million-year-old Homo erectus maxilla from Sangiran (Central Java, Indonesia). Journal of Human Evolution 61, 363–376. https://doi.org/10.1016/j.jhevol.2011.04.009

Zanolli, C., Bondioli, L., Coppa, A., Dean, C.M., Bayle, P., Candilio, F., Capuani, S., Dreossi, D., Fiore, I., Frayer, D.W., Libsekal, Y., Mancini, L., Rook, L., Medin Tekle, T., Tuniz, C., Macchiarelli, R., 2014. The late Early Pleistocene human dental remains from Uadi Aalad and Mulhuli-Amo (Buia), Eritrean Danakil: Macromorphology and microstructure. Journal of Human Evolution 74, 96–113. https://doi.org/10.1016/j.jhevol.2014.04.005

Zanolli, C., Dean, M.C., Assefa, Y., Bayle, P., Braga, J., Condemi, S., Endalamaw, M., Engda Redae, B., Macchiarelli, R., 2017. Structural organization and tooth development in a Homo aff. erectus juvenile mandible from the Early Pleistocene site of Garba IV at Melka Kunture, Ethiopian

highlands. American Journal of Physical Anthropology 162, 533–549. https://doi.org/10.1002/ajpa.23135

Zhang, G., Xing, S., Martinón-Torres, M., Bermúdez de Castro, J.M., Wang, S., 2023. A Late Middle Pleistocene human tooth from the Luonan Basin (Shaanxi, China). Journal of Human Evolution 178, 103343. https://doi.org/10.1016/j.jhevol.2023.103343

Zhao, L., Xuan, L.I., Xuejun, G.U., Baopu, D.U., Jiazhen, S.H.I., Xing, G. a. O., 2018. Middle Pleistocene hominins from the Sunjiadong site, Luanchuan county, Henan Province, Central China. Acta Anthropologica Sinica 37, 192.

Zhao, L., Zhang, L., Du, B., Nian, X.-M., Zheng, Y., Zhang, Z., Wang, C., Wang, X., Cai, H., 2016. New Discovery of Human Fossils and Associated Mammal Fauna from Mawokou Cave in Bijie, Guizhou Province of Southern China. Acta Anthropologica Sinica 35.

Zhu, R.X., Potts, R., Pan, Y.X., Yao, H.T., Lü, L.Q., Zhao, X., Gao, X., Chen, L.W., Gao, F., Deng, C.L., 2008. Early evidence of the genus Homo in East Asia. Journal of Human Evolution 55, 1075–1085. https://doi.org/10.1016/j.jhevol.2008.08.005

APPENDIX II. Sample specimen list (Table 2)

Accessory cusps (Cusp 6 and Cusp 7)

Dental casts		3D models	
Specimens	**Molars**	**Specimens**	**Molars**
AL 288-1	**LRM2, LRM3**	**Montmaurin Mandible**	**LRM3**
STW 14	**LRM2, LRM3**	**Tighennif 2**	**LLM2, LLM3**
Qafzeh 9	**LRM1/ LLM1**	**Dmanisi D2735**	**LRM1, LRM2, LRM3**
Sangiran 1b	**LRM1, LRM2, LRM3**		
Amud 1	**LRM3/ LLM3**		
Arago 13	**LRM3**		
KNM-ER 992	**LRM2/LLM2, LRM3/LLM3**		
Tabun C1	**LLM3**		
Vindija 206	**LRM2, LRM3**		
Montmaurin Mandible	**LRM3**		
ZKD B3	**LRM1**		

Protoconid

Dental casts	
Specimens	**Molars**
Arago 13	**LRM1, LRM2, LRM3**
Tabun C1	**LLM3**
Vindija 206	**LRM1, LRM2, LRM3**
Montmaurin Mandible	**LLM1, LLM2, LLM3**

APPENDIX III – Pairwise scatterplots of variables on molar-level measurements

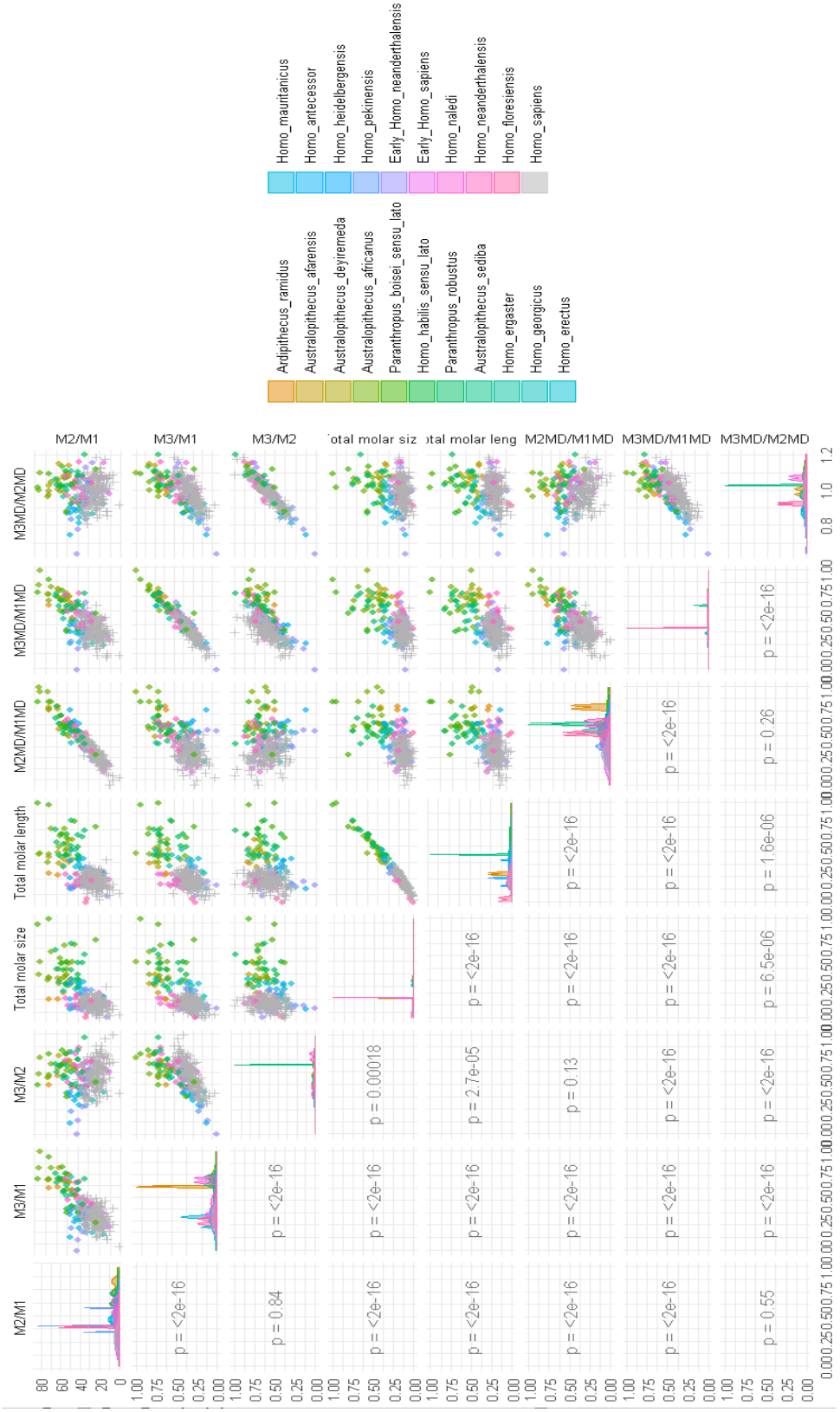

APPENDIX IV- RMA/ PRMA regressions of IC model application on upper consecutive (UC – Scenario 3) molars and upper isolated (UI – Scenario 4) molars

Scenario 3

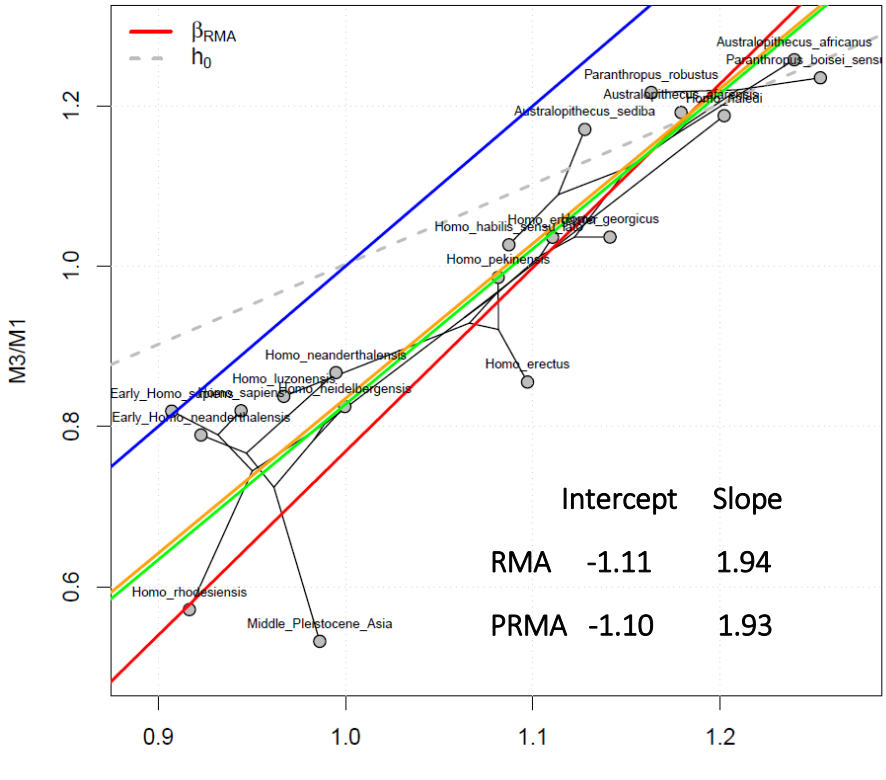

Slopes in colours :

Lambda = 0 (RMA)

Lambda optimised (PRMA)

Lambda = 1 (PRMA) & BetaRMA=Coefficient of PRMA with the assumption of full phylogeny

IC model: intercept=-1, slope=2

Scenario 4

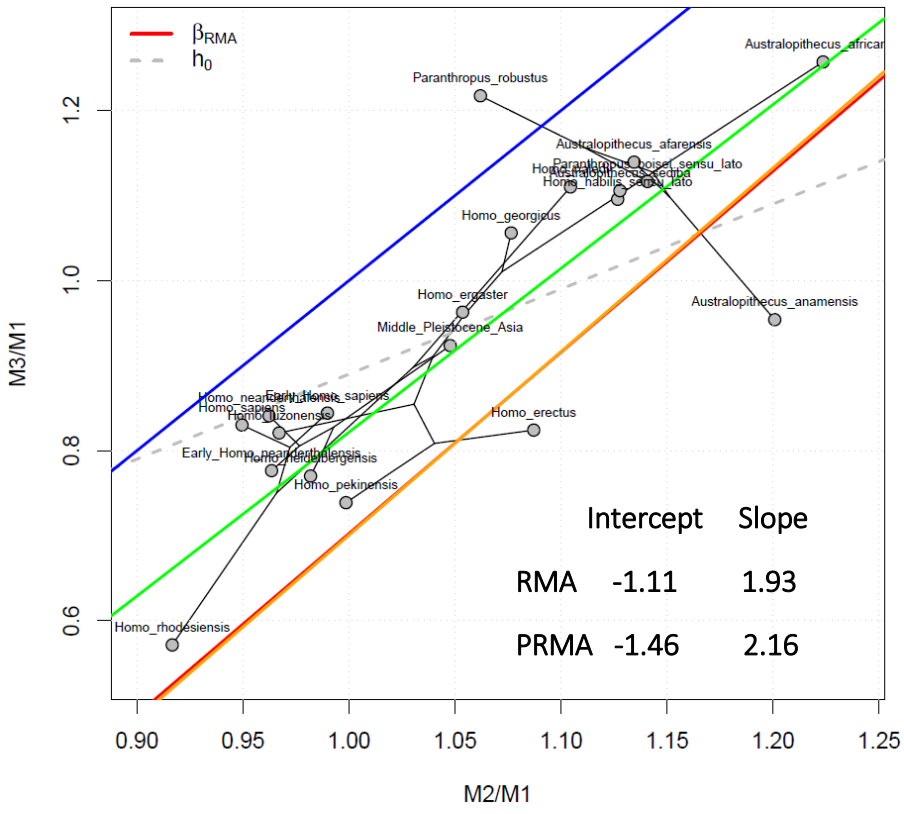

APPENDIX V(a)– Means of molar sizes by OTUs, and the respective variance between observed vs expected M2 size

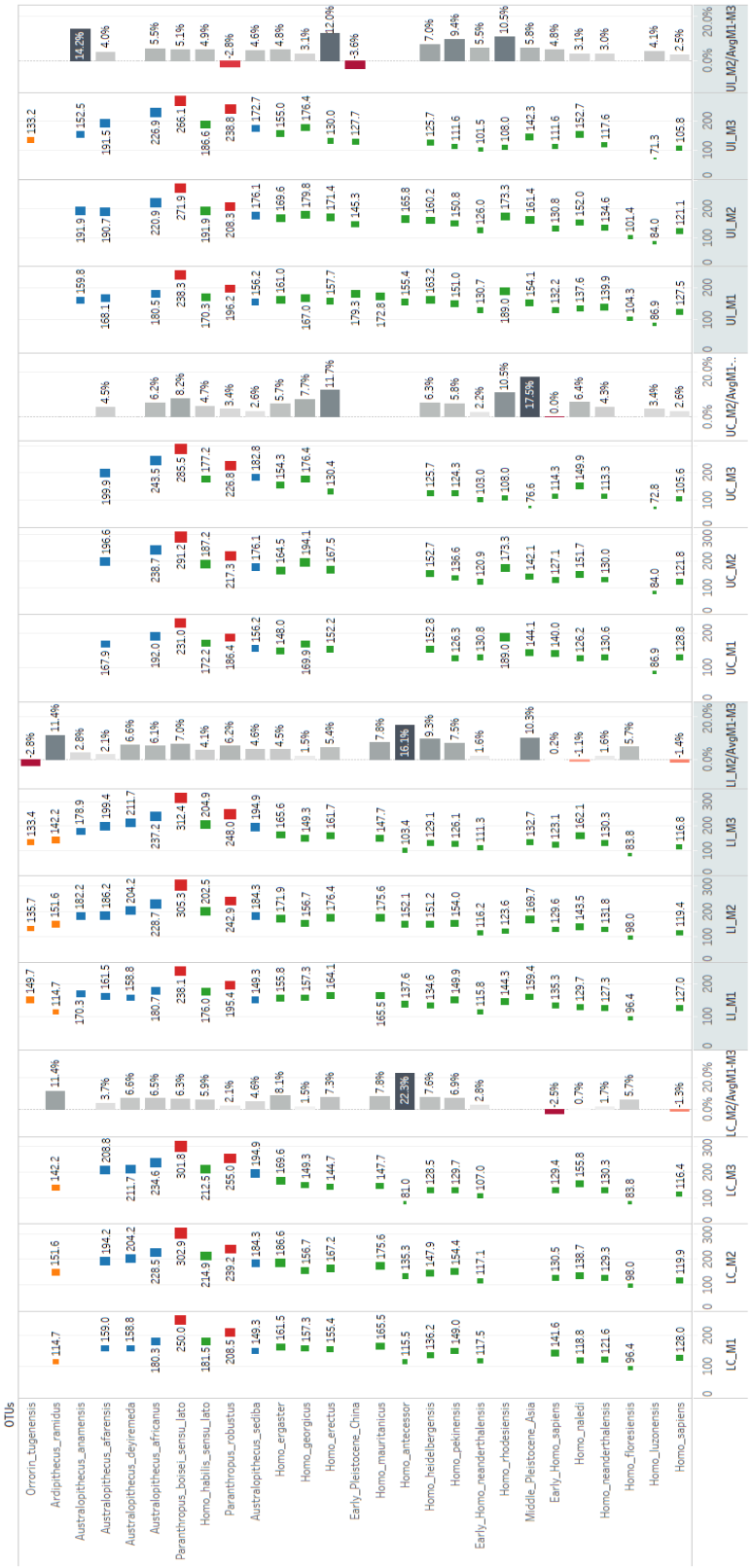

Scaling: square size, and the size position horizontally along the x-axes (0-300) are both proportional to the mean molar size by OTUs

Colour: represents the genus

Orange=Early hominins (i.e. *Orrorin, Ardipithecus*)

Blue=Australopithecus

Red=Paranthropus

Green=Homo

Abbreviations:

LC=Lower consecutive

LI=Lower isolated

UC=Upper consecutive

UI=Upper isolated

M1= mean size of M1

M2=mean size of M2

M3=mean size of M3

M2/AvgM1-M3= ratio of

M2 to average (M1+M2+M3)

APPENDIX V(b)– The respective variance between observed vs expected M2 size by OTUs (only OTUs with data available in both consecutive and isolated molar dataset are listed)

	Lower consecutive	Lower isolated	Upper consecutive	Upper isolated
Ardipithecus ramidus	11.4%	11.4%		
Australopithecus afarensis	3.7%	2.1%	4.5%	4.0%
Australopithecus deyiremeda	6.6%	6.6%		
Australopithecus africanus	6.5%	6.1%	6.2%	5.5%
Paranthropus boisei sensu lato	6.3%	7.0%	8.2%	5.1%
Homo habilis sensu lato	5.9%	4.1%	4.7%	4.9%
Paranthropus robustus	2.1%	6.2%	3.4%	-2.8%
Australopithecus sediba	4.6%	4.6%	2.6%	4.6%
Homo ergaster	8.1%	4.5%	5.7%	4.8%
Homo georgicus	1.5%	1.5%	7.7%	3.1%
Homo erectus	7.3%	5.4%	11.7%	12.0%
Homo mauritanicus	7.8%	7.8%		
Homo antecessor	22.3%	16.1%		
Homo heidelbergensis	7.6%	9.3%	6.3%	7.0%
Homo pekinensis	6.9%	7.5%	5.8%	9.4%
Early *Homo neanderthalensis*	2.8%	1.6%	2.2%	5.5%
Homo rhodesiensis			10.5%	10.5%
Middle Pleistocene Asia			17.5%	5.8%
Early *Homo sapiens*	-2.5%	0.2%	0.0%	4.8%
Homo naledi	0.7%	-1.1%	6.4%	3.1%
Homo neanderthalensis	1.7%	1.6%	4.3%	3.0%
Homo floresiensis	5.7%	5.7%		
Homo luzonensis			3.4%	4.1%
Homo sapiens	-1.3%	-1.4%	2.6%	2.5%
Average deviation	**5.5%**	**5.1%**	**6.0%**	**5.1%**

APPENDIX VI - PGLS regression graph of individual molar size of M2 *vs.* mandibular width at M1

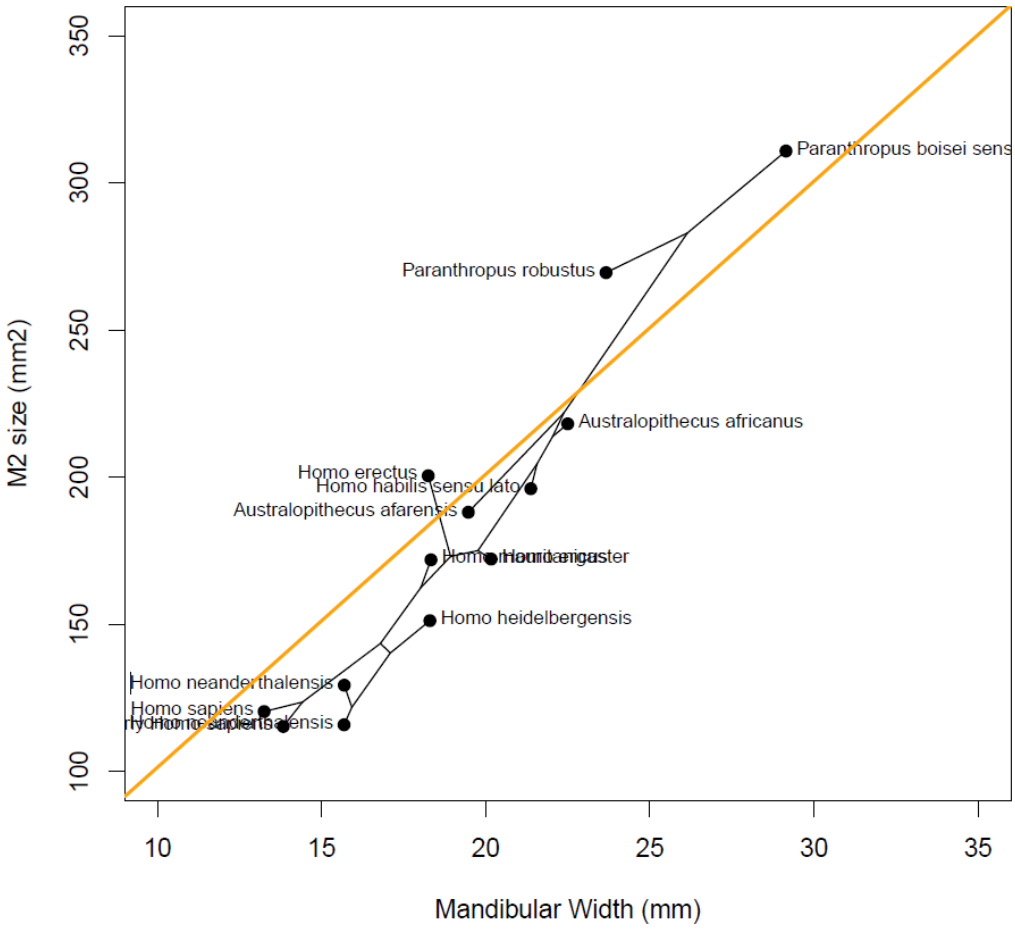

APPENDIX VII – PCA of cusp-related variables of M1

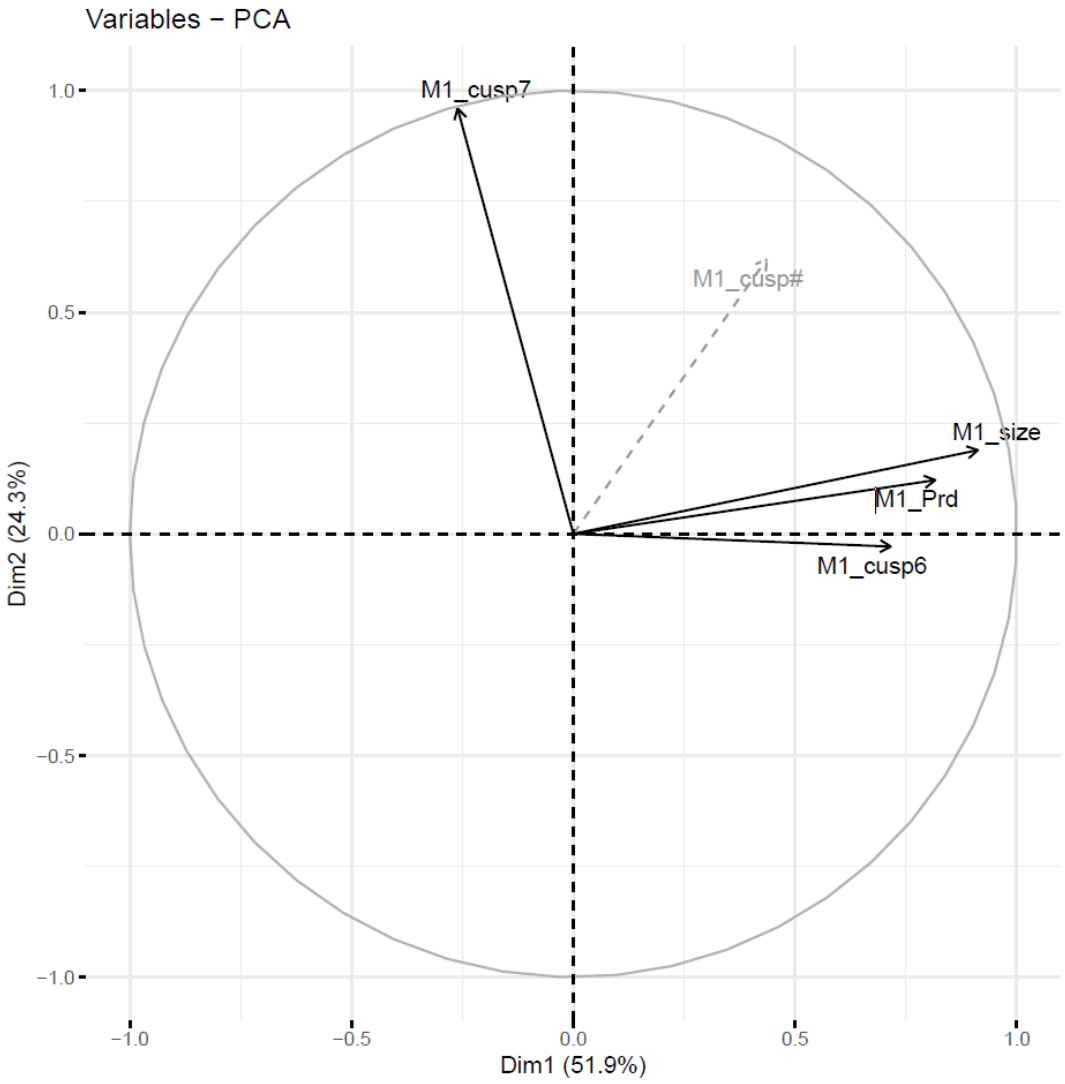

APPENDIX VIII – Visual illustration of the clustering of the variables

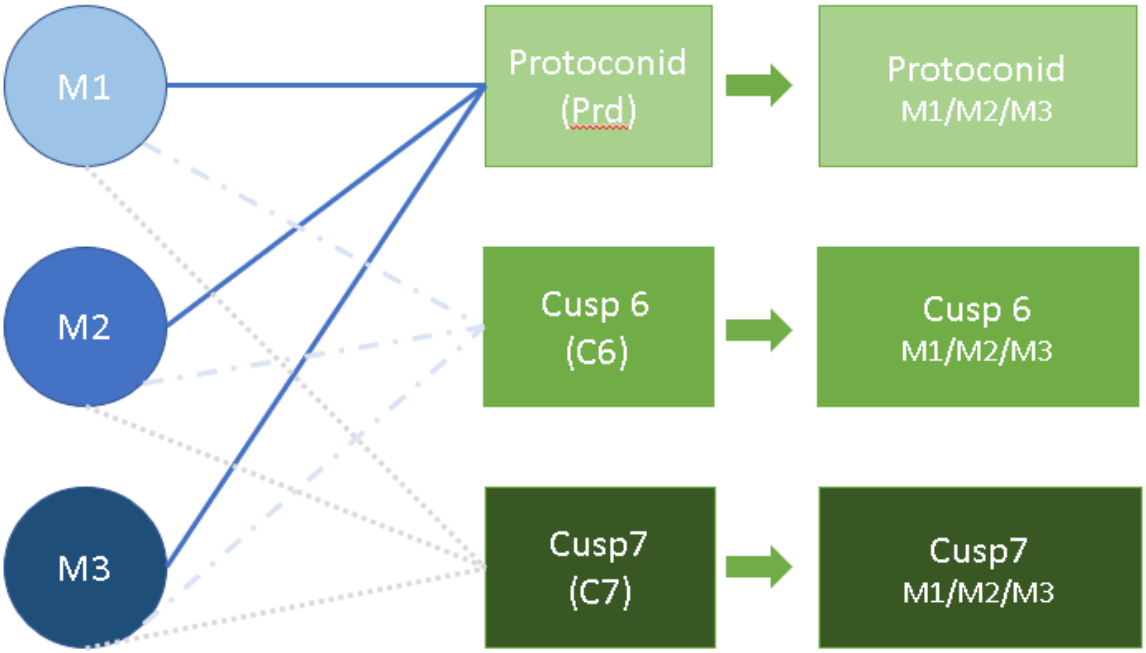

APPENDIX IX – Protoconid cusp size *versus* molar size

(a) Complete cups, molar size and sample size data

OTUs	M1 Prd	M2 Prd	M3 Prd	M1	M2	M3	M1 Prd%	M2 Prd%	M3 Prd%	M1#	M2#	M3#
Orrorin tugenensis	21.00			149.70			14.0%			1	0	0
Australopithecus africanus	35.33	44.65	43.77	183.00	219.92	228.29	19.3%	20.3%	19.2%	6	5	7
Paranthropus boisei sensu lato	38.86	56.46	54.42	237.79	315.41	324.54	16.3%	17.9%	16.8%	7	6	6
Homo habilis sensu lato	35.45	42.08	39.15	172.73	206.48	203.59	20.5%	20.4%	19.2%	5	6	11
Paranthropus robustus	36.66	45.46	46.27	210.47	245.36	252.86	17.4%	18.5%	18.3%	15	12	11
Homo ergaster	30.79	34.54	33.08	154.58	171.18	167.99	19.9%	20.2%	19.7%	6	7	6
Homo erectus	29.25	38.67	34.87	164.92	178.69	159.30	17.7%	21.6%	21.9%	4	5	7
Homo heidelbergensis	26.96	41.01	43.27	170.30	198.65	162.44	15.8%	20.6%	26.6%	1	1	1
Early Homo neanderthalensis	28.93	31.73	37.52	126.26	121.00	133.35	22.9%	26.2%	28.1%	1	1	1
Early Homo sapiens	29.54	35.15	31.86	143.84	124.26	126.99	20.5%	28.3%	25.1%	1	2	2
Homo neanderthalensis	23.71	26.86	25.22	129.95	126.56	122.44	18.2%	21.2%	20.6%	1	1	2

(b) PGLS on M1 protoconid size *vs.* molar size

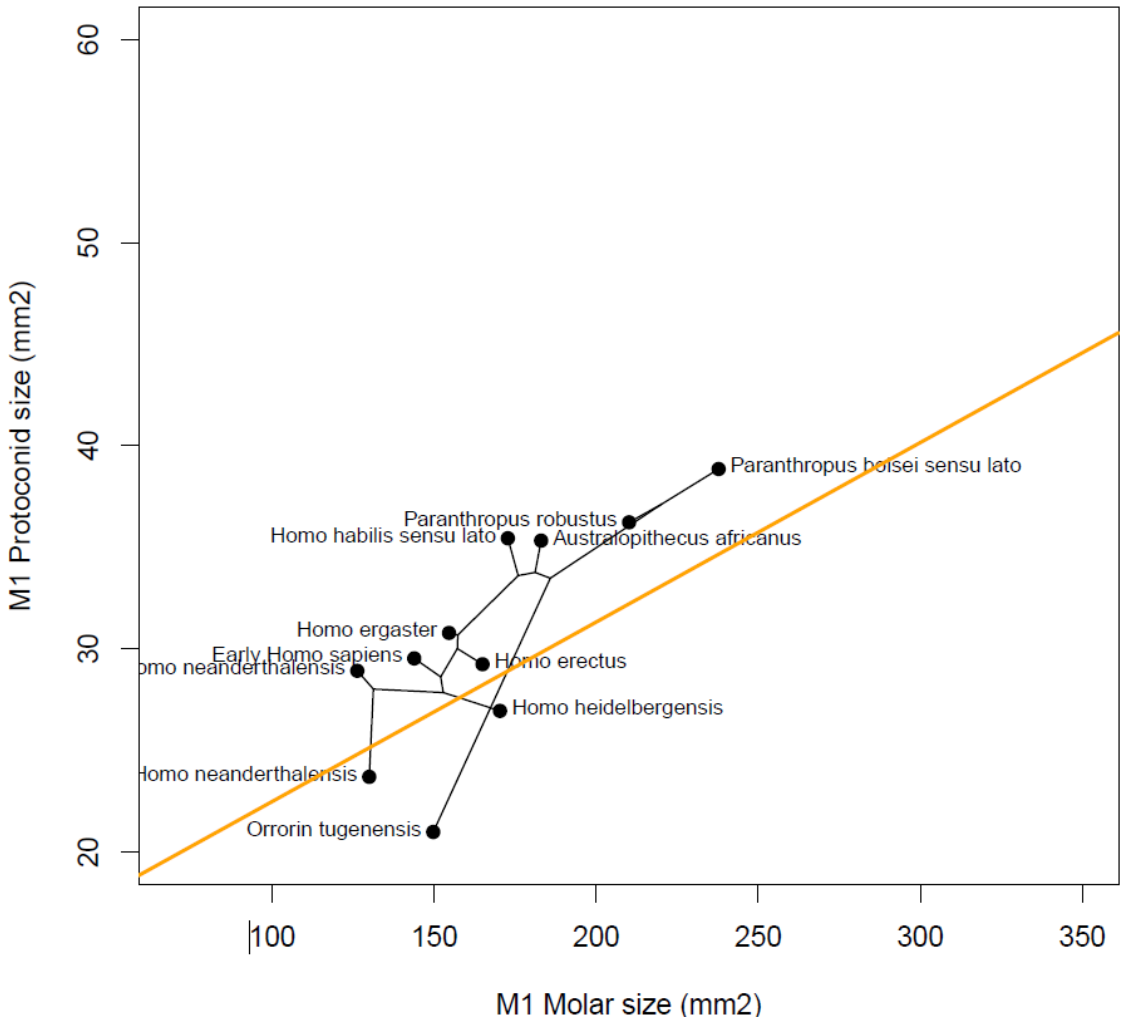

APPENDIX X – Visual illustration of tooth formation process by Jernvall and Jung (2000: 176)

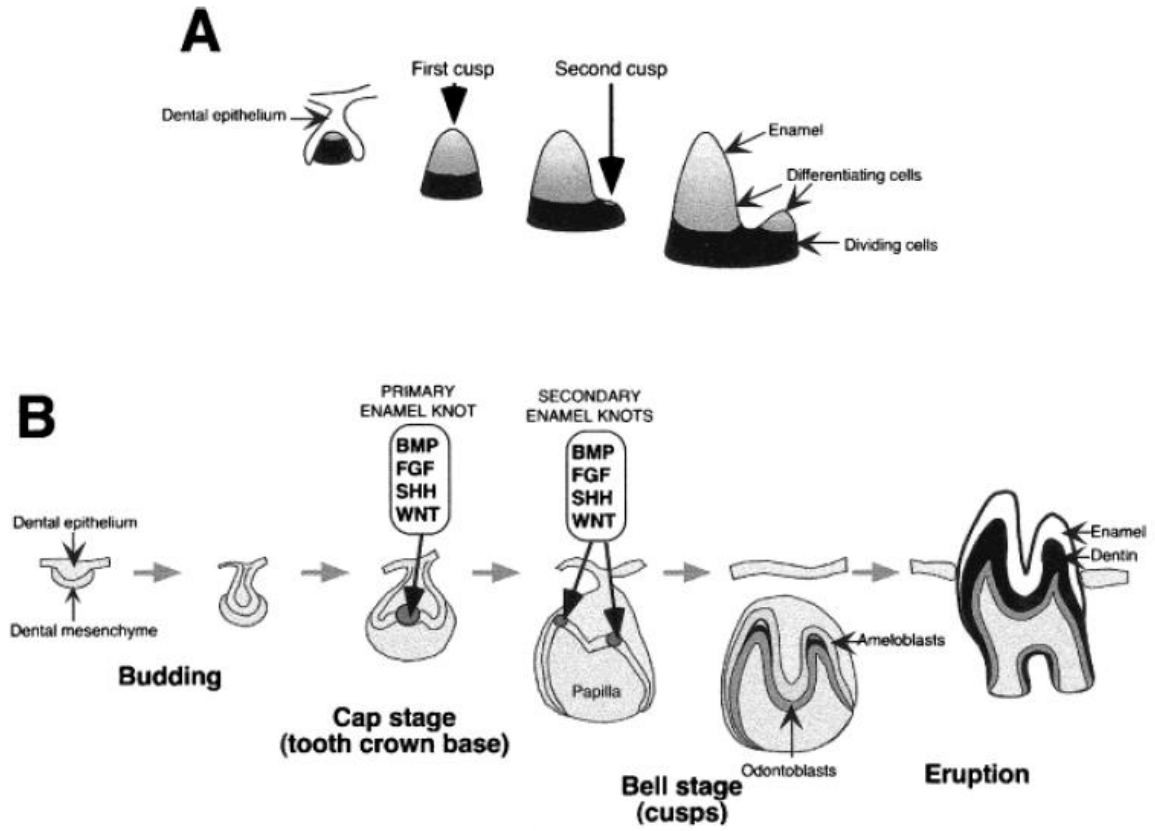

Fig. 3. Schematic representations of tooth development. **A:** Beginning in the cap stage, the tooth crown forms by unequal growth of the inner enamel epithelium (shaded). **B:** Molecular signals considered to be important for particular developmental stages are indicated above the morphology. Note how the same signaling pathways are used repeatedly during advancing tooth development. BMP, bone morphogenetic protein; FGF, fibroblast growth factor; SHH, sonic hedgehog; WNT, wingless-integrated.

Reference source:

Jernvall, J., Jung, H., 2000. Genotype, phenotype, and developmental biology of molar tooth characters. *Am. J. Phys. Anthropol*. 113, 171–190. https://doi.org/10.1002/1096-8644(2000)43:31+<171::AID-AJPA6>3.0.CO;2-3

APPENDIX XI

a. Cusp 6 - complete cups and molar size and sample size data

OTUs	NM1	NM2	NM3	M1	M2	M3	M1 C6%	M2 C6%	M3 C6%	NM1#	NM2#	NM3#	M1#	M2#	M3#
Orrorin tugenensis	149.70									1					
Australopithecus afarensis		158.60				171.41			5.6%		1				1
Australopithecus africanus	184.74	242.70		176.89	209.64	247.99	4.8%	3.6%	5.1%	4	2		1	4	5
Paranthropus boisei sensu lato	231.96	260.40	277.89	240.12	326.41	340.54	4.5%	4.9%	9.6%	2	1	1	5	5	4
Homo habilis sensu lato	172.73	186.74	182.38		226.83	206.61		3.6%	8.4%	5	3	2		2	7
Paranthropus robustus	197.77		250.35	213.81	253.90	247.68	4.5%	5.3%	11.4%	3		5	9	9	2
Homo ergaster	154.58	161.87			199.12	177.16		3.0%	6.0%	6	5			1	4
Homo georgicus	144.48				139.32	110.58		2.8%	4.0%	1				1	1
Homo erectus	170.28				184.92	182.70		6.1%	8.4%	1				1	1
Homo mauritanicus					189.00	167.50		3.1%	1.9%					1	1
Homo heidelbergensis	170.30	198.65				162.44			7.2%	1	1				1
Homo pekinensis				171.36			2.0%						1		
Early Homo neanderthalensis	126.26	121.00	133.35			131.84			1.3%	1	1	1			1
Early Homo sapiens	152.87	124.26	126.99							2	2	2			
Homo neanderthalensis	129.95	126.56	123.16							1	1	3			

b. PGLS of M1 cusp 6 size *vs.* molar size

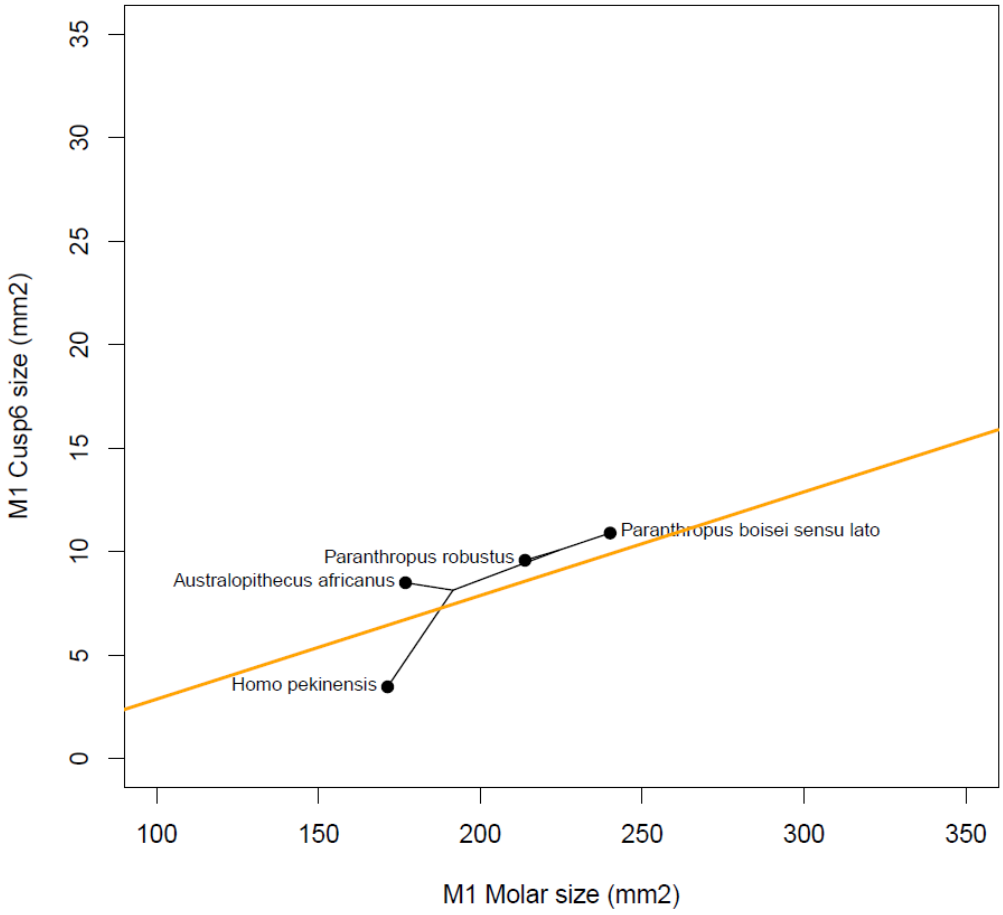

APPENDIX XII

a. Cusp 7 - complete cups and molar size and sample size data

	NM1	NM2	NM3	M1	M2	M3	M1 C7	M2 C7	M3 C7	NM1#	NM2#	NM3#	M1#	M2#	M3#
Orrorin tugenensis	149.70									1					
Australopithecus afarensis					158.60	171.41		3.4%	5.9%					1	1
Australopithecus africanus	183.17	212.44	233.95		237.10	237.96		3.1%	4.9%	5	4	2		2	5
Paranthropus boisei sensu lato	233.97	333.66	346.41		260.40			2.8%		6	5	3		1	
Homo habilis sensu lato	171.28	165.39	180.97	174.90	227.70	192.45	3.8%	2.9%	4.0%	3	2	3	2	3	4
Paranthropus robustus	209.75	256.56	247.93	214.50		259.55	4.7%		4.8%	10	10	6	1		1
Homo ergaster	150.86	162.68	181.46	162.01	178.86	164.82	4.3%	4.2%	5.3%	4	4	2	2	2	1
Homo georgicus				144.48	139.32	110.58	6.2%	2.7%	12.3%				1	1	1
Homo erectus			182.70	170.28	184.92		5.7%	4.5%				1	1	1	
Homo mauritanicus		189.00				167.50			3.9%		1				1
Homo heidelbergensis	170.30	198.65	162.44							1	1	1			
Homo pekinensis				171.36			4.1%						1		
Early Homo neanderthalensis	126.26	121.00	132.60							1	1	2			
Early Homo sapiens	143.84	124.26	126.99	161.90			5.8%			1	2	2	1		
Homo neanderthalensis	129.95				126.56	123.16		4.1%	3.6%	1				1	3

b. PGLS of M1 cusp 7 size *vs.* molar size

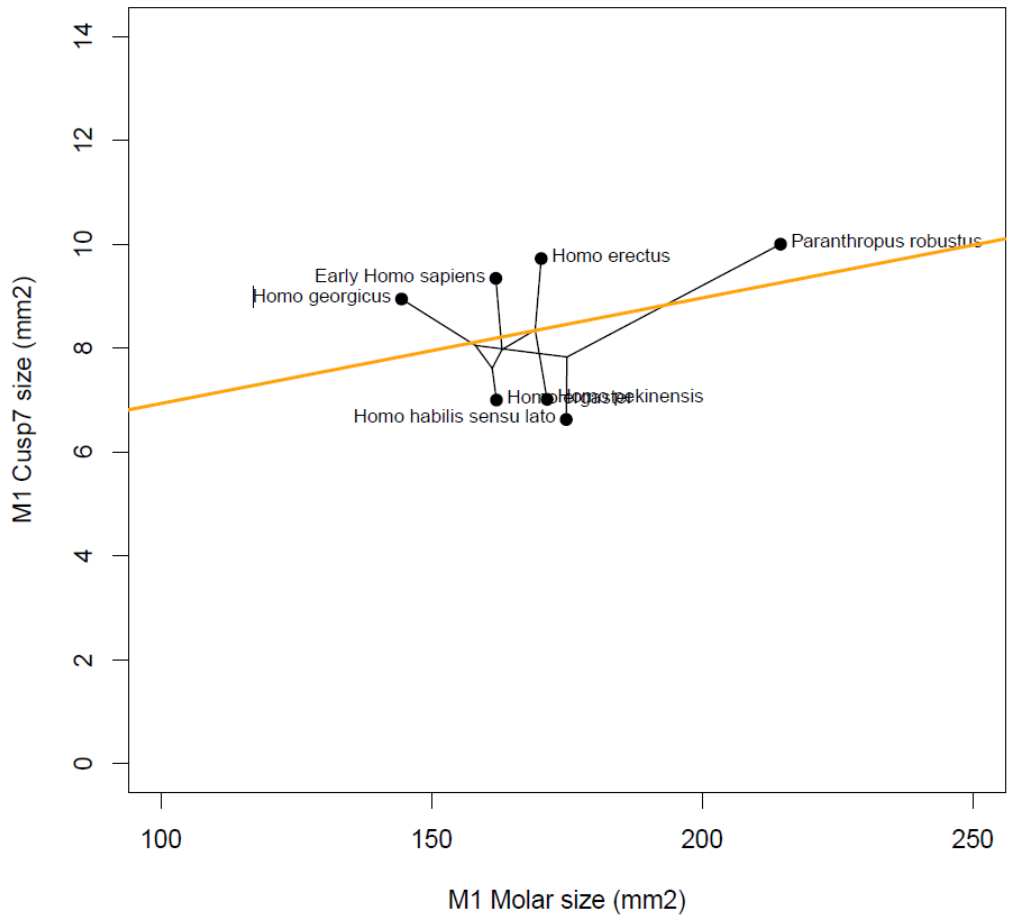

APPENDIX XII (cont'd)

c. PGLS of M2 cusp 7 size *vs.* molar size

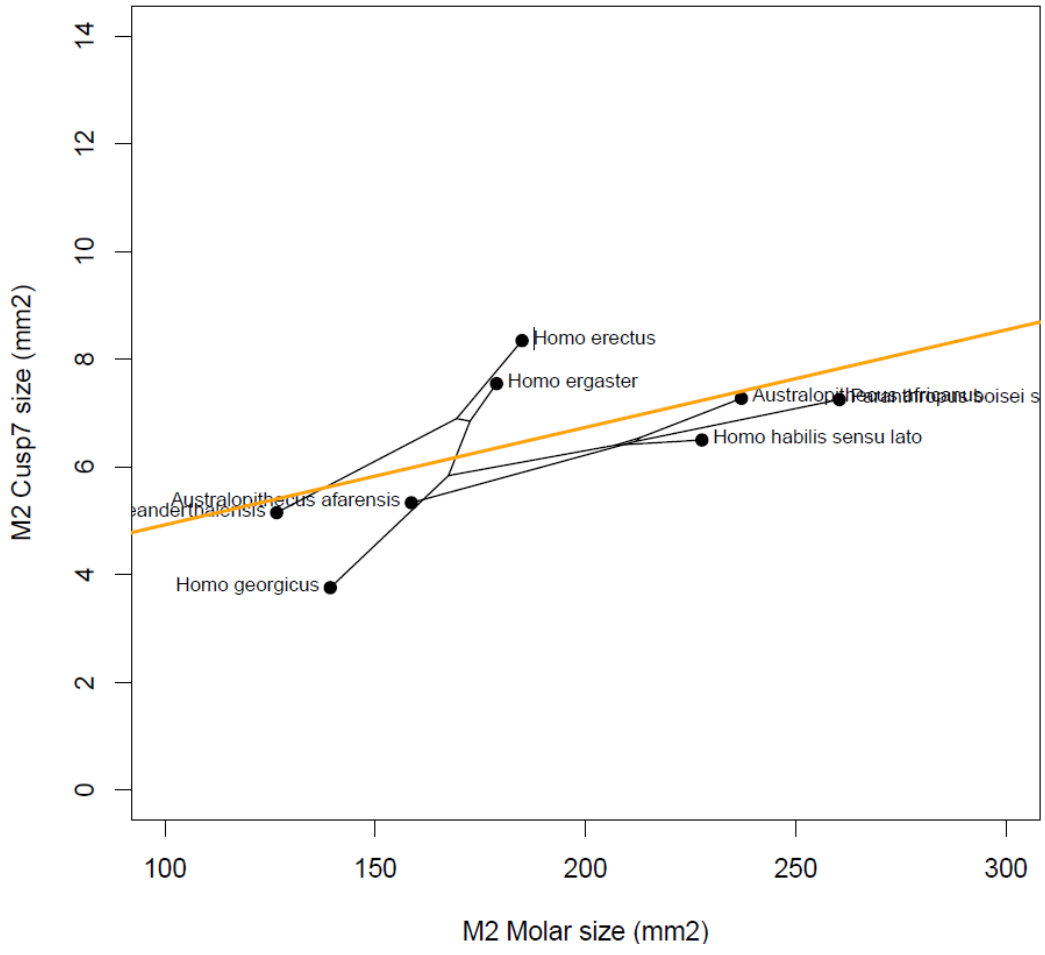

APPENDIX XIII - D5099 cusp 7 on 3D model

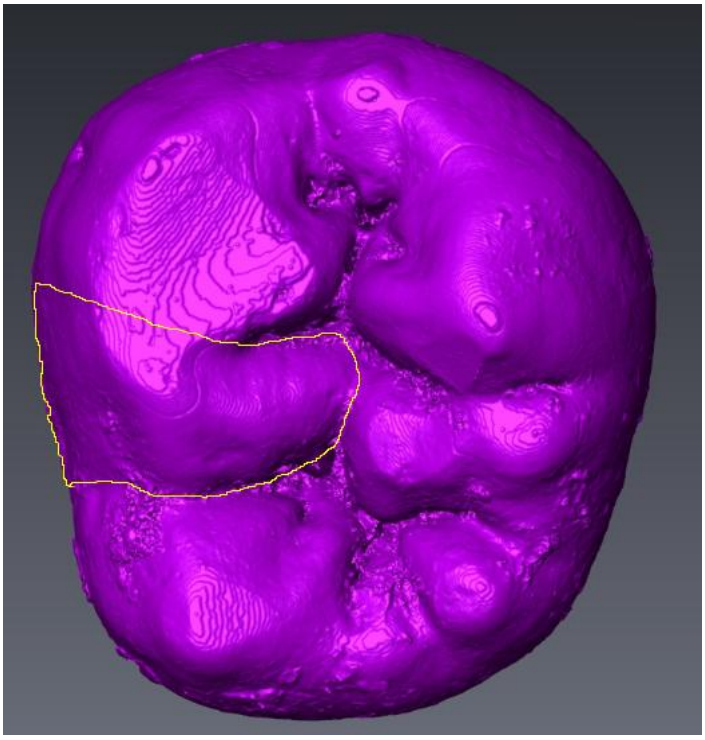

Supplementary image: cusp 6 defined, and with no drawn boundary overlapping the fissures

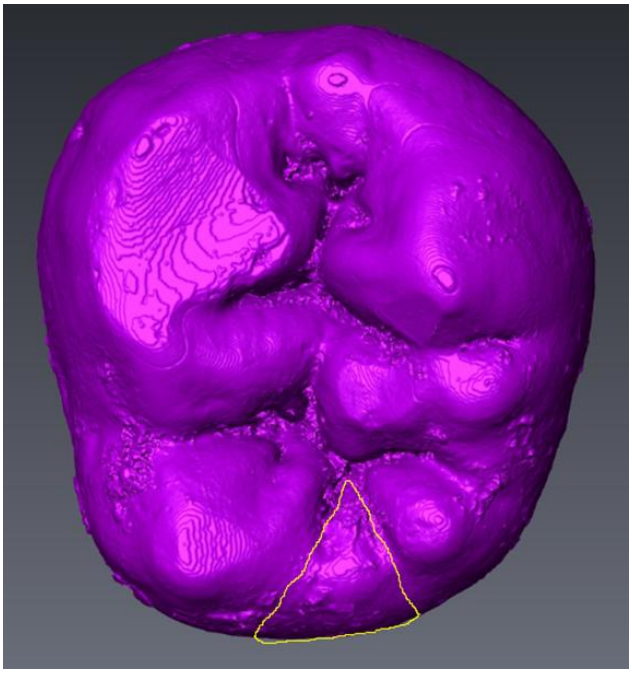

ABSTRACT

Activator-inhibitor networks are a common mechanism in development, and have been demonstrated to govern different cusp sizes of mammalian teeth through a sequential cascading mechanism. Yet it was not until the introduction of inhibitory cascade (IC) model that this mechanism became formalised into a statistical framework that allows predictions of relative molar sizes across species on evolutionary paths. While the model's applications to hominins report mixed results and raise questions about whether other factors influence sizes as well, in addition to the timing of initiation, the debates on the better proxy in reflecting developmental pattern: crown size *vs.* mesiodistal (MD) length, further complicate our understanding of developmental rules and the underlying genetic basis.

This study investigates molar size determination in hominins at multiple organisation scales: MD length, crown size, mandibular width and cusps, analysed by phylogenetic regressions. Our results show that the hominin molar size is determined not only by the cascading mechanism, but also by a hierarchical nesting of constraints. The smallest scales at which cascading dynamics are expressed were revealed to be the crown size. MD length carries no clear advantage in capturing phylogeny, which is considered an articulation of the underlying genetic pattern. The high dependence of the lower first and third molar size on mandibular width suggests spatial constraints from the jaw during development. The IC mechanism governs relative molar sizes in both jaws within these constraints, but the dynamics differ: maxillary molars align more closely with the IC predictions than those of the mandible, possibly linked to the stronger M3 reduction as indicated by more positive M3 allometry. The hierarchy is mirrored on cusps, with their sizes being regulated by sequential cascading in response to the available space, which is, in turn, shaped by crown area and the molar initiation order. We therefore conclude that rather than the IC mechanism alone, its interaction with spatial factors across jaws and crowns jointly determines the molar and cusp sizes of hominins.